CATALYTIC REACTIONS OF PLATINUM GROUP METAL PHTHALOCYANINES

THESIS

Submitted to

Rhodes University

in fulfilment of the requirements for the degree of

DOCTOR OF PHILOSOPHY

by

MANTOA MAKOENA C. SEKOTA

January 1999

Department of Chemistry

Rhodes University

Grahamstown

ACKNOWLEDGMENTS

I would like to give my heart felt thanks to my supervisor, Professor T. Nyokong, for her guidance and constant encouragement thoughout the duration of this project. It has been both a pleasure and an excellent learning experience to work under her supervision.

My very special thank goes to my husband, Simon M. Sekota, for the support and encouragement he has given me throughout the course of this project. I greatly appreciate the help he has given me in proof-reading this thesis.

I would also like to thank

- Lesotho government for financial assistance.
- Sibulelo Vilakazi for proof-reading my introduction.
- Stuff chemistry department at Rhodes University for their assistance in different ways.
- My fellow students and friends for making it a pleasure to work in this department.

Abstract

The voltammetric behaviour of *l*-cysteine and other organic compounds such as hydrazine, hydroxylamine and methionine has been studied on GCE modified with phthalocyanine complexes of osmium, rhodium and ruthenium. For cysteine oxidation, the catalytic activity of the electrode was dependent the nature of the axial ligand. When cyanide and dimethylsulphoxide (DMSO) were used as axial ligands, giving (DMSO)(Cl)Rh(III)Pc, $[(CN)_2Rh(III)Pc]^-$, $(DMSO)_2Os(II)Pc$ and $[(DMSO)_2Ru(II)Pc].2DMSO$ complexes, the peak current increased with repetitive scanning, indicating the increase in catalytic activity of the electrode after each scan. This behaviour was not observed when pyridine was used as axial ligand. The improvement of the catalytic activity of the GCE after the first scan has been attributed to the formation of the dimeric π-cation radical species at the electrode surface.

Water soluble phthalocyanine complex ($[(CN)_2Os(II)Pc]^{2-}$) and the tetramethyltetra-pyridinoporphyrazine complexes of Pd(II) and Pt(II), ($[Pd(II)2,3Tmtppa(-2)]^{4+}$, $[Pd(II)3,4Tmtppa(-2)]^{4+}$, $[Pt(II)2,3Tmtppa(-2)]^{4+}$ and $[Pt(II)3,4Tmtppa(-2)]^{4+}$) have been prepared. $[(CN)_2Os(II)Pc]^{2-}$ is soluble in water at pH greater 4 without the formation of dimers. The $[M(II)Tmtppa(-2)]^{4+}$ (M = Pd or Pt) show high solubility in water and are stable only in acidic pHs. The cyclic voltammetry of the MPc and $[M(II)Tmtppa(-2)]^{4+}$ complexes prepared, is also reported.

The interactions of amino acids *l*-histidine and *l*-cysteine with the $[M(II)Tmtppa(-2)]^{4+}$ complexes of Pd(II) and Pt(II) were studied. All the $[M(II)Tmtppa(-2)]^{4+}$ are readily reduced to the monoanion species $[M(II)Tmtppa(-3)]^{3+}$ in the presence of histidine and cysteine. The rate constants for the interaction of $[M(II)Tmtppa(-2)]^{4+}$ complexes of Pt(II) and Pd(II), with

histidine and cysteine range from approximately 2 x 10^{-3} to 0.26 dm^3 mol^{-1} s^{-1}. Kinetics of the interaction of $[Co(II)TSPc]^{4-}$ with amino acids, histidine and cysteine in pH 7.2 buffer were studied. The rate constants were found to be first order in both $[Co(II)TSPc]^{4-}$ and the amino acid. The formation of $[Co(III)TSPc]^{3-}$ in the presence of histidine occurred with the rate constant of 0.16 dm^3 mol^{-1} s^{-1}, whereas the formation of the $[Co(I)TSPc]^{5-}$ species in the presence of cysteine gave the rate constant of 2.2 dm^3 mol^{-1} s^{-1}.

The relative quantum yield (Q_Δ) for singlet oxygen production by $[(CN)_2Os(II)Pc]^{2-}$, and $[(CN)_2Ru(II)Pc]^{2-}$ in DMF using diphenylisobenzofuran (DPBF) and a chemical quencher were determined. The quantum yield values were obtained as 0.39 ± 0.05, and 0.76 ± 0.02 for $[(CN)_2Os(II)Pc]^{2-}$ and $[(CN)_2Ru(II)Pc]^{2-}$ respectively. The differences in quantum yield values have been explained in terms of donor abilities of both the central metal and the axial ligands

Table of Contents

List of abbreviations

B.M	=	Bohr Magneton
BAS	=	Bio-Analytical Systems
BSA	=	Bovin Serum Albumen
CME	=	Chemically Modified Electrode
CMGCE	=	chemically modified glassy carbon electrode
CO	=	Carbon monoxide
CTT	=	Charge Transfer Transitions
CV	=	cyclic voltammogram
DMA	=	N,N-dimethylacetamide
DMF	=	N,N-dimethylformamide
DMSO	=	dimethylsulphoxide
DNA	=	Deoxyribonucleic Acid
DPBF	=	Diphenylisobenzofuran
ESR	=	Electron Spin Resonance
FTIR	=	Fourier Transform Infrared
GCE	=	Glassy Carbon Electrode
HDP	=	Haematoporphyrin Derivative
HOMO	=	Highest Occupied Molecular Orbital
imid	=	imidazole
IR	=	Infrared
LMCT	=	Ligand to Metal Charge tranfer Transition
LUMO	=	Lowest Occupied Molecular Orbital
MCD	=	Magnetic Circular Dichroism
MLCT	=	Metal to Ligand Charge transfer Transition
MPc	=	Metallophthalocyanine
MT	=	Metallothionein

MTmtppa	=	Metal tetramethyltetrapyridinoporphyrazine
MTSPc	=	Metal tetrasulphonated phthalocyanine
NCS	=	thiocyanate
pa	=	porphyrazine
Pc	=	Phthalocyanine
PDT	=	Photodynamic Therapy
py	=	pyridine
$RSCH_3$	=	Methionine
RSH	=	Cysteine
RSSR	=	Cystine
SCE	=	Saturated Calomel Electrode
Sen	=	Sensitizer
SH	=	Hydrogen donor
SHE	=	Saturated Hydrogen Electrode
TEAP	=	Tetraethyl ammonium perchlorate
Tm	=	tetramethyl
Tmtppa	=	Tetramethyltetrapyridinoporphyrazine
tp	=	tetrapyridino
tppa	=	tetrapyridinoporphyrazine
TSPc	=	Tetrasulphonated phthalocyanine
UV	=	Ultra-violet
Vis	=	Visible
VR	=	Vibrational Relaxation

List of symbols

α	=	transfer coefficient
ΔE	=	separation between peak potentials
λ_{max}	=	wavelength
ν	=	stretching vibrations (IR)
π	=	pi
σ	=	sigma
τ_p	=	excited-state phosphorescence lifetime
$^1O_2$	=	singlet oxygen
C	=	concentration of the electroactive species
D	=	diffusion coefficient or donor
D_o	=	diffusion coefficient of oxidized species
D_R	=	diffusion coefficient of reduced species
$E_{1/2}$	=	half wave potential
E_f	=	final potential
E_i	=	intial potential
E_o	=	oxidation potential
E^o	=	formal reduction potential
E_{pa}	=	anodic peak potential
E_{pc}	=	cathodic peak potential
F	=	Faraday's constant
hv	=	light energy
i_p	=	peak current
i_{pa}	=	anodic peak potential
i_{pc}	=	cathodic peak potential
n	=	number of electrons transferred during redox process
n_a	=	number of electrons involved in charge transfer step
Q	=	charge in coulombs
R	=	gas constant in joules/Kelvin/mole

S_1	=	singelet excited state
S_o	=	ground state
T	=	temperature in Kelvin
T_1	=	triplet excited state
v	=	scan rate
ze/r	=	polarizing power

List of Figures

List of Schemes

List of Tables

1. INTRODUCTION

Metallophthalocyanines (MPc, Pc = phthalocyanine dianion) **Figure 1(a)**, are molecules of great commercial importance as they resemble, structurally, the biologically important metalloporphyrins **Figure 1(b)**. MPc complexes have established themselves as blue or green dyestuffs. They have a wide variety of uses including artists' colours, printing inks (especially for bank notes), colouring for plastics, surface coating, paper dyes, floor covering, dyestuffs for jeans and other clothing [1].

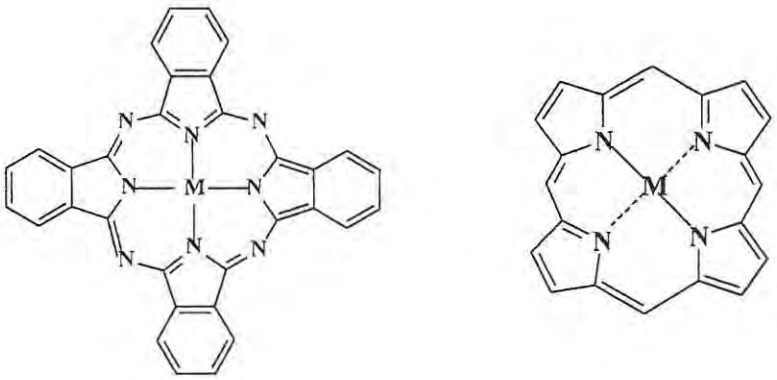

(a) **(b)**

Figure 1. Molecular structures of a) metallophthalocyanine and b) metalloporphyrin.

In recent years there have been a remarkable progress on the use of MPc complexes as photosensitizers in photodynamic therapy (PDT) [2], a new modality for treatment of tumours. PDT is the technique that uses light activated sensitizers, ie, compounds that are non-toxic until irradiated with light of an appropriate wavelength tuned to the absorption band of the sensitizer. Disulphonated aluminium phthalocyanine ($AlPcS_2$) has been reported to be very effective sensitizer in PDT [2]. The possible use of MPc complexes as photosensitizers in artificial solar energy devices has been investigated [3]. MPc complexes have potential use in electronic

display devices since they show dramatic variation of colour with change in potential. Research leading to the possible use of MPc in photovoltaic devices is also receiving increasing attention.

Metallophthalocyanine complexes are inexpensive and readily available catalysts with a potential for the degradation of environmental pollutants such as sulphur dioxide and chlorinated aromatic compounds [4,5]. Research into the application of MPc complexes as electrocatalysts is continuing to receive considerable attention [6]. Many of the applications of MPc complexes involve the exchange of electrons and coordination of the reactants or products to the MPc species. The catalytic activity is strongly dependent on the nature of the central metal ion. MPc complexes whose central metal can reversibly bind both the reactants and products are expected to show good catalytic activity.

The discovery of metallophthalocyanines complexes happened by chance in 1928 during the course of the industrial production of phthalimide at Messrs Scottish Dyes, Ltd [7]. The process involved passing ammonia into a molten phthalic anhydride in iron vessels. It was found that during certain preparations traces of a dark blue substance were formed in the molten amide and this dark blue product was later shown to be ferrous phthalocyanine. The geometric structure of metallophthalocyanine, **Figure 1 (a)**, was elucidated by Robertson *et al* [8], using crystal X-ray diffraction analysis.

The structure of metallophthalocyanine, **Figure 1 (a)**, consists of a ring system made up of four isoindole units linked by aza nitrogen atoms [9]. This structure resembles that of the naturally occurring metalloporphyrins, **Figure 1(b)**, except that the porphyrin ring system is made up of pyrrole units instead of the isoindole, and the pyrrole units in porphyrins are linked by carbon atoms in place of nitrogen atoms.

1.1 Methods of preparation of metallophthalocyanines

Metallophthalocyanines may be prepared by various methods. Commonly used methods involve the reaction of either *O*-cyanobenzamide, **Scheme 1**, or phthalonitrile, **Scheme 2**, with metal salts in the presence of a solvent.

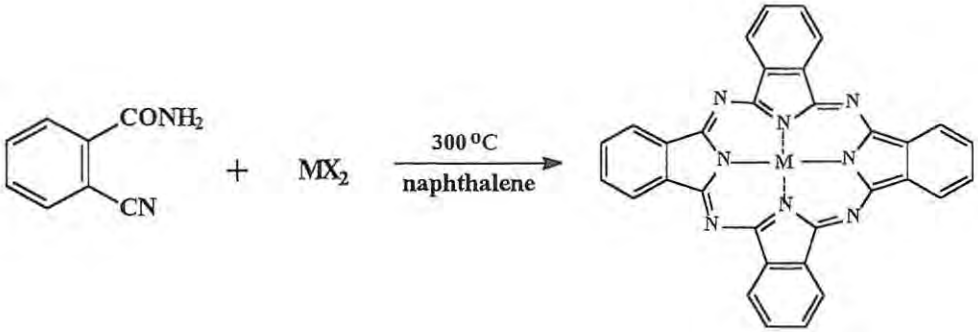

Scheme 1 A simplified synthetic route for metallophthalocyanine from *o*-cyanobenzaminde

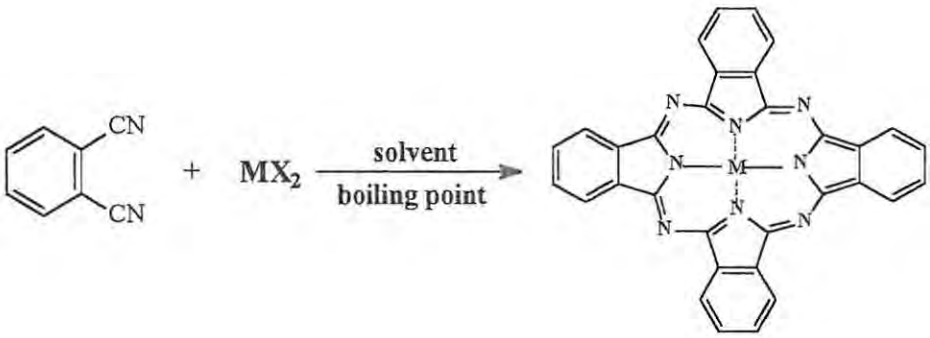

Scheme 2 A simplified synthetic route for metallophthalocyanine from phthalonitrile.

Axially coordinated MPc complexes (L_2MPc) are normally synthesized by refluxing the unligated MPc species in a coordinating solvent, **Scheme 3.**

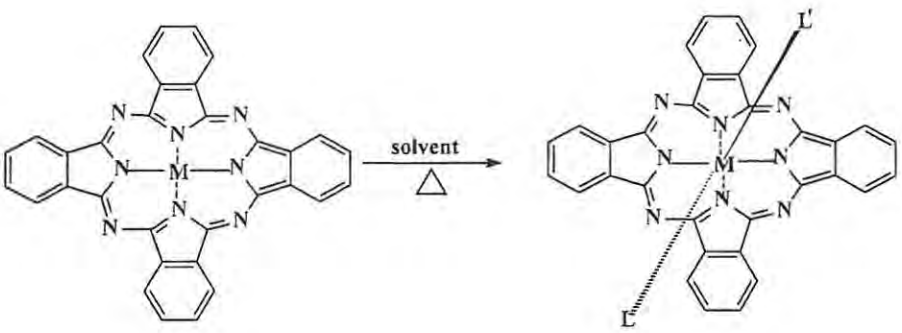

L and L' = axial ligands

Scheme 3 A simplified synthetic route for axially ligated MPc complexes.

Synthesis of substituted metallophthalocyanine complexes

Most unsubstituted MPc complexes have very low solubility in most of the organic solvents, and show no solubility at all in aqueous solvents. Introduction of ring substituents to the MPc system renders these complexes soluble in most of the organic solvents. Tetrasulphonated MPc species are known to be soluble in water [10]. These species are normally synthesized from the metal salt and the monosodium salt of 4-sulphophthalic acid in the presence of a catalyst, **Scheme 4.**

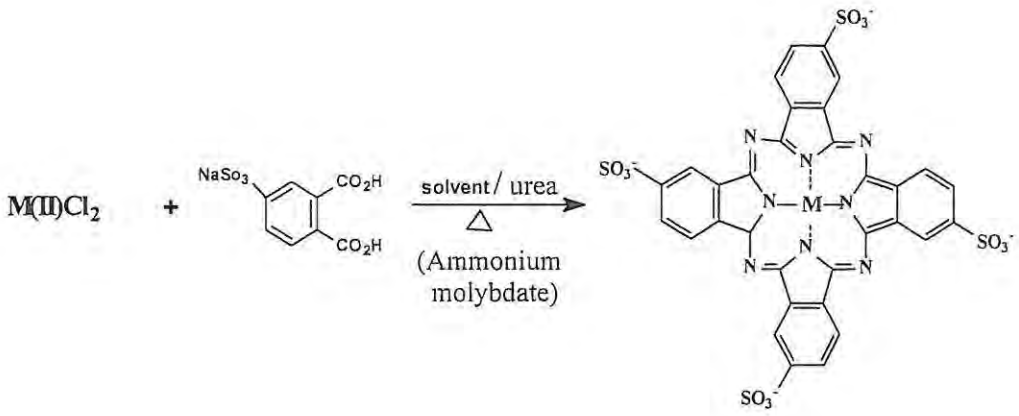

Scheme 4 A simplified synthetic route for M(II)tetrasulphophthalocyanine, ([M(II)TSPc]$^{4-}$).

Soluble octasubstituted MPc complexes are normally synthesized from the substituted phthalonitriles and the metal salt [11], **Scheme 5**.

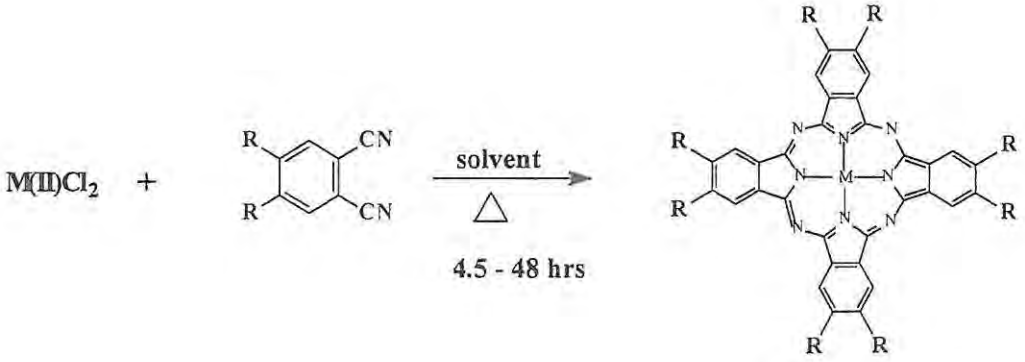

Scheme 5 A simplified synthetic route for the octasubstituted MPc complex prepared from the substituted phthalonitrile. R = organic ring substituents.

1.2 Absorption spectral properties of metallophthalocyanines

Most of the applications of MPcs result from their absorption spectra in the visible region, **Figure 2,** especially their intense band in the 600 - 750 nm regions. The spectrum is due to the $\pi \rightarrow \pi$ transitions within the phthalocyanine ring and charge transfer transitions between the phthalocyanine ring and the central metal.

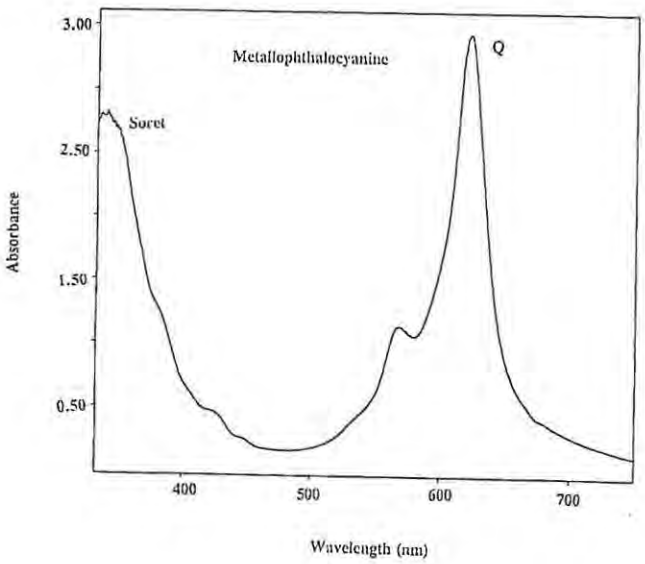

Figure 2 Absorption spectra of a typical metallophthalocyanine complex.

1.2.1 Electronic structure of Metallophthalocyanine

It has been shown that MPc has a square planer structure and therefore belongs to the D_{4h} point group [12]. According to Gouterman's four orbital theory [13], the highest occupied molecular orbital (HOMO) of the Pc ring is the $a_{1u}(\pi)$, the next low lying filled orbital is the $a_{2u}(\pi)$. The lowest unoccupied molecular orbital (LUMO) of the ring is the $e_g(\pi^*)$ and the next highest unfilled orbital is the $b_{1u}(\pi^*)$, **Figure 3**. The intense band observed near the 600 - 750 nm region, known as the Q band, is due to the transition from the highest occupied molecular orbital to the lowest unoccupied molecular orbital of the ring (HOMO to LUMO).

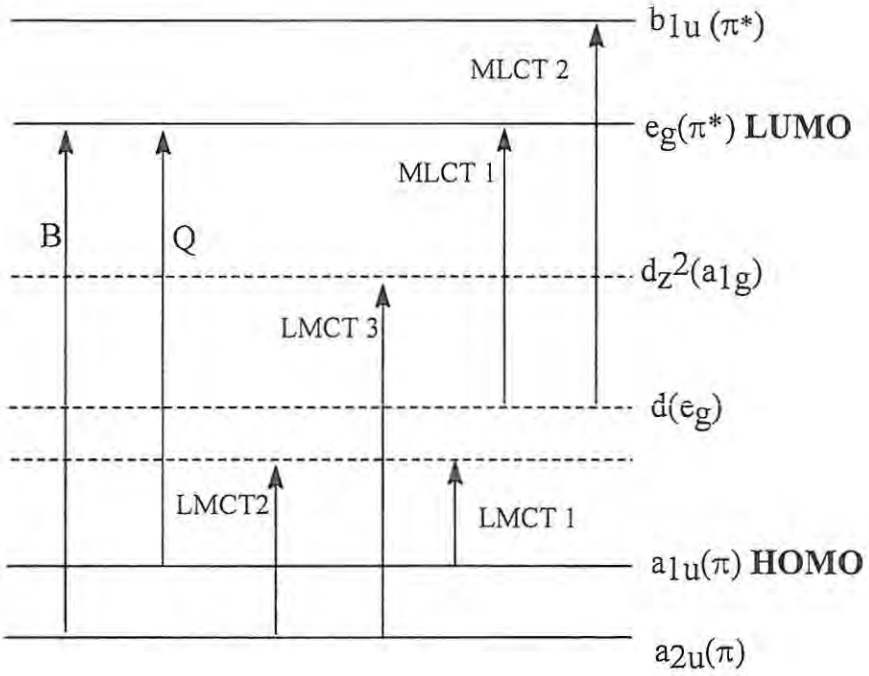

Figure 3. A simplified energy levels diagram for metallophthalocyanine [14].

_____ ring energy levels -------- central metal energy levels.

Transition from the $a_{2u}(\pi)$ to the LUMO yields the Soret band, also known as the B band, which is normally observed in the near 300 - 450 nm region. If the central metal has d-orbitals lying within the HOMO - LUMO gap, **Figure 3**, there is a possibility of an electron being transferred from the occupied phthalocyanine ring orbital to the unfilled metal d-orbital, or from the occupied metal d-orbital to the unfilled phthalocyanine ring orbital. Such transitions are called charge transfer transitions (CTT). Ligand to metal charge transfer transitions (LMCT) are observed when an electron is transferred from the occupied orbital of the ring to the unfilled d-orbital of the metal, while the metal to ligand charge transfer transitions (MLCT)

are observed when an electron transfer is from the occupied metal d-orbital to the unfilled orbitals of the Pc ring [15,16]. Charge transfer transitions are normally characterized by weak absorption bands near the infrared region or between the Q and the Soret band, normally in the 500 nm region. It has been reported that the CTT absorption bands are not typical of the MPc spectra in general, but are confined to those MPc complexes whose central metal ion has d-orbitals lying within the HOMO-LUMO gap, for example Fe(II) and Co(III) [17].

The electronic absorption spectra of the MPc complex is known to vary considerably depending on the nature of the ligands coordinated on the axial positions of the MPc complex. When axial ligands are attached to the MPc complex two new bands have been reported to form to the red of the B band, in the 300 to 400 nm region [17]. The intensity and the resolution of these two new bands have been reported to vary depending on the σ-donor strength of the axial ligands [17,18]. Studies by Dale [17] have shown that for $(L)_2Fe(II)Pc$, (where L = dimethylsulphoxide, (DMSO), pyridine (py), NH_3, CN^-, carbon monoxide (CO) and imidazole (imid)), the two new bands formed to the red of the B band intensify or become more resolved as the σ-donor strength of the ligand increased.

The properties of the absorption spectra of the MPc complexes are also affected by the nature of the solvent. The weakly coordinating solvents such as dimethylacetamide (DMA), DMSO and dimethylformamide (DMF) provide a consistent environment from which to compare different metal and different axial ligands. For most MPc species the Q band is found within 600-700 nm region [18] in weakly coordinating solvents. Spectra recorded in sulphuric acid solutions exhibit a red-shifted Q band, which lies between 700 an 850 nm.

1.2.2 Absorption spectra of cation and anion radical species of the metallophthalocyanines

Oxidation and reduction in metallophthalocyanines can occur at the central metal or at the phthalocyanine ring. Identification of the nature of a given redox product is usually based on the absorption spectra of the species. It is possible to deduce whether a reduction or oxidation occurred at the central metal or at the phthalocyanine ring, since the absorption spectra of the oxidized and reduced metallophthalocyanine are different from each other and from that of the neutral MPc species.

Oxidation at the phthalocyanine ring in MPc(-2) occurs by successive removal of one or two electrons from the HOMO resulting in the formation of the $[MPc(-1)]^{+}$ and $[MPc(0)]^{2+}$ cation radicals. The formation of $[MPc(-1)]^{+}$ cation radical species results in the partially filled highest occupied molecular orbital. The presence of a hole in $a_{1u}(\pi)$ permits the allowed transition from $e_g(\pi)$ levels lying below the $a_{1u}(\pi)$, **Figure 4**. The formation of $[MPc(-1)]^{+}$ is normally characterized by the loss of intensity of the Q band, the formation of weak bands in the 700 and 825 nm regions, and the observation of a broad band being centred near 500 nm. Generally the band around 700 nm is associated with the dimerization of the radical species [19 - 24].

Reduction at the Pc ring corresponds to successive addition of up to four electrons to the LUMO, resulting in the formation of MPc(-3) to MPc(-6) species [25]. The addition of electrons to the lowest unoccupied molecular orbital permits the π^*- π^* transitions to occur from the $e_g(\pi^*)$ to the higher energy π^* molecular orbitals of the ring, **Figure 4.** The formation of the MPc(-3) anion radical is characterized by the formation of a blue coloured solution and the appearance of two absorption bands near 620 and 580 nm, while MPc(-4) has a purple colour and absorbs near 520 nm. These are very weak absorption bands since the Pc ring is perturbed. MPc(-5) trianion and MPc(-6) tetraanion anions are blue in colour and blue - green respectively [23,25].

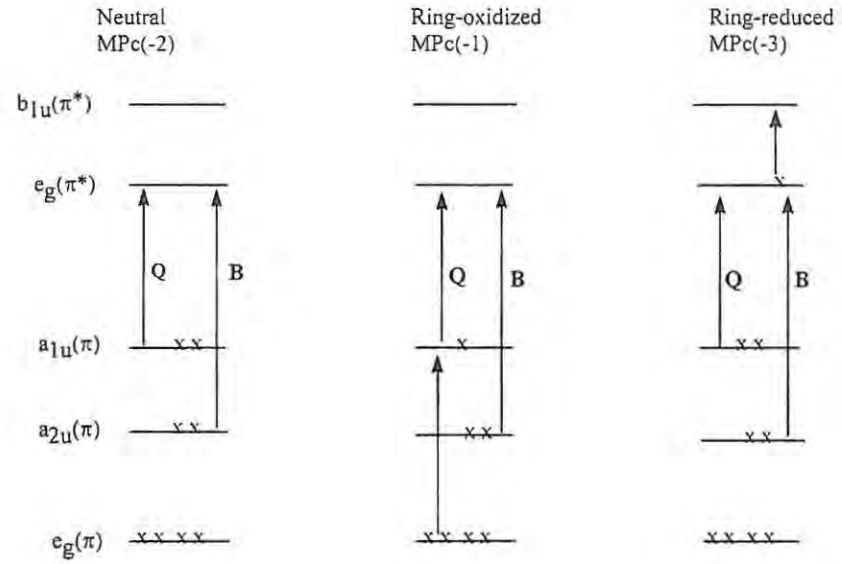

Figure 4. A simplified energy level diagram for ring-oxidized and ring-reduced MPc.

In MPc complexes the site of oxidation or reduction depends on the nature of the central metal ion, and for those metals which do not have d-orbitals positioned within the HOMO - LUMO gap of the Pc ring, oxidation or reduction occurs exclusively on the phthalocyanine ring. The spectra of metal oxidized or reduced MPc species are quite different from those observed for ring oxidation. Metal oxidation or reduction is characterized by the shift in the Q band without much reduction in intensity [26].

1.3 Electrochemistry: an overview

1.3.1 Cyclic voltammetry

Cyclic voltammetry [27,28] is commonly used as an initial electrochemical technique to characterize a reduction/oxidation (redox) system. It is used to determine the half wave potential ($\mathbf{E_{1/2}}$) and the number of electrons (**n**) transferred during the redox reaction. The solution of the species to be characterized is normally saturated with an inert gas, nitrogen or argon, in order to remove oxygen from the solution, as the presence of oxygen in the solution may interfere with the response of the species. In cyclic voltammetry, the potential is scanned linearly from an initial value E_i to the second value $\mathbf{E_f}$ and then back to $\mathbf{E_i}$, **Figure 5.**

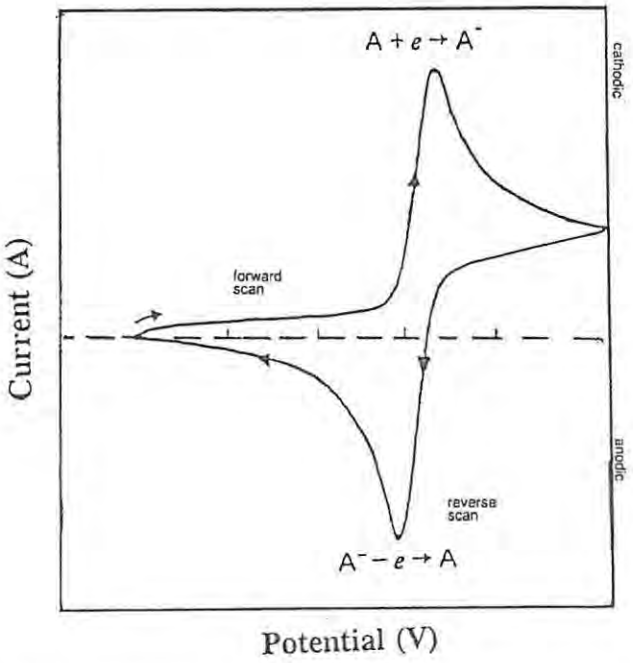

Figure 5. Cyclic voltammogram showing cathodic and anodic current peaks.

During the forward scan A is reduced to A^- resulting in a cathodic peak. When the scan direction is switched to the opposite direction, A^-, which has been accumulating near the electrode, is oxidized back to A, resulting in an anodic peak. One or more potential cycles can be performed, hence the term "cyclic voltammetry".

Reversible systems

A redox system in which both the oxidized and the reduced species are stable and rapidly exchange electrons with the working electrode is termed an electrochemically reversible couple [27]. The half wave potential, $\mathbf{E}_{1/2}$, for the reversible system is related to the formal reduction potential, $\mathbf{E}^{\circ}$, by **Equation 1**.

$$E^{\circ} = E_{1/2} + (RT/nF)\ln[(D_o/D_R)^{1/2}] \qquad \text{Equation 1}$$

where $\mathbf{D}_O$ and $\mathbf{D}_R$ are the diffusion coefficients of the oxidized and reduced species respectively,

$\mathbf{E}^{\circ}$ = formal potential (V)

F = Faraday's constant in coulombs/ mole.

R = gas constant in joules/Kelvin/mole.

T = temperature in Kelvin.

n = the number of electrons transferred.

$\mathbf{E}^{\circ} = \mathbf{E}_{1/2}$ when $\mathbf{D}_O = \mathbf{D}_R$ and this is a common approximation employed, which means that the formal reduction potential ($\mathbf{E}_{1/2}$ corrected for the reference electrode being used) for the reversible system is centred between the anodic potential ($\mathbf{E}_{pa}$) and cathodic potential ($\mathbf{E}_{pc}$), **Equation 2.**

$$E_{1/2} = \frac{E_{pa} + E_{pc}}{2} \qquad \text{Equation 2}$$

The number of electrons transferred in the electrode reaction for a reversible couple can be determined from the separation between the peak potentials ($\Delta\mathbf{E}$), **Equation 3** [27].

$$\Delta E = E_{pa} - E_{pc} = \frac{RT}{nF} \qquad \text{Equation 3}$$

For a one-electron process such as the reduction of **A** to A^-, ΔE should ideally be 0.058 V at 25°C and is independent of the scan rate (v). The peak current (i_p) for the reversible system is described by the Randle-Sevcik equation for the forward sweep of the first cycle, **Equation 4.**

$$i_p = 2.69 \times 10^5 \times n^{3/2} A D^{1/2} C v^{1/2} \qquad \text{Equation 4}$$

Where **n** is as described above, **A** the electrode surface area, **C** the concentration of the electroactive species in solution and **D** the diffusion coefficient . According to **Equation 4**, peak current increases with the square root of scan rate ($v^{1/2}$) and is directly proportional to concentration for a reversible couple. The dependence of the peak current on $v^{1/2}$ is indicative of a diffusion controlled process. The anodic to cathodic peak current ratio (i_{pa}/i_{pc}) is unity for reversible systems.

Irreversible and quasi-reversible systems

Electrochemical irreversibility is caused by a very slow electron exchange between the redox species and the working electrode. In a quasi-reversible system the anodic and cathodic peak currents are reduced in size and the anodic to cathodic peak current ratio is not unity. Totally irreversible systems are characterized by a single oxidation or reduction peak without the return peak, and the peak current for such systems is given by **Equation 5**:

$$i_p = (2.99 \times 10^5) n (\alpha n_a)^{1/2} A C D^{1/2} v^{1/2} \qquad \text{Equation 5}$$

where α is the transfer coefficient and n_a is the number of electrons involved in the charge-

transfer step. The rest of the symbols are as described above for **Equation 4**.

1.3.2 *Controlled potential electrolysis*

Cyclic voltammetry is capable of rapidly generating a new species during the forward scan and then regenerating the starting species on the reverse scan. It provides the information about the potentials at which the species get oxidized and reduced, and the site of reduction or oxidation is normally confirmed by controlled potential electrolysis. In controlled potential electrolysis [27,28], the current is integrated during the course of the experiment. When the electrolysis of the species is complete, the total charge is used to calculate the amount of material electrolysed by means of Faraday's law, **Equation 6**:

$$Q = nvFc \qquad \text{Equation 6}$$

where **Q** = charge, in coulombs (C)

F = Faraday's number, in coulombs/mole ($C\ mol^{-1}$)

n = number of electrons transferred per mole of ion.

v = volume of the solution in the cell (ml)

c = concentration of the solution ($mol\ dm^{-3}$)

The products generated from controlled potential electrolysis are normally characterized by electronic spectroscopy in order to determine the site of the redox process; the number of electrons transferred can be calculated from **Equation 6**. Other methods such as magnetic circular dichroism (MCD) and electron spin resonance (ESR) may also be used to characterise the species. If the solid form of the products can be isolated, the infrared spectroscopy of the species can also be obtained.

1.4 Electrochemical properties of metallophthalocyanines

1.4.1 Main group metallophthalocyanines

Main group metallophthalocyanines are said to be redox inactive since the central metal d-orbitals do not lie within the HOMO - LUMO gap of the phthalocyanine ring and the redox processes in these species are expected to occur exclusively on the phthalocyanine ring. Substitution of electron withdrawing ligands, such as cyanide, on the phthalocyanine ring decreases the average electron density of the total conjugated system, thus resulting in lowering of the lowest unoccupied molecular orbital of the ring. This increases the electron affinity of the macrocycle, thus leading to easier reduction of the ring [29]. For the same kind of substituents on the ring, the individual potentials of the first ring reduction or oxidation depend on the polarizing power (*ze*/**r**) of the central metal ion. The more polarizing the central metal the easier it is to reduce the ring and the more difficult to oxidize it [30].

Most of the studies on the solution electrochemistry of the main group phthalocyanines are on magnesium and zinc phthalocyanines. This might be due to the low solubility of most of the main group MPcs. For both MgPc and ZnPc, all the six redox processes have been reported, $[M(II)Pc(0)]^{2+}$ to $[M(II)Pc(-6)]^{4-}$ [31 -35]. Ring substitution with electron attracting groups such as cyanides and chlorides on Zn(II)Pc species has been reported to shift the reduction potentials to positive values when compared to the unsubstituted counterparts [32,36].

1.4.2 Transition metal phthalocyanine

Transition metal phthalocyanines have been classified into redox inactive and redox active metallophthalocyanines. The redox inactive metallophthalocyanines have redox properties very similar to that of main group MPcs, and all the redox properties are expected to occur on the phthalocyanine ring. NiPc and CuPc are examples of the redox inactive

metallophthalocyanines. Their electrochemical properties have been reported to be more like those for the zinc phthalocyanine, where the redox processes occur exclusively on the phthalocyanine ring [37- 43].

In redox active transition metal phthalocyanines, the central metal has the d-orbitals lying within the HOMO - LUMO gap. The redox processes for these species can occur either on the Pc ring or on the central metal depending on the nature of the axial ligand, the solvent, the electrolyte and ring substituents. CrPc, FePc, MnPc and CoPc are examples of the redox active transition metal phthalocyanine. These metallophthalocyanine complexes have been reported to exhibit redox processes at potentials lying within the HOMO - LUMO gap [15].

Manganese phthalocyanines.

Reports on the electrochemistry of Mn(II)Pc [40, 44- 47] have shown that in the presence of electron donating solvents, Mn(II) is slightly stabilized and oxidation occurs on the Pc ring. Reduction of Mn(II)Pc occurs on the central metal to form Mn(I) and the reduction couple has been reported to be independent of the solvent or the counter ion [29]. The stabilization of Mn(II)Pc for ring oxidation by the electron donating solvents has been reported to follow the following sequence: py > DMSO > DMA = DMF. In the presence of strong coordinating anions metal oxidation on Mn(III) is favoured, in the sequence: Cl^-, > Br^- > ClO_4^- [45,48].

Iron phthalocyanine

The first reduction in Fe(II)Pc is reported to occur on the central metal to form $[Fe(I)Pc(-2)]^-$. Unlike the situation in M(II)Pc, reduction in Fe(II)Pc is reported to be highly dependent on the solvent, with potentials shifting negatively in the sequence: DMA < DMSO < py. The second

reduction process occurs at the phthalocyanine ring, with the formation of $[Fe(I)Pc(-3)]^{2-}$ and it shows very little dependence on the nature of the solvent [49]. In the presence of strongly binding donor solvents, Fe(II)Pc is reported to get oxidized at the central metal to form $[Fe(III)Pc(-2)]^{+}$. However, pyridine is known to stabilize Fe(II)Pc, through the formation of $(py)_2Fe(II)Pc(-2)$ to such a degree that $[Fe(III)Pc(-2)]^{+}$ is unstable in pyridine [45].

Cobalt phthalocyanine

In Co(II)Pc, metal oxidation occurs prior to ring oxidation in the presence of donor solvents. Donor solvents coordinate along the axis to form a six-coordinate $L_2Co(III)Pc$ species. In non -donor solvents oxidation to Co(III) is inhibited and ring oxidation occurs first. Reduction in Co(II)Pc occurs at the central metal to give Co(I)Pc [40,45,47,50,51].

1.4.3 Electrochemical properties of Platinum group metal phthalocyanines

Ruthenium phthalocyanine complexes

The electrochemical oxidation of $L_2Ru(II)Pc(-2)$ complexes (L = axially coordinated ligand), **Figure 6**, has been reported to occur at the phthalocyanine ring to generate a cationic ruthenium(II) phthalocyanine radical species, $[L_2Ru(II)Pc(-1)]^{+}$, and not metal oxidized, $[L_2Ru(III)Pc(-2)]^{2+}$ species [20].

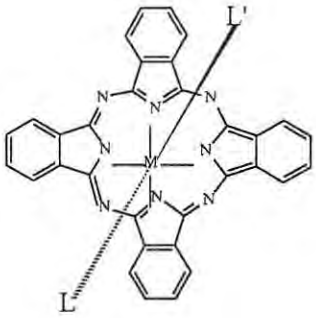

M = Ru, Rh, Os

L and L' = axially coordinated ligan

	M	L	L'	Compound
a	Ru	CN	CN	$[(CN)_2Ru(II)Pc]^{2-}$
b	Rh	Cl	py	Rh(III)Pc(Cl)(py)
c	Rh	Cl	DMSO	Rh(III)Pc(Cl)(DMSO)
d	Rh	CN	CN	$[(CN)_2Rh(III)Pc]^{-}$
e	Os	py	py	$Os(II)Pc(py)_2$
f	Os	CN	CN	$[OsPc(CN)_2]^{2-}$

Figure 6 Molecular structure of axially coordinated platinum group metallophthalocyanine complex.

The position of the first oxidation couple for the $L_2Ru(II)Pc(-2)$ complexes has been shown to depend on the nature of the axial ligands and also on the solvent molecules that serve as axial ligands. Coordination of electron donating ligands such as pyridines on the axial position decreases the oxidation half wave potential ($E_{1/2}$) values, since the donor ligands increase the

electron density of the MPc complex, thus making the ring easier to oxidize and more difficult to reduce. The $E_{1/2}$ for the first ring oxidation of $L_2Ru(II)Pc$ complexes (L= pyridines, imidazole, dimethylformamide, dimethylsulphoxide, and acetonitrile) studied by Dolphin *et al* [20], lie between 0.7 and 0.9 V vs saturated calomel electrode (SCE). The $E_{1/2}$ values have been reported to decrease in accordance with increasing electron donor strength of the coordinated ligand [20]. π-acceptor ligands such as carbon monoxide and cyanide are known to pull the electron density away from the MPc complex, making it difficult to oxidize the ring and resulting in highly positive oxidation half wave potentials.

The $E_{1/2}$ for the first oxidation of dicyanoruthenium(II) phthalocyanine has been observed at 0.45 V vs SCE in acetonitrile and the second oxidation at $E_{1/2}$ = 1.15 V vs SCE [42]. The $E_{1/2}$ for the first oxidation $[(CN)_2Ru(II)Pc]^{2-}$, like other $L_2Ru(II)Pc$ complexes, has been assigned for the removal of one electron from the phthalocyanine ring [19,52]. The $E_{1/2}$ for the second oxidation has been attributed to the removal of the second electron from the phthalocyanine ring [19]. $[(CN)_2Ru(II)Pc]^{2-}$ is reported to be soluble in water. The oxidation couple for this complex in water has been observed at 0.3V vs SCE and at 0.29 V vs SCE in buffered solutions (pH = 9). Oxidation of $[(CN)_2Ru(II)Pc]^{2-}$ in water is also reported to occur on the phthalocyanine ring.

Rhodium(III) phthalocyanine complexes

Electrochemical properties of $[RhPc(CN)_2]^-$, [RhPc(Cl)(py)] and RhPc(Cl)(DMSO), have been reported. The first oxidation in all of the complexes occurs at the phthalocyanine ligand with the formation of a phthalocyanine π-cation radical species [52-54]. Addition of one electron to dicyanorhodium(III)phthalocyanine $[(CN)_2RhPc(-2)]^-$ results in the formation of a phthalocyanine radical $[(CN)_2RhPc(-3)]^{2-}$ through the addition of the electron to the phthalocyanine ring [53,54]. Studies on the electrochemistry of RhP(Cl)(py) and

RhPc(Cl)(DMSO) [53] have shown that one electron addition in these species occurs at the central metal to give a short lived Rh(II)Pc complex, which rapidly dimerizes to dinuclear $[Ru(II)Pc]_2$ with the loss of both anionic and neutral ligands. However, Lever *et al* [54] have recently shown that there are three different dinuclear species formed by dimerization of Rh(II)Pc following one electron reduction of RhPc(Cl)(L) species.

According to Lever *et al* [54] one electron reduction of chlororhodium (III) phthalocyanine species ClRh(III)Pc(-2), results in the formation of $[ClRh(II)Pc(-2)]^{2-}$, which rapidly dimerizes at room temperature to form a six coordinate [Pc(2-)(Cl)Rh(II)-Rh(II)(Cl)Pc(2-)]. This dinuclear species may further be reduced to form $[Ru(II)Pc(3-)]_2$ dinuclear anion. Whether reduction in chlororhodium(III)phthalocyanine species occurs on the central metal or on the phthalocyanine ring, depends generally on the relative energies of the metal d_z^2 orbital and the Pc π^* orbital [54]. Substitution with electron withdrawing ligands such as CN^- may promote ring reduction since the π back-bonding ability of CN^- tends to depress the d-orbitals to below the HOMO level of the ring, hence making it possible for ring reduction to occur. The fact that oxidation in RhPc complexes is reported to occur exclusively at the Pc ring, suggests that metal d-orbitals in this complex lie below the HOMO level of the Pc ring.

Osmium(II) phthalocyanine complexes

The electrochemical properties of osmium(II)phthalocyanine complexes remain unexplored. In this thesis the electrochemical properties of axially coordinated osmium(II) phthalocyanines are investigated. The insolubility of metallophthalocyanine complexes, especially in aqueous solution, is a serious drawback in most applications of these species. The synthesis of water soluble metallophthalocyanine is therefore very crucial. In this thesis the water soluble diacyanophthalocyaninatoosmium(II), $[CN_2Os(II)Pc]^{2-}$ has been synthesised and its

electrochemistry is reported. We also report the electrochemisty of other axially coordinated osmium(II) complexes such as bispyridinophthalocyaninatoosmium(II), $(py)_2Os(II)Pc$.

Palladium(II), platinum(II) and iridium phthalocyanines complexes

Electrochemical data reported for PtPc and PdPc complexes is minimal. There are no reports available on the electrochemistry of iridium phthalocyanines complexes. Very brief reports have indicated that oxidation of PdPc and PtPc complexes occurs exclusively on the phthalocyanine ring [55,56]. In this study, the electrochemical properties of the tetramethyltetrapyridinoporphyrazine complexes of Pd(II) and Pt(II) are explored.

1.5 Tetrapyridinoporphyrazines complexes

The tetrapyridinoporphyrazine (tppa) complexes were first prepared by Linstead *et al* [57]. These complexes are phthalocyanine derivatives in which the outer benzene ring has been replaced by the pyridines, **Figure 7(a)**.

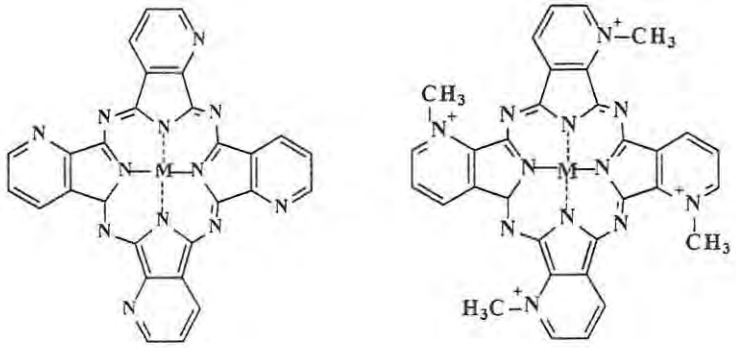

Figure 7 Molecular structure of a metal complex of a) tetrapyridinoporphyrazine and b) tetramethyl-tetra-2,3-pyridinoporphyrazine.

The metal complexes of tetrapyridinoporphyrazines, M(tppa), are synthesized by similar procedures to that of metallophthalocyanines. The synthesis of M(tppa) generally involves the use of 2,3- or 3,4- pyridine dicarboxylic acid and the metal salt [58]. The synthetic route for these complexes is shown in the discussion section.

The tetrapyridinoporphyrazine complexes are highly insoluble in water. They dissolve very slightly in organic solvents. Unlike the phthalocyanines, the M(tppa) complexes are known to be less resistant to heat. On prolonged exposure to high temperatures they tend to decompose [51,58]. Their tetramethylated derivatives, normally prepared by quaternization of pyridine nitrogen with dimethylsulphate, **Figure 7(b)**, are highly soluble in water. These water soluble tetramethyltetrapyridinoporphyrazines, $[MTmtppa(-2)]^{4+}$ have an advantage over water soluble tetrasulphonatedphthalocyanines, $[MTSPc]^{4-}$, since they do not form aggregates in aqueous solutions. The $[MTmtppa(-2)]^{4+}$ complexes are stable in low pH solutions and are normally characterized by a blue or green colour with strong absorption in the visible region. In slightly alkaline pHs these complexes decompose [58].

Since they do not form aggregates in aqueous solutions, the water soluble $[MTmtppa(-2)]^{4+}$ have potential applications as photosensitizers [59]. Their catalytic role in the autooxidation of sulphide and sulphur containing organic compounds has been reported [60,61]. $[Co(II)Tmtppa(-2)]^{4+}$ is known to catalyse the oxidation of hydrazine and hydroxylamine [62]. The $[MTmtppa(-2)]^{4+}$ complexes also find application in intercalation into DNA and as electroconductors [63,64].

Electrochemical properties of Metalloporphyrazine complexes.

Unlike the metallophthalocyanines, the electrochemical properties of metalloporphyrazines have received little attention. Most of the literature on the electrochemistry of $[MTmtppa(-2)]^{4+}$ has concentrated on $[Co(II)Tmtppa(-2)]^{4+}$ [58,59,60]. Reduction processes in this complex are reported to occur on the central metal first, resulting in the formation of $[Co(I)Tmtppa(-2)]^{3+}$. Further reduction processes occur on the ring. Reduction of $[Co(II)Tmtppa(-2)]^{4+}$ to $[Co(I)Tmtppa(-2)]^{3+}$ is reported to occur at relatively more positive potentials than the Co(II)/Co(I) couple in the other water soluble cobalt phthalocyanine species. This is due to the electron-withdrawing ability of four methylated aza groups, which stabilizes the Co(I) oxidation state [60].

As mentioned in section 1.4.3 above, in this thesis we explore the electrochemical properties of the following water soluble tetramethyltetrapyridinoporphyrazine complexes: NN'N"N'"-tetramethyltetra-2,3-pyridinoporphyrazine palladium(II), $[Pd(II)2,3Tmtppa(-2)]^{4+}$, NN'N"N'"-tetramethyltetra-3,4-pyridinoporphyrazine palladium(II), $[Pd(II)3,4Tmtppa(-2)]^{4+}$, NN'N"N'"-tetramethyltetra-2,3-pyridinoporphyrazine platinum(II), $[Pt(II)2,3Tmtppa(-2)]^{4+}$ and NN'N"N'"-tetramethyltetra-3,4-pyrdinoporphyrazine platinum(II), $[Pt(II)3,4Tmtppa(-2)]^{4+}$, **Figure 8**.

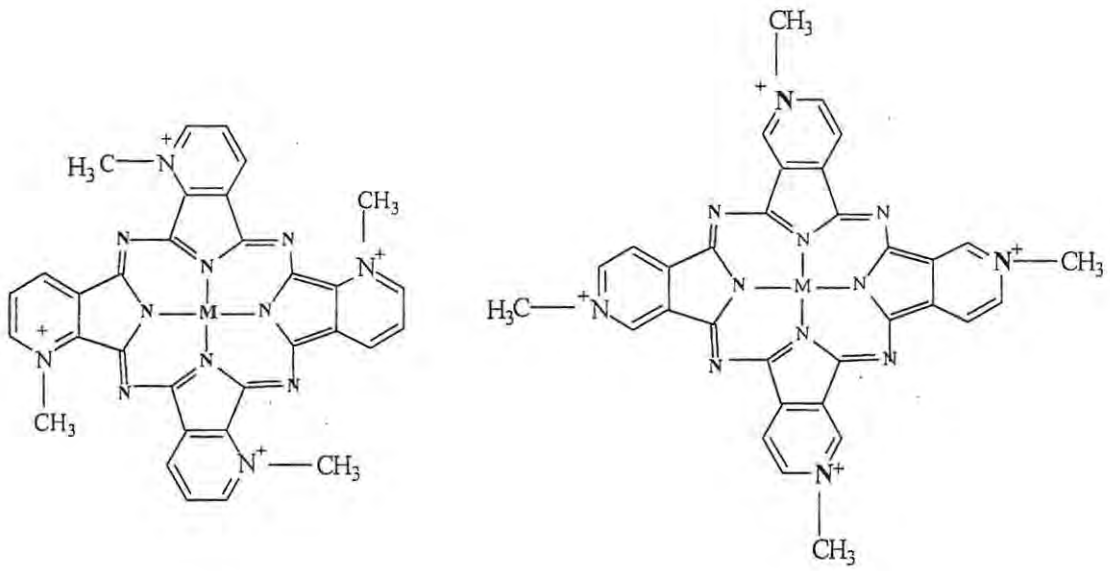

M = Pd or Pt

Figure 8 Molecular structures of a) [Pd(II)2,3Tmtppa(-2)]$^{4+}$ and b) Pd(II)3,4Tmtppa]$^{4+}$

1.6 Electrocatalysis

Many electrode reactions, such as oxidation of cysteine, occur at potentials that are greater than the expected thermodynamic potential. Such high overpotentials affect the selectivity and the sensitivity of the electrochemical measurements. Sometimes the electrode reaction may require an overpotential that is beyond that of solvent electrolysis, thus making the measurement infeasible. This problem is normally overcome by the use of mediators (catalysts) which will catalyse the oxidation or reduction of the specific solute species (substrate) at substantially reduced potentials. The catalyst normally provides alternative reaction pathways and allows the reaction to be carried out at increased current density closer to the reversible potential. The reactions in which the substrate and the charged mediator react are called electrocatalytic reactions [65]. **Figure 9** shows the cyclic voltammogram observed on catalysed reduction of a

substrate by MPc species.

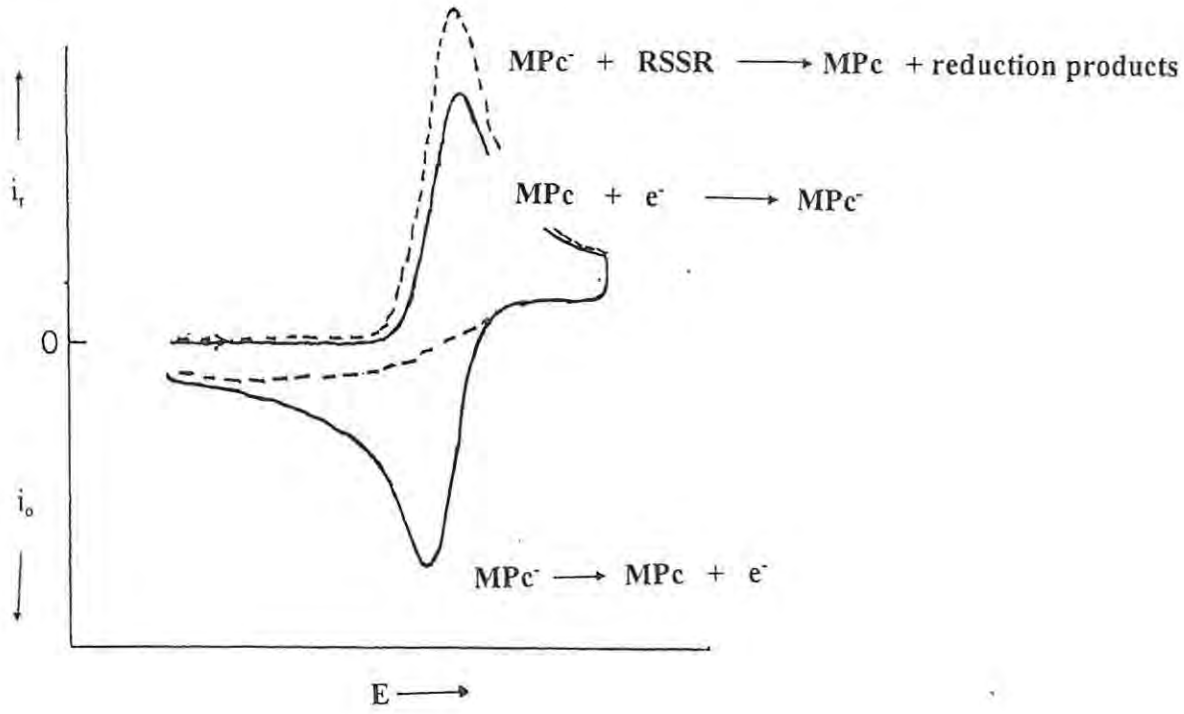

Figure 9 The diagram showing the changes expected on the cyclic voltammogram of a catalysed reaction..

In redox catalysis the catalyst couple, couple **I**, is involved in an outer-sphere electron transfer reaction with the substrate. The catalyst simply plays the role of an electron carrier between the electrode and the substrate [66]. In catalytic reaction, the cyclic voltammogram shows the peak on the single scan and there is no return peak as shown in **Figure 9**.

In general, a catalyst may be in a solution form (homogeneous catalysis) or it may be attached to the surface of an electrode (heterogeneous catalysis). When specific molecules are attached to the surface of an ordinary electrode for the purpose of catalysing the electrode reaction, the electrode is said to be chemically modified. Chemically modified electrodes (CMEs) have an advantage over conventional electrodes in that they have the possibility of lowering

overpotential and increasing the rate of electrode reaction, hence increasing the sensitivity and selectivity of the methods of analysis.

Chemically modified electrodes can be prepared by various methods including the following: (a) direct deposition of the catalyst on the glassy carbon electrode (drop dry method) or dip coating [67], (b) mixing of the catalyst with carbon paste to make a catalyst conductive cement (carbon paste electrode) [6,65], (c) electrochemical deposition [68,69] and (d) vacuum sublimation.

Drop dry method

In this method, a droplet of a solution of a catalyst (of known volume), is applied to the electrode surface and the solvent is allowed to evaporate in air or nitrogen atmosphere before the electrode is transferred to the substrate solution. A major advantage of this approach is that the coverage of the catalyst on the electrode surface can be known from the original concentration of the catalyst and the droplet volume. A very similar procedure, known as dip coating, consists of immersing the electrode material in a solution of a catalyst for a period sufficient for a spontaneous film to occur by adsorption. After a desired period of time the electrode is withdrawn from the solution and the film of the solution on the electrode surface is allowed to dry. The disadvantage of dip coating is that the film coverage on the electrode surface is not accurately known.

Electrochemical deposition

This procedure relies on the variation of catalyst solubility with oxidation or reduction (and ionic) state. An irreversible film formation often occurs when a catalyst is oxidized or reduced to its less soluble state. The deposition of film is normally achieved by scanning the electrode in a solution of the catalyst within the particular potential range for a specific period of time. The

time taken for scanning will control the amount of film deposited on the electrode.

Carbon paste electrode

This method involves mixing a desired amount of the catalyst with graphite powder plus a binder (normally mineral oil). The mixture is packed in one end of a fused silica capillary and the electrical conduct is established *via* nickel/chromium wire. The advantage of this kind of modified electrode is that it is easy to construct and shows reproducibility since the surface may be renewed by pushing more paste from the capillary [69].

The use of MPc as electrocatalysts, both in solution and on chemically modified electrodes, for sulphide and sulphur containing organic compounds such as cysteine and methionine, has been reported [6,67,70]. MPcs are also known to catalyse the reduction of molecular oxygen [67,71].

Metallophthalocyanines are normally adsorbed onto the surface of the electrode by the methods based on chemisorption. Chemisorption is an adsorptive interaction between a molecule and a surface in which the electron density is shared between the adsorbed molecule and the surface. When the electrode is modified with MPc species, the π-electron density is shared between the electrode surface and the MPc. In chemisorption direct contact between the chemisorbed molecule and the electrode surface is required, as a result, the highest coverage achievable is usually a monomolecular layer [28].

Electrocatalytic reactions of MPc species involve the oxidation or reduction of MPc followed by electron transfer between the oxidized or reduced MPc and the species to be electrocatalysed. It is believed that oxidation or reduction occurs at the central metal, followed by electron transfer between the reduced or oxidized species and the substrate. Halbert *et al* [67] have shown that

electrooxidation of cysteine catalysed by cobalt phthalocyanine occurs according to **Equations 7, 8 and 9**.

$$Co(II)Pc \rightarrow [Co(III)Pc]^{+} + e^{-} \qquad \text{Equation 7}$$

$$[Co(III)Pc]^{+} + RSH \rightarrow Co(II)Pc + RS^{\cdot} + H^{+} \qquad \text{Equation 8}$$

$$RS^{\cdot} + RS^{\cdot} \rightarrow RSSR \qquad \text{Equation 9}$$

Where RSH = cysteine and RSSR = cystine.

MPc complexes with electroactive central metal, such as CoPc and FePc are known to be better catalysts. Electrocatalytic reactions involving ring-based electron transfer in MPc have not been reported prior to the present investigation. In this work we use platinum group metal phthalocyanines to modify the electrodes, and we study the electrocatalytic activities of these complexes in relation to electrooxidation of cysteine, hydrazine, hydroxylamine and methione. We study the effects of axial ligands and solvents towards the electroactivity of the MPc species. The MPc complexes used as electrocatalysts in this work are (DMSO)Rh(III)Pc, (py)(Cl)Rh(III)Pc, $[(CN)_2Rh(III)Pc]^{-}$, $[(CN)_2Os(II)Pc]^{2-}$, $(py)_2Os(II)Pc$, $(DMSO)_2Os(II)Pc$, $[(CN)_2Ru(II)Pc]^{2-}$, $(py)_2Ru(II)Pc$ and $[(DMSO)_2Ru(II)Pc].2DMSO$, see **Figure 6**.

1.6.1 Electro catalysed oxidation of cysteine on MPcs

Cysteine (R-SH) is a sulphur-containing amino acid which has a very important role in living systems. It is known to undergo one-electron oxidation to give cystine which is also important biologically. The use of electrochemical methods for the analysis of cysteine have been limited by the extreme potentials required for its oxidation at most conventional electrodes. On unmodified electrodes cysteine oxidation occurs at 1.4 V vs SCE. When the electrode is modified with cobalt tetrasulphophthalocyanine, $[(Co(II)TSPc]^{4-}$, **Figure 10(a)**, cysteine oxidation occurs at 0.77V vs SCE [67], and at 0.28V vs Ag/AgCl when oxomolybdenum(V) tetrasulphophthalocyanine $[OMo(V)(OH)TSPc]^{4-}$, was employed as a catalyst [6].

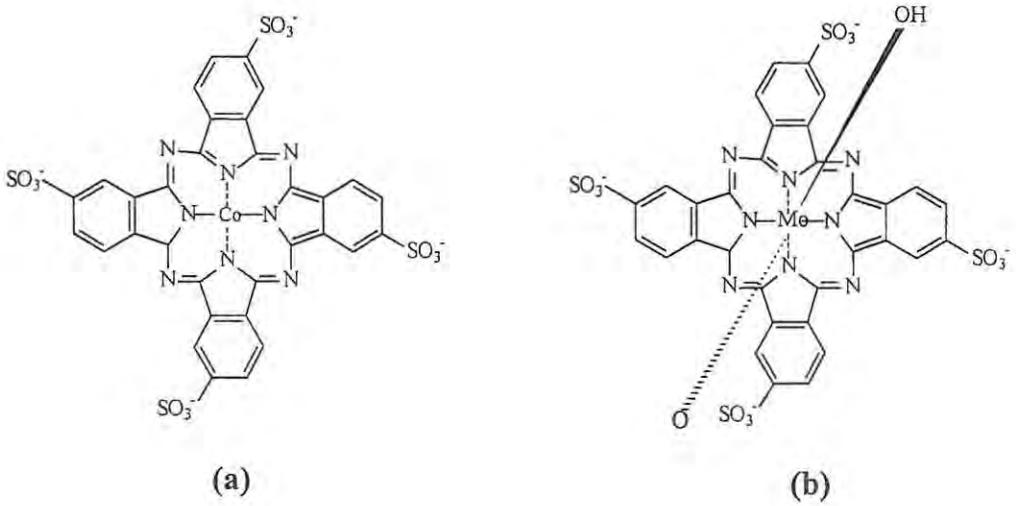

Figure 10 Molecular structure of a)$[Co(II)TSPc]^{4-}$ and b) $[OMo(V)OHTSPc]^{4-}$.

Even though lower potentials were observed for $[OMo(V)(OH)TSPc]^{4-}$ the sensitivity (10^{-3}) was poorer than on CoPc (10^{-7}).

The oxidation of cysteine on carbon electrodes modified with MPcs is believed to be a two-step electrocatalytic process. This process is believed to be initiated by central metal electrochemical oxidation, followed by the chemical oxidation of cysteine by the oxidized MPc species and the regeneration of the original MPc complex, **Equations 7 to 9**.

It is believed that cysteine coordinates axially to $[OMo(IV)(OH)TSPc]^{4-}$ when this species is employed as a catalyst and that this coordination occurs prior to electron transfer [6].
At pHs greater than 4 the autocatalytic oxidation of cysteine to cystine by $[Co(II)TSPc]^{4-}$ has been reported to occur according to **Equation 10**.

$$2[Co(II)TSPc]^{4-} + 2RSH \rightarrow 2[Co(I)TSPc]^{5-} + RSSR \qquad \text{Equation 10}$$

The electrochemical behaviour of cysteine on graphite electrodes modified by tetrasulphonated phthalocyanines of cobalt, iron, manganese, nickel and copper has been reported, and the catalytic activity has been shown to decrease as follows: Co> Fe > Mn > Ni > Cu. The catalytic activity is believed to vary linearly according to the number of *d*-electrons in the central metal [72].

1.6.2 Electrooxidation of Hydrazine and Hydroxylamine

Hydrazine

Hydrazine (N_2H_4) is a highly reactive molecule which has applications in fuel cells, herbicides, pesticides and rocket propellants [73-75]. It possesses two free electron pairs located on the nitrogen atoms having sp^3-hybridization. This accounts for both the basic and neucleophilic

character of the molecule. At ordinary pyrolytic graphile electrode (OPGE), oxidation of N_2H_4 is known to occur at very high potential [76]. Electrooxidation of hydrazine to nitrogen via four electron path has been reported to occur at E_o = 1.16 V vs SHE [76]. Phtholocyanines of several transition metals, for example Fe, Co, Cu and Ni, and their tetrasulphonated analogues are known to substantially decrease the overpotential for the electro-oxidation of hydrazine, when these complexes are attached or adsorbed to surface of the graphite electrode [66,67,76,77].

The catalytic process has been reported to occur at potentials close to the M(I)/M(II) redox couple in the MPc, thus illustrating the importance of the redox properties of the catalyst in determining its activity. The mechanism proposed [76] for the electro-oxidation of hydrazine is shown by Equations 11,12 and 13. The mechanism takes into account the M(I)/M(II) reversible couple of the metal in the phthalocyanine.

$$M(II)L + N_2H_4 \rightarrow [L\text{-}M(I)^{\cdot} (N_2H_4)^{+}] \qquad \text{Equation 11}$$

$$[L\text{-}M(I)\text{-} (N_2H_4)^{+}] + OH^{-} \rightarrow L\text{-}M(II)\text{-}N_2H_3 + H_2O + e^{-} \qquad \text{Equation 12}$$

$$[L\text{-}M(II)\text{-}N_2H_3] + OH^{-} \rightarrow M(II)L + N_2H_2^{\cdot} + H_2O \qquad \text{Equation 13}$$

where L = Pc, TSPc and M = Fe, Mn and Cr.

Hydroxylamine

Electro-oxidation of hydroxylamine (NH_2OH) at unmodified glassy carbon electrode has been reported to occur at potentials greater than 1 V vs Ag/AgCl. Phthalocyanine complexes of Mn, Fe, Co, Ni and Cu are known to catalyse electro-oxidation of NH_2OH. On GCE modified

by CoPc, potential for electro-oxidation has been reported to be between 0.25 to 0.55 V vs Ag/AgCl. The oxidation products for the oxidation of NH_2OH on CoPc chemically modified electrode include oximes, azoxy compounds and dimeric products [76,77].

FeTSPc adsorbed on pyrolytic graphite eletrodes in known to catalyse electro-oxidation of hydroxylamine to N_2O. The activity of FeTSPc for the electro-oxidation of hydroxylamine has been reported to be less pronounced as compared to that reported for hydrazine electro-oxidation. This has been attributed to the formation of the adduct formed between hydroxylamine and FeTSPc, which inhibit the reaction [76,77]. The proposed [76] mechanism for electro-oxidation of hydroxylamine is shown by **Equations 14** and **15**.

$$M\text{-}L + NH_2OH \rightarrow L\text{-}M\text{-}H_2OH \qquad \text{Equation 14}$$

$$L\text{-}M\text{-}NH_2OH + OH^- \rightarrow [L\text{-}M\text{-}NH_2OH]^- + H_2O \qquad \text{Equation 15}$$

where L and M are as described above in Equations 11 to 13.

For both hydrazine and hydroxylamine, the electrocatalytic activity of the MPc or MTSPc depends on the redox potential and the electronic structure of the transition metal centred within the phthalocyanine ring [79]. Studies have shown that NiTSPc shows the highest activity for the electro-oxidation of hydroxylamine in contrast to what has been found for hydrazine where FeTSPc and CoTSPc show highest activity [79]. NN'N"N'"-tetramethyl-3,4-pyridinopophyrazinecobalt(II), $[Co(II)Tmtppa]^{4+}$ has been reported to show electrocatalytic activity towards oxidation of both hydrazine and hydroxylamine, when this complex is adsorbed on graphite electrode [62].

1.7 Photochemical properties of metallophthlocyanines

1.7.1 Photochemistry: an overview

Ordinary thermal reactions take place between molecules in their ground state (S_0), activation energy of the reaction being acquired through random collisions between molecules.

In a photochemical reaction, however, the reacting molecule is initially promoted to an electronically excited state by an absorption of light. This light energy is used to energize an electron and cause it to jump from a low energy orbital to a higher energy unoccupied orbital of the molecule. The electron jump can occur without a change in spin resulting in the formation of a very short-lived singlet excited state ,S_1, which in most cases soon loses its energy with a change of spin, resulting in the formation of a triplet excited state,T_1 [80].

In order to place itself in equilibrium with the surrounding medium the excited molecule soon loses its excitation energy either through physical or chemical processes. The physical deactivation processes are classified into radiative (energy loss in the form of light) and radiationless (energy loss in the form of heat) processes, **Figure 11**.

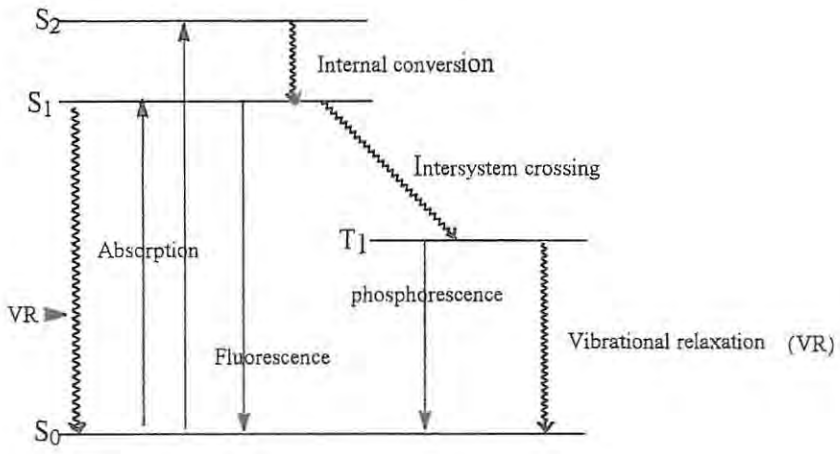

Figure 11 A modified Jablonski diagram showing transitions between excited states and ground state. Radiative processes are shown by non-wavy lines , radiationless processes by wavy lines.

A radiative process that occurs without a change of spin is termed fluorescence; if the spin changes the process is called phosphorescence. Internal conversion is the radiationless process which does not involve a change of spin, while intersystem crossing is radiationless but involves spin change.

The chemical deactivation process involves the transfer of energy by the excited molecule, the **donor**, to another molecule in its vicinity, the **quencher**, and this energy transfer process can be described by **Equation 16** [81].

$$D^* + A \rightarrow D + A^* \qquad \text{Equation 16}$$

The asterisk indicates an excited molecule.

1.7.2 Photo-oxidation and photo-reduction of metallophthalocyanines

Irradiation of metallophthalocyanines at the Q band produces the low-lying ligand-centred triplet ($^3\pi\pi^*$) excited states [26,37,82-87]. These states can be quenched by electron transfer to a number of electron acceptors such as carbon tetrabromide, nitroaromatics, and benzoquinone. The photoexcited MPc species may be deactivated, in the presence of an electron acceptor, generally by one electron oxidation at the ring with the formation of π-cation radical species [26], **Equations 17 and 18**.

$$M(II)Pc(-2) \rightarrow M(II)Pc(-2)^* \qquad \text{Equation 17}$$

$$M(II)Pc(2-)^* + Q \rightarrow [M(II)Pc(-1)]^+ + \textbf{Reduction products} \qquad \text{Equation 18}$$

MPc* indicates the phthalocyanine at an excited triplet state and Q is the quencher.

The $[M(II)Pc(-1)]^+$ π-cation species are characterized by the formation of new bands in the visible region of the absorption spectra at 710 and 510 nm, as discussed in section 1.2.2. These bands have been reported for the photooxidation of Ru(II)Pc and Zn(II)Pc in the presence of acceptors and they are characteristic of $[RuPc(-1)]^+$, $[ZnPc(-1)]^+$ species [22,25]. Studies by Nensala *et al* [5] have shown that photolysis of the following diphthalocyanine complexes; $[(Pc(-2)Nd(III)Pc(-2)]^-$, $[(Pc(-2)Dy(III)Pc(-2)]^-$ and $[(Pc(2)Lu(III)Pc(-2)]^-$, in the presence of pentachlorophenol (PCP) or SO_2 results in one electron oxidation of the diphthalocyanine species to form Pc(-1)Nd(III)Pc(-2), Pc(-1)Dy(III)Pc(-2), and Pc(-1)Lu(III)Pc(-2), respectively.

Photoreduction of metallophthalocyanine complexes can be achieved by Q band irradiation in the presence of electron donors and in most cases it occurs on the phthalocyanine ring. It has been shown that Q band irradiation of the monomeric $(Br)_2Sn(IV)Pc(-2)$ in the presence of sulphur dioxide and in pyridine, results in the formation of $[(Br)_2Sn(IV)Pc(-3)]^-$ anion radical species [4].

Illumination of the metallophthalocyanines at the Soret or B band results in a population of nπ* excited states. Unlike the ($^3\pi\pi^*$) excited states, the (nπ*) excited states of MPcs are not quenched by electron acceptors; instead they go through chemical transformations which involve abstraction of hydrogen from the solvent, **Equation 19.**

$$M(Pc) + \xrightarrow{hv} n\pi^* + \xrightarrow{SH} M(Pc\text{-}H) + S^- \qquad \text{Equation 19}$$

SH = hydrogen donor.

In general, irradiation of metallophthalocyanine dimers $(MPc)_2$ in the Q band produces the same low-lying $^3\pi\pi^*$ excited states of the monomers, but irradiation in the Soret band region tends to induce the photoredox dissociation of dimers and the products of photodissociation are either reduced and oxidized ligand radicals, or species with an oxidized and reduced metal centre, **Equations 20 and 21**.

$$[M(II)Pc]_2 \xrightarrow{hv} [M(II)Pc]_2^* \longrightarrow [M(II)Pc]^- + [M(II)Pc]^+ \qquad \text{Equation 20}$$

$$[M(II)Pc]_2 \xrightarrow{hv} [M(II)Pc]_2^* \longrightarrow [M(I)Pc]^- + [M(III)Pc]^+ \qquad \text{Equation 21}$$

The products of the photodissociation of the dimeric metallophthalocynines are largely determined by the nature of the central metal. Photodissociation into ligand radicals, **Equation 20**, has been observed in Soret band irradiations of dimeric Cu(II) , Fe(II) and cobalt(III) tetrasulphophthalocyanines. A photoinduced dissociation into metal oxidized and metal reduced species, ($[M(III)Pc]^+$ and $[M(I)Pc]^-$), **Equation 21**, has been reported for photolysis of the dimeric cobalt(II) tetrasulfophthalocyanine [89,90].

1.7.3 Photochemical properties of platinum group metal phthalocyanines

Ruthenium(II) phthalocyanine complexes

Several reports have shown that Q band irradiation of ruthenium complexes of the type L_2 Ru(II)Pc(-2), (where L = py, CO, DMF, or DMSO), see **Figure 6** section 1.4.3, results in formation of low-lying $^3\pi\pi^*$ excited states. Quenching of these states by carbon tetrabromide is known to produce π-cation radical species $[L_2 Ru(II)Pc(-1)]^+$ [25]. Nitroaromatics are also known to quench the $^3\pi\pi^*$ formed by Q band photolysis of axially coordinated ruthenium

phthalocyanine species, but the formation of the π-cation radical species in this case is highly dependent on the nature of the axial ligand. Quenching of the excited states of $L_2Ru(II)Pc(-2)$, L= py or DMF, by various nitroaromatics results in the formation of oxidized phthalocyanine ligand species. However, quenching of the excited states of Ru(II)Pc(-2)(py)(CO), Ru(II)Pc(-2)(DMF)(CO) or $Ru(II)Pc(-2)(DMSO)_2$ results in the formation of exciplexes. The formation of the exciplexes is believed to occur when the $^3\pi\pi^*$ states of these ruthenium complexes react with the aromatic quenchers [84,85].

The life times of the $^3\pi\pi^*$ excited states of ruthenium phthalocyanine species have been reported to be largely determined by the nature of the axial ligand. The life times are said to be associated with perturbations of the phthalocyanines' electronic structure induced by the electron withdrawing and electron donating tendencies of the axial ligand. Generally the triplet lifetime increases with increasing electron-withdrawing capacity of the axial ligands in $(L)_2RuPc(-2)$ [86].

The Soret band irradiation of $Ru(II)Pc(-2)(py)_2$ has been reported to result in the formation of nπ* excited states, and these states are known to undergo chemical transformations which involve hydrogen abstraction from the solvent (discussed above, see **Equation 19**) and ligand exchange reactions. For example, photolysis of $RuPc(py)_2$ in CO-saturated dichloromethane has been reported to result in the formation of Ru(II)Pc(-2)(py)(CO) [87].

Rhodium(III) phthalocyanine complexes

Reports on the photochemistry of acido(phthalocyanine)rhodium(III) complexes, where acido = Cl^-, Br^- or I^-, have shown that ultraviolet irradiation in these species induce the formation of ligand centred nπ* excited states. These nπ* species, as in $RuPc(py)_2$ and monomeric

tetrasulphophthalocyanines of cobalt(II) and copper(II), induce the abstraction of hydrogen from the appropriate donors and may even result in ligand photolibilization processes [91].

1.7.4 Metallophthalocyanines as photosensitizers

It is known that the triplet states of many porphyrins and phthalocyanines readily undergo net electron transfer with suitable redox quenchers to form separated ion products. Even though they are known to have high quenching constants, the singlet excited states of the MPc species do not yield ion products. Since photosensitization by phthalocyanines occurs *via* the triplet excited state, necessary requirements for the phthalocyanine complex to be a good sensitizer are that its triplet excited state be populated in high yield and be long lived.

Metallopthalocyanine complexes are extremely resistant to degradation and can be synthesized by convenient routes. The disadvantages associated with these complexes is their insolubility in water. Their water soluble derivatives, tetrasulphonated metallophthlocyanines (MTSPcs) can easily be synthesized, but these species form dimers in aqueous solutions and dimers are known to be photoinactive.

The triplet quantum yields of metallophthlocyanines are greatly influenced by the nature of the central metal ion. Heavy metal ions such as Rh(III) and Pd(II) or paramagnetic metal ions such as Cr(III)Pc or Cu(II)Pc enhance the yield of the triplet state, but also shorten the life time of these states. Phthalocyanines with paramagnetic transition metal ions possess very short triplet life times values and this imposes severe limitations upon their use as photosensitizers.

The excited state life-times (τ_p) that have been reported for some platinum metal phthalocyanines [3,88] are shown in **Table 1**.

Table 1 Excited states life-times for some platinum group metal phthalocyanines.

Compound	phosphorescence life-time (τ_p) in ms	Reference
PdPc	0.025	3
PtPc	0.006	3
RhPc(Cl)	0.016	88
IrPc(Cl)	0.0035	88
$RuPc(py)_2$	0.00135	88

1.7.5 Metallophthalocyanines as photosensitizers in photodynamic therapy

Photodynamic Therapy, **PDT**, is a cancer treatment that uses a combination of red light (usually from a laser), photosensitiser (**Sen**) and molecular oxygen to obtain therapeutic effect. It is believed that tumour damage is achieved only when these three components come together in the tissue at the same time, and it is assumed that singlet oxygen is the active species responsible for tumour damage [92]. The photosensitizer acts in a catalytic manner since it does not react directly with the cellular targets, its function being to absorb light energy and transfer it to molecular oxygen, regenerating the ground state photosensizer.

The processes related to the activation of molecular oxygen by its interaction with light and photosensitiser are often described as Type I and Type II mechanisms [2]. The Type II

process involves the production of singlet oxygen *via* energy transfer from the triplet state of the sensitiser to molecular oxygen, **scheme 6**, while the Type I process involves an electron transfer from the sensitizer either to molecular oxygen or to the biological substrate, **scheme 7**.

$$\mathbf{Sen} \xrightarrow{\text{red light}} \mathbf{Sen^*}$$

$$\mathbf{{}^1Sen^*} \longrightarrow \mathbf{Sen + Fluorescence}$$

$$\mathbf{{}^1Sen^*} \longrightarrow \mathbf{{}^3Sen^*}$$

$$\mathbf{{}^3Sen^* + {}^3O_2} \longrightarrow \mathbf{Sen + {}^1O_2}$$

$$\mathbf{{}^1O_2 + \text{Biological substrates (BS)} \longrightarrow \text{destruction via substrate photooxidation}}$$

Scheme 6 The processes involved in Type II mechanism.

$$\mathbf{{}^3Sen^* + O_2 \rightarrow Sen^+ + O_2^-}$$

or

$$\mathbf{{}^3Sen^* + BS \rightarrow Sen^+ + BS^-}$$

Scheme 7 The processes involved in Type I mechanism.

For the optimal efficiency of PDT, the sensitizer should absorb strongly in the red region of the spectrum, it should be non-toxic, selectively retained by tumours relative to normal adjacent tissue, and it must have a high triplet quantum yield to become an efficient generator of singlet oxygen. It should be of defined chemical composition and should dissolve in water [2].

A mixture of porphyrins known as haematoporphyrin derivative (**HPD**) has been successfully used as a photosensitiser in PDT and is known to have low toxicity and is selectively retained in tumours [93]. However, there are some disadvantages associated with the use of HPD as a photosensitisers in PDT. The major disadvantage is that this mixture absorbs very poorly in the red region of the spectrum. It is an extremely complex mixture which may aggregate to different extents in different environments resulting in alterations in its biological efficiency. An additional complication is that patients treated with HPD as photosensitiser have been found to suffer from photosensitive reaction to daylight, and need to be kept away from light for several weeks after the treatment, since HPD tends to accumulate in normal tissue [2].

In order to overcome many of the disadvantages associated with HPD, alternative "second generation" photosensitisers have been investigated and the search has recently focussed on metallophthalocyanines. Metallophthalocyanines have several advantages over HPD as photosensitisisers. They absorb strongly in the red region of the spectrum where light penetration of tissue is slight, they have a well-defined composition, they are chemically stable and are easily synthesized. Some of them are reported to be non-toxic to mammals [94].

The only drawback in using metallophthalocyanines as photosensitisers in PDT is their insolubility, especially in water. Water soluble sulphonated metallophthalocyanines have been prepared by attaching sulphonates to the phthalocyanine ring. These sulphonated MPc species, however, have a great tendency to form aggregates (or dimmers) in aqueous solutions and this is a drawback when these complexes are used in PDT since the dimers are photoinactive, which reduces the usefulness of sulphonated MPc species as photosensitizers. The aggregation problem has been overcome by the addition of ethanol or by working in micellar media [93,95].

Aluminium and zinc phthalocyanines have been tested as photosensitizers in PDT and have been reported to be very effective, especially aluminium phthalocyanines. These species are known to have very high quantum yields for singlet oxygen production and do not aggregate in aqueous solution [93,96]. The photobiological activity of the sensitizer is affected significantly by the nature of the central metal in the MPc species, and paramagnetic metals like Fe, Co and Cu reduce the activity of the phthalocyanine drastically [97].

Following injection of dye into the body, during PDT treatment, it is possible that some reaction with the biological substrate occurs prior to photosensitization; that is, the photoexcitation of the MPc complex occurs on MPc already linked to protein or amino acids. There have been reports of direct coordination of bovine serum albumen to ClAlPc prior to photosentization [98].

1.8 Aims of the project

The mechanism of PDT is not clearly understood. It has been suggested [2] that the type II mechanism predominates. But there is a possibility of both mechanisms being involved. It has been proved that singlet oxygen ($^1O_2$) is involved in PDT. The type II mechanism is known to involve the production of $^1O_2$. As a first step towards understanding which mechanism is involved in PDT, in this study we use RuPc and OsPc complexes as photosensitizers for singlet oxygen production. We determine the quantum yields of these complexes for singlet oxygen production, and compare these with the reported quantum yields. The determination of quantum yield for singlet oxygen production by Os(II) and Ru(II) phthalocyanine complexes is outlined in chapter 6 of this work.

As a first step in understanding the interaction between MPcs or related complexes with biological substrates, we studied the interactions of amino acids with water soluble $[Pd(II)2,3Tmtppa(-2)]^{4+}$, $[Pd(II)3,4Tmtppa(-2)]^{4+}$, $[Pt(II)2,3Tmtppa(-2)]^{4+}$ and $[Pt(II)3,4Tmtppa(-2)]^{4+}$. Some tetrasulphophthalocyanine complexes of Co, Ni and Pd have also been studied. We studied the effect of the central metal and the effects of ring substituents on the interaction of these MPc or $[MTmtppa(-2)]^{4+}$ complexes with amino acids. The study of the interactions of MPcs or related complexes with amino acids is outlined in chapter 5 of this thesis.

The fact that most MPc complexes are insoluble in water, is a serious drawback for the use of these complexes as photosensitizers in PDT. Even though the tetrasulphonated MPc complexes are soluble in water there is still a problem in their use as photosensitizers in PDT because in aqueous solutions MTSPc complexes form dimers which are photoinactive. In this work we synthesise water soluble MPc or related complexes, for example, $[(CN)_2Os(II)Pc(-2)]^{2-}$ and the tetramethylatedtetrapyridionporphyrazine complexes of Pd(II) and Pt(II). The synthesis and characterization of these complexes are dealt with in chapter 3.

At most conventional electrodes, such as glassy carbon and graphite electrodes, oxidation of cysteine and other sulphhydryl compounds requires extreme positive overpotentials. The selectivity and detection limits in electrochemical methods depends, to an extent, on the oxidation potential of the analyte. Modification of carbon electrodes with MPc complexes lowers the potential for oxidation of cysteine and other organic compounds significantly. One major disadvantage of using chemically modified electrodes in electrochemical measurements is the poisoning of the electrode after the first scan, thus requiring the renewal of the electrode surface after each scan. It is important, therefore, to find the catalyst which can improve both

the stability and the detection limit of the electrode and at the same time lower the potential needed for oxidation of cysteine and other organic compounds. In this work the electrocatalytic activity of the platinum group metal phthalocyanines towards oxidation of cysteine , hydrazine, hydroxylamine and methionine have been explored.

The behaviour of cysteine in electrochemical measurements tends to depend on the pH of the solution in which cysteine is dissolved. Most of the physical properties of cysteine, like all other amino acids, are consistent with the dipolar ion structure for amino acid **I** [139].

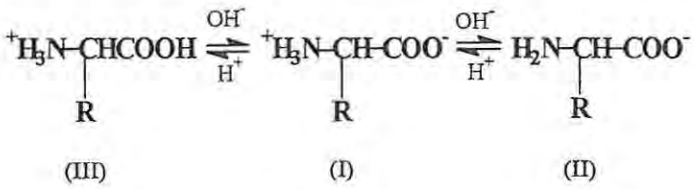

(III) (I) (II)

R = $HSCH_2$ (for cysteine)

In alkaline solutions, the dipolar ion **I** in converted to anion **II** and in acidic solutions the dipolar **I** is converted to the cation **III**. The pH at which the anion **II** and the cation **III** are in equilibrium is known as the isoelectric point of the amino acid. For cysteine the isoelectric point occurs at pH = 5.02. Most of the reported studies for the oxidation of cysteine have been carried out in acidic medium where the predominant form of cysteine is the cation **III**. We intend to show in this work that the phthalocyanine complexes of Rh, Os and Ru catalyse the oxidation of cysteine in the pH range of 5.8 to 7.2 when these complexes are attached to the surface of the glassy carbon electrode. The catalytic behaviour of Os(II), Rh(III) and Ru(II) phthalocyanine towards the electrooxidation of cysteine, hydrazine, hydroxylamine and methionine on glassy carbon electrodes is outlined in chapter 4 of this thesis.

2. Experimental

The cyano-osmium phthalocyanine complexes, and also palladium and platinum porphyrazine complexes were prepared for the first time in this work and the characterization data (elemental analysis, infrared and electronic absorption) are given for each compound following the description of the synthetic procedures.

2.1 Synthesis of metallophthalocyanines and metalloporphyrazine complexes

The ruthenium and rhodium phthalocyanine complexes were prepared following established procedures using the references given for each complex. The electronic absorption and infrared data for this complexes are listed in Table 2 and 3, respectively, following the description of the synthesis.

2.1.1 Ruthenium(II) phthalocyanine complexes

(Phthalocyaninato)ruthenium(II) (RuPc)

Following the method of Farell *et al* [97], crude ruthenium phthalocyanine (RuPc) was prepared by heating $RuCl_3.3H_2O$ (Aldrich) (0.31g, 1.19×10^{-3} mol), *o*-cyanobenzamide (2.0g, 1.5×10^{-2} moles) and naphthalene (PAL) (0.80g, 6×10^{-2} mol) in a ratio of 1:12.6:5.06. The mixture was heated for approximately 20 minutes at 290°C. The mixture was then cooled, washed with 95% ethanol and filtered. The dried residues were Soxhlet-extracted with glacial acetic acid until the washings were colourless. The remaining greenish black solid was dried in the oven in order to remove excess acetic acid. The crude RuPc thus prepared was used as a precursor for the preparation of various L_2RuPc complexes. Yield (0.20g, 65%).

The *o*-cyanobenzamide was prepared by dissolving phthalamide (8.0g, 0.06 moles) in acetic anhydride (30 ml) in a round bottom flask fitted with a water condenser. The mixture was heated as fast as possible to boiling point and the solution was refluxed for 3 hours. On cooling the solution, white needle shaped crystals were formed. The crystals were washed with ice cold ethanol (95%) and dried at 100°C. Yield (1.80g, 22%). Melting point 172°C.

Phthalamide was prepared by adding phthalimide (Kodak) (20g, 0.36 moles) to ammonia (60 ml) and stirring the solution for 24 hours. The resulting mixture was filtered and the white crystals formed, were dried at 100°C. Melting point 220 - 230 °C. Yield (90%).

Potassium (biscynato)(phthalocyaninato)ruthenium(II) ($K_2[(CN)_2RuPc]$)

$K_2[(CN)_2RuPc]$ was prepared according to the reported synthetic procedures for $[(CN)_2MPc]^{2-}$ complexes [19,98-101] by treating crude RuPc (0.037g, 5.75×10^{-5} moles) with excess potassium cyanide (0.035g, 5.34×10^{-4} moles) in refluxing dimethylformamide (DMF, 30 ml) for 3 hours. After evaporation of the solvent, the resulting solid was washed with chloroform and recrystallized three times from distilled acetonitrile. Yield (0.026g, 79%). UV-vis data is shown in Table 2 and infrared data in Table 3. Found: C, 50.9; H, 3.3; N, 17.1%. Calculated for $K_2C_{34}H_{22}N_{10}O_3Ru$: C, 51.2; H, 2.8; N, 17.6%.

Carbonyl(N,N-dimethylformamide)(phthalocyaninato)ruthenium(II)

(RuPc(CO)(DMF))

RuPc(CO)(DMF) was synthesized following the method of Dolphin *et al* [102], by refluxing crude RuPc (0.05g, 8.15×10^{-5} moles) in DMF (20 ml) for 3 hours under nitrogen atmosphere and the resulting solution filtered. The deep blue filtrate was added to an alumina column containing hexane and the column was eluted with hexane until all the DMF has been removed.

Elution with diethyl ether and evaporation to a low volume afforded purple crystals of the complex. Yield (0.048g, 96%). UV-vis data is shown in Table 2 and infrared in Table 3. Found: C, 54,9; H, 3.5; N, 16.2 %. Calculated for $C_{36}H_{27}N_9O_3Ru$: C, 58.8; H, 3.7; N, 17.0 %.

Bis(dimethylsulfoxide)(phthalocyaninato) ruthenium(II) **(RuPc(DMSO)$_2$.DMSO)**

RuPc(DMSO)$_2$.DMSO was synthesized according to the method of Dolphin *et al* [102] by refluxing crude RuPc (0.05g, 8.15 x 10^{-5} moles) in dimethylsulfoxide (20 ml) under nitrogen atmosphere for 3 hours. The resulting blue solution was filtered and the filtrate was collected. Evaporation of the solvent afforded purple crystals which were washed with hexane to remove excess DMSO. The sample was then recrystallised from chloroform. Yield (0.034, 68%). The UV-vis and infrared data are shown in Table 2 and 3, respectively.

2.1.2 Rhodium(III) phthalocyanine complexes

Chloro(phthalocyaninato)rhodium(III) (RhPcCl)

Following the procedure of Farell *et al* [97], Rh(Pc)Cl was prepared from Rh(III)Cl$_3$ and *o*-cyanobenzamide as follows: a mixture of Rh(III)Cl$_3$ (Aldrich) (0.02g, 9.6 x 10^{-4} moles), *o*-cyanobenzamide (1.8g, 1.4 x 10^{-2} moles) and naphthalene (PAL) (0.6g, 4.7 x 10^{-3} moles) was heated at 290 °C for one hour and the resulting blue solid was Soxhlet extracted with glacial acetic acid until the washings were colourless. The solid was then dried at 100 °C for 12 hours to remove traces of acetic acid. Yield: (0.12g, 60%). The crude RhPc(Cl) was then used to prepare RhPc(Cl)(L) or RhPc(L)$_2$ complexes as follows:

Chloro(phthalocyaninato)(pyridine)rhodium (III) (Rh(Pc)Cl(py))

Chloro(phthalocyaninato)(pyridine)rhodium(III) (Rh(Pc)Cl(py)) was prepared in our laboratory [53] by refluxing Rh(Pc)Cl (0.1g, 4.8 x 10^{-4} moles) in pyridine (20 ml) for 8 hours. The resulting blue solution was chromatographed on an aluminium oxide column and eluted with chloroform to give a purple solid. Yield (0.08g, 80%). The UV-vis and infrared data are shown in Tables 2 and 3 respectively. Found : C, 60.6; H, 2.6; N,16.0%. Calculated for $C_{37}H_{21}ClN_9Rh$: C, 60.3; H, 2.9; N, 17.3%.

Chloro(dimethylsulphoxide)(phthalocyaninato)rhodium(III) (Rh(Pc)Cl(DMSO)

Chloro(dimethylsulphoxide)(phthalocyaninato)rhodium(III) (Rh(Pc)Cl(DMSO) was prepared following the reported procedures [53] by refluxing Rh(Pc)Cl (0.1g, 4.8 x 10^{-4} moles) in dimethyl sulphoxide (30 ml) for 3 hours. The solution was then evaporated to dryness and the resulting blue solid was recrystallized twice from distilled acetonitrile. Yield (0.07g, 70%). The UV-vis and infrared data are shown in Tables 2 and 3. Found: C, 55.0; H, 3.4; N, 14.3%. Calculated for $C_{34}H_{22}ClN_8Rh$: C, 56.0; H,3.0; N, 15.4 %.

Potassium dicyano(phthalocyaninato)rhodium(III) K[Rh(Pc)(CN)$_2$].3H$_2$O

Potassium dicyano(phthalocyaninato)rhodium(III) $K[Rh(Pc)(CN)_2].3H_2O$], was prepared according to literature [53] by refluxing Rh(Pc)Cl (0.05g, 2.4 x 10^{-4} moles) with an excess of potassium cyanide (0.03g, 4.6 x 10^{-4} moles) in dimethyformamide (30 ml) for 3 hours. The resulting blue solution was evaporated to dryness, and the residue was washed with water and recrystallized twice from distillied acetone. Yield (0.035g, 70%). Found: C,53.9; H,2.3; N,17.0% Calculated for $C_{34}H_{16}KN_{10}Rh.3_2O$: C ,53.7; H, 2.9; N,18.5 %. UV-vis data in shown in Table 2 and infrared in Table 3.

Table 2: Electronic absorption data in DMF for ruthenium and rhodium phthalocyanine complexes. Where λ = wavelength in nm and ϵ = extinction coeffecient in $dm^3\ mol^{-1}\ cm^{-1}$.

Complex	λ_{max} (log ϵ)
$K_2[(CN)_2RuPc]$	622 (4.8), 567(4.3), 452(3.7), 426(3.9), 354(4.7)
RuPc(CO)(DMF)	642(5.2), 581(4.6), 345(4.7)
$RuPc(DMSO)_2.DMSO$	638(4.1), 581(3.8), 307(4,3)
$K[Rh(Pc)(CN)_2]$	650(5.2), 623(4.6), 587(4.7),403(4.3), 375(4.3), 345(4.6)
Rh(Pc)(DMSO)	653(5.3), 623(4.6), 588(4.6)
Rh(Pc)Cl(py)	647(5.2), 620(4.6), 585(4.6)

Table 3: Infrared spectral data for ruthenium and rhodium phthalocyanine complexes in the range 4000 to 300 cm^{-1}. Where: s = strong, v = very, m = medium, w = weak.

$[RuPc(CN)_2]^{2-}$	RuPc(CO)(dmf)	$RuPc(DMSO)_2$	$[RhPc(CN)2]^-$	ClRhPc(DMSO)	$ClRhPc(py)_2$	Assingments for main bands
				345	350	ν(Rh - Cl)
			574 m	574 m	573 m	
	647 m		640 sh			
	669 m					
	716 s	714 m				
757 w	755 m		757 s		732 vs	C-H bending
	778 w		779 sh	777 sh	756 s	C-H bending
	910 m		913 s	912 m	911 m	
				946 m		ν(Rh - S)

Table 3 continued.

$[RuPc(CN)_2]^{2-}$	$RuPc(CO)(dmf)$	$RuPc(DMSO)_2$	$[RhPc(CN)_2]^-$	ClRhPc(DMSO)	$ClRhPc(py)_2$	Assingments for main bands
1064 w	1063m		1068s	1068s	1068m	
1172m	1169 s		1169s	1168 s	1168 s	
1290 m	1287 s		1289 s	1288 vs	1287s	
1385 w	1307 m	1378 m	1330 vs	1330 vs	1330 vs	
	1329 m					
1492 s	1489 s		1498 s	1418 s	1418 s	C-C stretching
1561 w				1500 s		
	1734 s	1724 vs		1610sh		C-C stretching
	1773 w			1639 sh		
	1969 vs					ν(Ru - CO)
2068 m						ν(Ru -CN)
			2130 m			ν(Rh - CN)
	2923 m		2921 s			

2.1.3 Osmium(II) phthalocyanine complexes

(Phthlocyaninato) osmium(II) (OsPc)

Crude osmium(II) phthalocyanine OsPc, was synthesised and purified by following the procedure of Hanack *et al* [103]. A mixture of $OsCl_3.3H_2O$ (Aldrich) (0.06g, 2.02 $x10^{-4}$ moles), *o*-cyanobenzamide (0.75g 4.86 x 10^{-3} moles) and naphthalene (PAL) (0.5g, 3.57 x 10^{-3} moles) was heated under nitrogen to boiling for 20 minutes and then allowed to cool. The melt was crushed with a pestle and motor, washed with 95% ethanol and extracted with glacial acetic acid for 48 hours. The residue was dried in the oven, yielding purplish blue powder. Yield: 0.08g, 75%. The crude OsPc thus prepared was used in synthesizing the $(L)_2OsPc$ species.

Bis(pyridine)(phthalocyaninato)Osmium(II) (OsPc(py)$_2$)

Bis(pyridine)(phthalocyaninato)osmium(II) OsPc(py)$_2$ was prepared following the method of Hanack *et al* [103,104] by dissolving OsPc (0.05g 7.40 x10^{-5} moles) in pyridine (25ml). The solution was refluxed under nitrogen for 6 hours. After evaporation of the solvent, the residue was dissolved in chloroform and filtered. The filtrate was evaporated to low volume. The solution was then chromatographed in activated neutral aluminium oxide (Al_2O_3) eluting with chloroform. Yield:0.02g, (40%) UV-vis(acetonitrile): λ_{max} (log ϵ) 612(4.3), 562(4.0), 459(3.7), 433(3.9), 425(4.0) and 36.7(4.2) nm. IR spectra (KBr disk): 1774m, 1605w, 1524s, 1491w, 1467w, 1438w, 1364s, 1307s, 1171m, 1126s, 1053s, 766w, 716s cm^{-1}. The IR spectra is shown in appendix 1. Found: C, 59.6; N,15.2; H, 3.2. Calculated for $C_{42}H_{26}N_{10}Os$: C, 58.6; N, 16.2; H, 3.0 %.

Potassium(biscyanato)(phthalocyaninato)osmium(II) ($K_2[(CN)_2OsPc]$)

Potassium(biscyanato)(phthalocyaninato)osmium(II) $K_2[(CN)_2OsPc]$ was prepared following the reported procedures for the synthesis of $[(CN)_2MPc]^{2-}$ complexes [19,97-100]. Crude OsPc (0.04g,0.06mmol) was reacted with excess potassium cyanide (0.035g, 5.37 x 10^{-4} moles) in refluxing dimethylformamide (DMF, 20 ml) for 4 hours under nitrogen atmosphere. After evaporation of the solvent the resulting solid was washed with chloroform and recrystallized three times from acetonitrile. Yield (0.02, 40%) UV-vis (pH 9 buffer) λ_{max} (Log ϵ) 625(4.7), 571(4.4), 474(4.1), 422(4.3), 377(4.4)nm. IR spectra (KBr disks):2070m, 1578w, 1520s, 1490m, 1410w, 1362m, 1330w, 1286m, 1168m, 1122s, 1065w, 895m, 750s, 745sh, 720m cm^{-1}. The IR spectra in appendix 1. Found: C, 50.1, N, 15.0, H, 2.2 . Calculated for $C_{34}H_{16}N_{10}OsK_2$: C, 49.0; N, 16.8; H, 2.9%

Bis(dimethylsulphoxide)(phthalocyaninato)osmium(II) (OsPc(DMSO)$_2$.DMSO)

$(DMSO)_2OsPc.DMSO$ was prepared according to procedures described for the preparation of $(DMSO)_2MPc$ complexes [102,105]. Crude Os(II)Pc (0.04g, 0.06mml) was refluxed in dimethylsulfoxide (DMSO) (25 ml) for 4 hours under nitrogen atmosphere. The solvent was evaporated and the resulting solid was recrystallized from distilled acetonitrile, and in acetone. Yield (0.02g,50%). UV-vis (DMF) λ_{max} (logϵ) 612(3.7), 573(3.5), 297(3.95) nm. Infrared spectra (KBr disk): 2922vs, 2854m, 1719s, 1491w, 1459w, 1287w, 1169m, 1125s, 942s, 729s cm^{-1}. The IR spectra is shown in appendix 1.

2.1.4 Palladium(II) porphyrazine complexes

Palladium(II) tetra-3,4-pyridinoporphyrazine **(Pd(II)3,4tppa)**

Palladium(II) tetra-3,4-pyridinoporpyrazine (Pd(II)3,4tppa), (tp = tetrapyridino, pa = porphyrazine), was prepared by the method described by Smith *et al* for the tetrapyridino porphyrazine complexes of copper and cobalt [58]. Urea (1.23g, 2.0×10^{-2} moles), ammonium molybdate (0.040, 3.24×10^{-5} moles) and 3,4-dicarboxylic acid (0.318g, 1.9×10^{-3} mol) were ground together with pestle and mortar to form a homogeneous mixture. The mixture was added to a round bottomed flask and 1,2,4- triclorobenzene (20ml) was added. The contents of the flask were then heated for one hour with temperature maintained at 160°C. A ground mixture of $PdCl_2$ (Aldrich) (0.20g, 1.85×10^{-5} moles) and urea (0.77g, 1.28×10^{-2} moles) was then added slowly to the flask under nitrogen atmosphere and the temperature was maintained at 205-210°C for 3 hours. The crude product thus obtained was washed successively with ethanol, warm aqueous sodium hydroxide solution (5%), and dilute hydrochloric acid (25%), with each washing followed by rinsing with warm water. The sample was then dried at 80°C in the oven. Yield:(0.099g, 49.5%)

Pd(II)tetra-2,3-pyridinoporphyrazine (Pd(II)2,3tppa)

Pd(II)tetra-2,3-pyridinoporphyrazine (Pd(II)2,3tppa) was prepared using the same procedure outlined above for Pd(II)3,4tppa except that 2,3-dicarboxylic acid was used instead of 3,4-dicarboxylic acid. The quantities of reagents used are shown in Table 4. Yeild (0.28g, 80%).

Table 4 Quantities of reagents used for the preparation of **Pd(II)2,3tppa, Pt(II)2,3-tppa** and **Pt(II)3,4-tppa** complexes.

	Pd(II)2,3tppa	**Pt(II)2,3tppa**	**Pt(II)3,4tppa**
Metal salt	0.34g $PdCl_2$ (Aldrich)	0.10g $KPtCl_4$ (Sigma)	0.104g $KPtCl_4$ (Sigma)
Urea (PAL)	1.80g	0.25g	0.25g
Ammonium molybdate	0.04g	0.006g	0.006g
Dicarboxylic acid (Aldrich)	0.32g; 2,3-dicarboxylic acid (Aldrich)	0.044g; 2,3-dicarboxylic acid (Aldrich)	0.044g 3,4 dicarboxylic acid (Aldrich)
Trichlorobenzene	20ml	20ml	20ml
Yield	0.28g, 80%	0.06g, 60%	0.017g,16%

***NN'N"N'"-tetramethyltetra-3,4-pyridinoporphyrazine palladium,* [Pd(II)3,4Tmtppa]$^{4+}$[$SO_3(OCH_3]_4^-$**

The tetraethoxysulphide salt of *NN'N"N'"*-tetramethyltetra-3,4-pyridinoporphyrazine palladium, [Pd(II)3,4Tmtppa]$^{4+}$[$SO_3(OCH_3]_4^-$, was prepared by the method also outlined by Smith *et al* for the tetramethyltetra-3,4-pyridinoporphyrazines complexes of cobalt and copper [58]. Pd(II)3,4tppa(-2) (0.099g, 1.59 x 10^{-4} moles) was heated to 120°C in freshly distilled DMF (10ml) in a three necked round bottom flask fitted with water condenser and a thermometer.

Nitrogen was slowly bubbled through the third neck of the flask. Dimethyl sulphate (10ml), distilled immediately before use, was added dropwise to the flask using a dropping funnel.

The mixture was heated with stirring for 30 minutes during which time the Pd(II)3,4tppa compound began to dissolve. The solution was cooled to room temperature and then poured into acetone (100 ml). The tetramethylated porphyrazine compound immediately precipitated and the product, $[Pd(II)3,4Tmtppa]^{4+}[SO_3(OCH_3)]_4^-$, was collected by centrifuge and washed successively with 95% ethanol and diethyl ether then dried at 80°C. The compound was further purified by recrystallizing from distilled water. Yield:(0.02, 20%), UV-vis (distilled water) λ_{max} (logϵ) 659(4.32), 643(3.9), 594(2.09), 332(3.27) nm. IR spectra was obtained with KBr disks and is shown in appendix 1. The IR data is also shown in Table 5. Found: C, 29.9; N, 15.1; H, 3.3. Calculated for $C_{32}H_{40}N_{12}O_{24}S_6Pd$: C, 30.1; N, 13.2; H, 3.2 %.

Table 5 The infrared data for the tetramethyltetrapyridinoporphyrazine complexes of palladium(II) and platinum(II) in the range 4000 to 400 cm^{-1}.

Pd(II)2,3Tmtppa	Pd(II)3,4Tmtppa	Pt(II)2,3Tmtppa	Pt(II)3,4Tmtppa	Assignments
443 s	432 s		457 m	
540 sh	555 sh			
559 m	580 m			
615 vs	614 vs	615 m	616 m	
799 vs	751 vs	757 vs	764 vs	ν (C-H) stretch
848 w	851 m			C-H out of plane
971 vs				
	1002 vs	1003 vs	1007 m	ν (C-N) stretch
1054 vs 1057 m	1057 m	1058 m	1063 m	
1110 w	1105 w			

NN'N"N'"-*tetramethyltetra-2,3-pyridinoporphyrazine palladium(I)*, [Pd(II)2,3Tmtppa]$^{4+}$[$SO_3(OCH_3)$]$_4^-$

The tetraethoxysulphide salt of *NN'N"N'"*-tetramethyltetra-2,3-pyridinoporphyrazine palladium(II), [Pd(II)2,3Tmtppa]$^{4+}$[$SO_3(OCH_3)$]$_4^-$, was prepared by heating 0.28g of Pt(II)2,3tppa 120°C in freshly distilled DMF in a three necked round bottom flask fitted with a water condenser and a thermometer. The rest of the procedure was followed exactly as outlined above for the preparation of [Pd(II)3,4Tmtpp]$^{4+}$[$SO_3(OCH_3)$]$_4^-$. Yield (0.08g, 28%). UV-vis (distilled water) λ_{max} (logϵ) 619(3.8), 610(3.6), 556(3.1), 335(3.5) nm. IR (KBr disks): The spectra is shown appendix 1 and the IR data in Table 5.

2.1.5 Preparation of platinum(II) porphyrazine complexes

***Platinum(II)tetra-3,4-pyridinoporphyrazine* (Pt(II)3,4tppa) *and platinum(II)tetra-2,3-pyridinoporphyrazine* (Pt(II)2,3tppa).**

The tetrapyridinoporphyrazine complexes of platinum(II) , Pt(II)3,4tppa and Pt(II)2,3tppa were synthesized following the procedure outlined above for the palladium tetrapyridino-porphyrazine complexes. The only difference being that the potassium tetrachloroplatinate ($KPtCl_4$) was used instead of palladium chloride ($PdCl_2$). The quantities of reagents used for the preparation of each complex and the percentage yields are shown in Table 4.

NN'N"N'"-*tetramethyltetra-3,4-pyridinoporphyrazine platimum(II)*, [Pt(II)3,4Tmtppa]$^{4+}$[$SO_3(OCH_3)$]$_4^-$

The tetraethoxysulphide salt of *NN'N"N'"*-tetramethyltetra-3,4-pyridinoporphyrazine platimum(II), [Pt(II)3,4Tmtppa]$^{4+}$[$SO_3(OCH_3)$]$_4^-$ was prepared by heating Pt(II)3,4tppa, (0.017g) in freshly distilled DMF (100 ml) at 120°C in a three necked round bottom flask fitted with a water condenser and a thermometer. Nitrogen was slowly bubbled through the third neck of the flask . The rest of the procedure was followed exactly as detailed in section 2.1.4 for the preparation of [Pd(II)3,4Tmtppa]$^{4+}$[$SO_3(OCH_3)$]$_4^-$. Yield (0.006g, 35%). UV-vis (distilled water) λ_{max} (logϵ) 685(3.80), 671(3.78), 627(3.49), 398(3.52). IR (KBr disks) shown in Table 5, the spectra also shown in Appendix 1. Found: C, 28.5; N, 12.6; H, 4.8. Calculated for $C_{32}H_{40}N_{12}0_{24}S_6Pt$: C, 28.2; N, 12.3, H, 3.0 %.

***NN'N"N'"-tetramethyltetra-2,3-pyridinoporphyrazine platinum(II)*, [Pt(II)2,3Tmtppa]$^{4+}$[$SO_3(OCH_3)$]$_4^-$**

The tetraethoxysulphide salt of *NN'N"N'"*-tetramethyltetra-2,3-pyridinoporphyrazine platinum(II), [Pt(II)2,3Tmtppa]$^{4+}$[$SO_3(OCH_3)$]$_4^-$, was also prepared following the method outlined above for the preparation of [Pd(II)3,4Tmtppa]$^{4+}$[$SO_3(OCH3)$]$_4^-$ complex, except that for [Pt(II)2,3Tmtppa]$^{4+}$[$SO_3(OCH_3)$]$_4^-$ complex the Pt(II)2,3tppa (0.006g) was used as a starting material. Yield (0.004g , 66%). UV-vis (distilled water) 609(4.82), 599(4.76), 548(4.35), 306(4.93). IR (KBr disks) shown in Table 4. The IR spectra shown in Appendix 1. Found: C, 28.5; N, 12.6; H, 4.5 %. Calculated for $C_{32}H_{40}N_{12}0_{24}S_6$ Pt: C, 28.2; N, 12.3; H, 3.0 %.

2.1.6 Tetrasulphonated metallophthalocyanines

Cobalt(II)4,4',4",4'"-tetrasulphophthalocyanine Na_4 [Co(II)TSPc].$2H_2O$

Tetrasodium salt of cobalt(II)4,4',4",4'"-tetrasulphophthalocyanine 2-hydrate (Na_4[Co(II)TSPc].$2H_2O$) was synthesised by the method described by Webber *et al* [10]. The monosodium salt of 4-sulphophthalic acid (4.32g, 0.016 moles), ammonium chloride (0.47g, 0.009 moles), urea (5.8g, 0.097 moles), ammonium molybdate 0.068g, 6 x 10^{-5} moles) and cobalt(II)sulphate 7-hydrate(1.4g, 0.0048 moles) were ground together with a pestle and mortar until homogeneous. The solid mixture was added with stirring to 40 ml of a hot (180°C) nitrobenzene in a three-necked round bottom flask fitted with a thermometer, a condenser and a glass cork. The mixture was heated for 3 hours with the temperature maintained between 160 and 190°C.

The crude product obtained (solid cake) was washed with methanol until the odour of nitrobenzene could no longer be detected and the solid was added to 100ml of 1M hydrochloric acid saturated with sodium chloride. The mixture was heated to boiling, cooled to room temperature and filtered. The resulting solid was dissolved in 100ml of 1M sodium hydroxide and the solution was heated to 180°C then filtered hot. Sodium chloride (3.2g) was added to the filtrate and the solid product began to precipitate. The slurry was heated to 80°C and the solid product was obtained by filtration. The product was then washed with 80% aqueous ethanol until the filtrate was chloride free and was refluxed in 40ml absolute ethanol for 2 hours. After evaporation of ethanol, purplish blue crystals were obtained which were dried over P_2O_5. Yield 80%. IR(KBr disks) 2336w,1624m, 1400m, 1329m, 1191s, 1058m, 1029vs, 934s, 831s, 698s, 636w, 593w, 419w, 386m. Found: C, 38.1; N,11.0; H, 1.6%. Calculated for $CoC_{32}H_{12}N_8O_{12}S_4Na_4.2H_2O$: C,37.8; N,11.0; H, 1.6%.

The monosodium salt of 4-sulphophthalic acid was prepared by the method outlined by Rollman *et al* [42], by reaction of sodium hydroxide with 30% aqueous sulphophthalic acid (Eastman). Evaporation of the solution afforded pinkish-white crystals.

Palladium(II) 4,4',4'',4'''-tetrasulphophthalocyanine Na_4[Pd(II)TSPc]

Tetrasodium salt of palladium(II) 4,4',4'',4'''-tetrasulphophthalocyanine, Na_4[Pd(II)TSPc], was synthesized following the similar prodedure detailed above for Na_4[Co(II)TSPc].$2H_2O$ but palladiuml chloride (0.85g, 0.0048 moles) was used instead of cobalt(II) sulphate. Yield(0.78g, 92%) UV-vis (distilled water): λ_{max} (logϵ) 658(4.76), 625(4.9), 342(4.78). IR (KBr disks): 2371w, 1637m, 1509m, 1400m, 1325s, 1189vs, 1189vs, 1113m, 1057s, 1030vs, 935s, 836s, 747s, 698s, 650s, 596m, 397w. Found: C, 36.0; N, 11.5; H, 1.6. Calculated for $PdC_{32}H_{12}N_8O_{12}S_4Na_4$: C,36.5; N,10.5; H,1.5 %.

Nickel(II) 4,4',4'',4'''-tetrasulphophthalocyanine Na_4[Ni(II)TSPc]

The tetrasodium salt of nickel(II) 4,4',4'',4'''-tetrasulphophthalocyanine, Na_4[Ni(II)TSPc], was also synthesized following the method of Webber *et al* [10] detailed above for Na_4[Co(II)TSPc], except that nickel chloride (0.62g, 0.0048 moles) was used instead of copper(II)sulphate. Yield(0.60g, 95%). UV-vis (distilled water) λ_{max} (logϵ) 663(4.76), 633(4.9), 343(4.74). IR (KBr disks) 2370w, 1629, 1400m, 1331s, 1189vs, 1150sh, 1112m, 1061s, 1030vs, 970sh, 935s, 833s, 750s, 700s, 650s, 602m, 387w. Found :C,38.4; N,10.5; H,1.6%. Calculated for $NiC_{32}H_{12}N_8O_{12}S_4Na_4$: C,37.8; N,11.0; H,1.6%.

2.2 Preparation of reagents for electrochemical studies

Tetraethylammonium perchlorate (TEAP)

Hot solutions of sodium perchlorate (1.00 mol dm^{-3}, 100 ml) and tetraethylammonimum chloride (Sigma) was mixed and the mixture was cooled in ice cold water. The precipitate formed was filtered, washed with ice cold ethanol (95%) and TEAP recrystallised from ethanol (95%). TEAP thus obtained was dried in the oven overnight and used as an electrolyte in electrochemical experiments in nonaqueous solvents. Yield, 80%. Sodium sulphate was recrystalized from ethanol and was used as an electrolyte for electrochemical studies in aqeous solvents. Ferrocene (BDH) was recrystallised from ethanol and was used as an internal standard for electrochemical measurements in non-aqueous solvents.

Solvents:

Dimethylformamide (DMF) was dried over aluminium oxide and distilled, then stored over molecular seives. Acetonitrile was dried over phosphorus pentoxide before distillation and was also stored over molecular sieves after distillation. Phosphate buffer pH7.2 was prepared by mixing 3.2 ml of 0.2M potassium dihydrogen sulphate with 50 ml of 0.2M potassium hydroxide in 100ml volumetric flask , and the volume was brought to the mark by adding distilled deionized water to the flask. For the experiments performed in water, triplly destilled deionized water was used.

2.3 Preparation of reagents for photochemical studies

Tetrathiocyanato(diamine)potassium chromate, $KCr(NH_3)_2(NCS)_4$, for actinometry.

Tetrathiocyanato(diamine)potassium chromate, $KCr(NH_3)_2(NCS)_4$, commercialy known as Reinecke's salt was prepared according to the procedure reported by Wegner *et al* [106]. Reinecke's salt is commercially available as tetrathiocyanato(diamine)ammonium chromate monohydrate salt, $NH_4[Cr(NH_3)_2(SCN)_4].H_2O$, and was purchased from Merck chemicals. This salt was converted to the potassium salt ($KCr(NH_3)_2(NCS)_4$) by dissolving (5.00g, 1.4×10^{-2} moles) of the salt in warm water (40-50°C) followed by addition of an excess of potassium nitrate (2.01g, 1.98×10^{-2} moles) to the solution. The solution was then cooled in ice cold water and filtered. The resulting product ($KCr(NH_3)_2(NCS)_4$) was recrystallised from 10% KNO_3 and the purified solid was dried over P_2O_5 in the vacuum desiccator to afford the anhydrous product. The preparations were carried out in a dark room under red light and the product was kept in a dark bottle covered with aluminium foil to keep it away from light.

Diphenylisobenzofuran (DPBF) was purchased from Aldrich and was used without further purification as a quencher for singlet oxygen production experiments.

2.4 Instrumentation

Electrochemical data were collected with the BioAnalytical systems (BAS) model CV-50W Voltammetric Analyser and all the electrochemical measurements were carried out under an atmosphere of purified nitrogen. Nitrogen was purchased from MG Fed gas and was purified by passing through drierite self-indicating mesh 8 (unhydrous $CaSO_4$) (SAAR chemicals). Infrared spectra (KBr pellets) were recorded with a Perkin-Elmer model 180 IR spectrophotometer or Perkin Elmer Fourier Transform Infrared (FTIR) spectrometer spectrum 2000. Electronic absorption spectra were recorded with a Cary 1E UV-Vis or Beckman UV 520 spectrophotometer using a quartz cell with 1 cm path length. Magnetic Susceptibility data were collected on a Faraday balance manufactured by Cahn Instrument Company and all the melting points were determined using Gallenkamp melting point apparatus. Bulk electrolysis data was collected with BAS CV 27 Voltammograph analyser.

2.5 Electrochemical methods

Cyclic Voltammetry.

For the determination of redox potentials for the MPc and $[MTmtppa(-2)]^{4+}$ complexes, a three electrode cell containing a solution of MPc or $[MTmtppa(-2)]^{4+}$ (10^{-4}-10^{-3} mol dm^{-3}) in acetonitrile, dimethylformamide or deionised distilled water was employed. Nitrogen was bubbled through the solution for about 15 minutes before running the cyclic voltammogram. In organic solvents, a platinum disk (1.6 mm diameter) was used as a working electrode, a platinum wire as an auxiliary electrode and silver wire coated with silver chloride was employed as a pseudo-reference electrode for non-aqueous solvents. In aqueous solutions, silver/silver chloride electrode (Ag/AgCl, 3 mol dm^{-3} KCl) was used as a reference electrode. For some cyclic voltammetric studies of $[MTmtppa]^{4-}$ complexes, a Bioanalytical systems (M F 2007) carbon fibre microelectrode

(11 μm diameter) was employed as a working electrode.

Tetraethylammonium perchlorate (0.03 - 0.1 mol dm^{-3}) was used as an electrolyte in non-aqueous solutions while sodium sulphate or phosphate buffer were electrolytes in aqueous solutions. Potentials in non-aqueous solutions were referenced internally to the ferrocenium/ferrocene (Fc^+/Fc) couple and this couple has been reported to have the potential of 0.44V vs SCE in CH_3CN containing TEAP [19] and 0.46V vs SCE in DMF containing TEAP [21,36,53]. Table 6 shows an example of how redox potentials of $OsPc(py)_2$ in acetonitrile were referenced to the ferrocinium/ ferrocene couple, with TEAP as an electrolyte.

Table 6: Example showing how redox potential of $OsPc(py)_2$ were referenced internally to the ferrocene in acetonitle using TEAP as an electrolyte.

	Fc^+/Fc couple	**$OsPc(py)_2$ oxidation couple**	**$OsPc(py)_2$ reduction couple**
$E_{1/2}$ vs Ag wire (Volts)	0.5	0.60	-0.63
$E_{1/2}$ vs Fc^+/Fc	0.0	0.10	-1.13
$E_{1/2}$ vs SCE	0.44	0.54	-0.69

Where: (1) $E_{1/2}$ vs Fc^+/Fc = $E_{1/2}$ vs Ag wire - $E_{1/2}$ (Fc^+/Fc couple) vs Ag wire.

(2) $E_{1/2}$ vs SCE = $E_{1/2}$ vs Fc^+/Fc + $E_{1/2}$ (Fc^+/Fc couple) vs SCE

Spectroelectrochemical methods (Bulk electrolysis)

For characterization of MPc or $[MTmtppa(-2)]4^{+}$ species formed following the reduction/oxidation reactions, bulk electrolysis was carried out in a three electrode cell with two compartments, one compartment containing MPc or $[MTmtppa(-2)]^{4+}$ complex (10^{-5} mol dm^{-3}), and the other compartment contained only the solvent plus an electrolyte without MPc or[$MTmtppa(-2)]^{4+}$. The working electrode (platinum sheet) and the reference electrode were housed in the same compartment and were separated from the auxiliary electrode (Pt sheet), in the other compartment, by a fine glass frit. A silver/silver chloride electrode (3 mol dm^{-3} KCl) was used as a reference in aqueous solutions and silver wire coated with AgCl, as pseudo-reference in non-aqueous solutions. Nitrogen was bubbled through the solution throughout the duration of the experiment. The products of electrolysis were accumulated in the compartment containing the working electrode and these products were characterized by electronic absorption spectroscopy.

Electrocatalytic methods

For electrocatalytic experiments, solutions of *l*-cysteine (Sigma), methionine (Sigma), metallothionein from rabbit liver (Sigma), hydroxylamine or hydrazine were freshly prepared in pH 7.2 buffer just before the analysis. The cyclic voltammetry was carried out in a three electrode cell and nitrogen, purified as mentioned in section 2.4, was bubbled through the solution. In these experiments, the working electrode was a glassy carbon electrode (GCE) modified or unmodified with MPc complexes. The complexes used to modify the electrode were (DMSO)(Cl)Rh(III)Pc, py(Cl)Rh(III)Pc, $[(CN)_2Rh(III)Pc]^{-}$, $(py)_2Os(II)Pc$, $(DMSO)_2Os(II)Pc.DMSO$, $(py)_2Ru(II)Pc$, and $[(DMSO)_2Ru(II)Pc].2DMSO$. The adsorbed films of MPc complexes on GCE were prepared by a drop dry method in which a drop of a saturated (ca. 1×10^{-3} mol dm^{-3}) solution of the MPc in dimethylformamide,

acetonitrile or pyridine were placed on the glassy carbon electrode surface then dried in air. Before coating with the MPc complexes, the glassy carbon electrode was polished with alumina on a Buehler felt pad, followed by soaking in dilute nitric acid and rinsing in distilled water. The cyclic voltammetry of the adsorbed species was run before and after the addition of the substrate to the buffer solution. Different concentrations of the substrate were studied. The electrode was washed and recoated for each new concentration run.

Since $[RuPc(CN)_2]^{2-}$ and $[OsPc(CN)_2]^{2-}$ are highly soluble in water it was difficult to work with these complexes when adsorbed on the electrode surface by drop dry method because as soon as the modified electrode is dipped into the buffer solution, the adsorbed film on the electrode leached out and the adsorbed MPc species dissolved from the electrode surface into the solution. Therefore, for these complexes the solution catalysis (or homogeneous catalysis) was employed. In homogeneous catalysis the MPc complex was dissolved in a known volume of phosphate buffer, pH7.2, and the cyclic voltammetry of the species was run using bare glassy carbon electrode as a working electrode. Then a desired amount of the substrate was added to the solution and the cyclic voltammetry was again determined.

Homogeneous catalysis was also employed for catalytic reactions of the tetramethyltetra-pyridino porphyrazine complexes of palladium and platinum, $[Pd(II)2,3Tmtppa(-2)]^{4+}$, $[Pd(II)3,4Tmtppa(-2)]^{4+}$ $[Pt(II)2,3Tmtppa(-2)]^{4+}$, and $[Pt(II)3,4Tmtppa(-2)]^{4+}$ because they are also highly soluble in water and like the cyano complexes of Ru(II)Pc and Os(II)Pc above, these complexes tend to leach from the electrode surface.

2.6 Studies of the interactions of MPc Complexes with amino acids

l-histidine and *l*-cystine were obtained from Sigma chemicals and were used without further purification. Solutions of the amino acids were prepared in phosphate buffer (pH 7.2) with concentrations ranging from 0.001 to 0.3 mol dm^{-3}. A known volume of $[M(II)TSPc]^{4-}$ solution was added to a spectrophotometric cell of 1 cm path length and the absorption spectrum of the solution was recorded. Then a known volume of a solution of *l*-histidine or *l*-cysteine in phosphate buffer (pH 7.2) was added to the cell. The cell was tightly closed with the stopper and the absorption spectrum of the solution was recorded immediately after addition of the amino acids and then at regular time intervals over the duration of the reaction. Since the concentration of phthalocyanine species (1×10^{-5} to 1×10^{-6} mol dm^{-3}) was much less than that of the *l*-histidine or *l*-cysteine species, pseudo-first order conditions were maintained for kinetic studies.

Tetrasulphonated MPc species are known to form aggregates in aqueous solutions hence the exact concentrations of the complexes may be difficult to determine. The concentration of the dimeric cobalt(II) tetrasulphophthalocyanine species was estimated with an absorption maximum at 624 nm to be 8.0×10^{-6} mol dm^{-3} using a published extinction coefficient of 5.8×10^4 dm^3 mol^{-1} cm^{-1} [100]. The concentration of $[M(II)TSPc]^{4-}$ species were kept constant for all reactions.

For tetramethylated tetrapyridinoporphyrazine complexes, $[3,4Pd(II)Tmtppa]^{4+}$, $[2,3Pd(II)Tmtppa]^{4+}$, $[3,4Pt(II)Tmtppa]^{4+}$, $[2,3Pt(II)Tmtppa]^{4+}$, the same procedure outlined for the $[MTSPc]^{4-}$ above was followed except that distilled deionized water was used as a solvent instead of phosphate buffer. Phosphate buffer could not be used in the case of tetramethylated tetrapyridino-porphyrazine because these complexes tend to be unstable in buffer even at low pHs. The concentration of the porphyrazine complexes was 1.7×10^{-5} mol dm^{-3} and this concentration was kept constant for all the reactions, while the *l*-cysteine and *l*-histidine concentration ranged from 0.001 to 0.003 mol dm^{-3}. These studies were carried out at room temperature.

2.7 Photochemical methods

Determination of light intensity, I_o, incident on the cell

The intensity of radiation I_o, was determined with $KCr(NH_3)_2(NCS)_4$ [106] commonly known as Reinecke's salt. This salt is commercially available as tetrathiocyanato(diamine)ammoniumchromate, ($NH_4[Cr(NH_3)_2(SCN)_4].H_2O$), and was converted into ($KCr(NH_3)_2(NCS)_4$) by the method described in section 2.3. Reinecke's salt shows maximum absorbance at 500 nm but it is usable with ease up to about 600nm and with more difficulty up to 735 nm. MPc complexes absorb strongly between 600 and 750 nm. When $KCr(NH_3)_2(NCS)_4$ is photolysed, one thiocyanate ion (NCS^-) is released. The NCS^- species forms an iron thiocyanate ($Fe(III)(NCS)_3$) complex when iron(III)nitrate ($Fe(NO)_3$) and hypocloric acid ($HClO_4$) are added to a photolysed solution of $KCr(NH_3)_2(NCS)_4$ [106]. The iron thiocyanate complex has an absorption maximum at 450 nm with an extinction coefficient of $4.3x10^3$ dm^3 mol^{-1} cm^{-1} and the absorbance at this wavelength gives the thiocyanate ion concentration directly [106].

The analysis of free thiocyanate was performed in the following manner: 3 ml of $2.1 x10^{-3}$ mol dm^{-3} $KCr(NH_3)_2(NCS)_4$ solution in distilled water, was added to a 1 cm path length spectrophotometric cell. The sample was photolysed with 50W tungsten lamp and a 600 nm cut off filter was used to exclude ultra-violet radiation. 1 ml of the photolysed sample was diluted with 4 ml of 0.1M $Fe(NO_3)_3.9H_2O$ in 0.5M $HClO_4$. The absorption spectrum of the diluted solution was recorded. Different dilutions were made for each photolysis time and absorption spectrum was recorded for each dilution. The procedure was carried out in the dark room under red light. The increase in the absorption band at 450 nm reflected an increasing concentration of iron thiocyanate complex. The change in absorbance (ΔA) at 450 nm, between the non-photolysed and photolysed samples, were plotted against the photolysis time and the slope ΔA/sec was

determined. The number of moles of NCS^- (per second of irradiation) were calculated as shown in **Equation 22** [107].

$$\text{Moles of } NCS^-/\text{sec} = \frac{V_1 \times V_3 \times \Delta A/\text{sec}}{\epsilon \times l \times 1000 \times V_2} \qquad \text{Equation 22}$$

Where V_1 (ml) is the volume of $KCr(NH_3)_2(NCS)_4$ solution irradiated, V_2 (ml) is the sample of the photolysed solution to be complexed to $Fe(III)(NCS)_3$, V_3 (ml) is the total volume after dilution of V_2, l is the path length of the spectrophotometric cell, ϵ is the molar extinction coefficient of the iron thiocyanate complex and $\Delta A/\text{sec}$ is the slope of the plot of ΔA versus photolysis time. The number of moles of the photoreleased thiocyanate ions divided by the quantum yield obtained from Wegner *et al* [106] for ($KCr(NH_3)_2(NCS)_4$) give I_o , **Equation 23.** The value of the quantum yield for the photoreleased thiocyanate ions by $KCr(NH_3)_2(NCS)_4$) at the wavelength of 600nm was used in **Equation 25** to calculate the incident intensity (I_o) in einsteins per unit time.

$$I_o/\text{sec} = \frac{\text{Moles of NCS/sec}}{0.27} \qquad \text{Equation 23}$$

Singlet oxygen production of $[RuPc(CN)_2]^{2-}$ and $[OsPc(CN)_2]^{2-}$

For the determination of quantum yield for production of singlet oxygen by the water soluble $[Ru(II)Pc(CN)_2]^{2-}$ and $[Os(II)Pc(CN)2]^{2-}$, oxygen was bubbled for 3 minutes (at 1 atm) through 100ml solution of $[Ru(II)Pc(CN)_2]^{2-}$ or $[Os(II)Pc(CN)2]^{2-}$ in DMF contained in a flask fitted with a rubber septum. The desired volume of the MPc solution was mixed with an appropriate

volume of oxygen saturated solution of diphenylisobenzofuran (DPBF) (Aldrich). The mixture was introduced into a spectrophotometer cell and the cell was tightly stoppered. The absorption spectra of the solutions were recorded before the photolysis and the solution was then photolysed for known periods with 50W tungsten lamp and 600 nm filter was used to exclude ultraviolet radiation. The absorption spectrum of the solution was recorded after each photolysis time. The concentration of the MPc species was 5.25×10^{-5} mol dm^{-3} and this concentration was kept constant for all the photolysis reactions. The concentrations of DPBF ranged from 1.0×10^{-4} to 2.0×10^{-5} mol dm^{-3}. Experiments were also performed where 60% acetonitrile/water was used instead of DMF for comparison purposes.

For each solution of DPBF, the decrease in concentration of DPBF was followed as a function of irradiation time by monitoring the disappearance of its absorbance due to DPBF at 415 nm. The concentrations of DPBF at each photolysis time were calculated from its absorbances using the extinction coefficient of DPBF in DMF (17360 dm^3 mol^{-1} cm^{-1}). Plots of concentration of DPBF versus photolysis time were obtained for each reaction from the data obtained, the relative quantum yeilds for singlet oxygen production were then calculated as shown in chapter 6.

3. Characterization of MPc complexes

*3.1 Potassium (biscyanato)(phthalocyaninato) osmium(II) $K_2[(CN)_2Os(II)Pc]$**

The preparation of potassium(biscyanato)(phthalocyaninato)osmium(II) $K_2[(CN)_2Os(II)Pc]$ was carried out by the reaction of crude OsPc with potassium cyanide in refluxing DMF, **Scheme 8**. The method of the preparation is outlined in section 2.1.3.

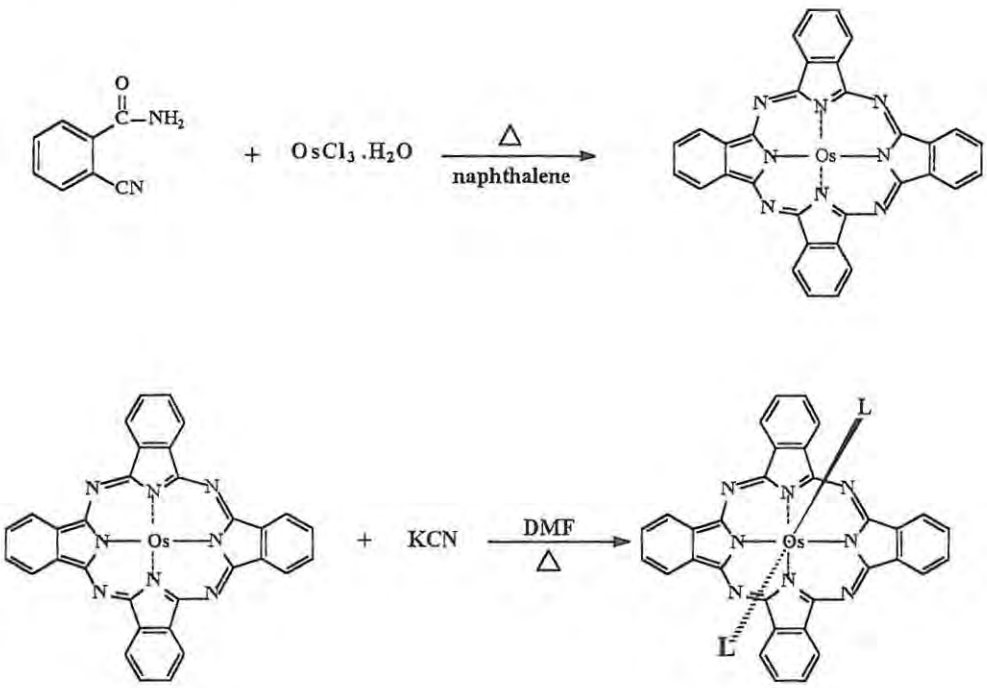

Scheme 8: Synthesis of $K_2[(CN)_2Os(II)Pc]$

*The following paper has resulted from the research work presented in this chapter and is not referenced further in this thesis: *Polyhedron*, 1996, **15(17)**, 2901- 2908.

3.1.1 Spectroscopic characterization of $K_2[(CN)_2Os(II)Pc]$

$K_2[(CN)_2Os(II)Pc]$ was found to be soluble in water at pHs greater than four, and the solubility was found to increase with the pH of the solution. This behaviour has been observed before in our laboratory [19] for $K_2[(CN)_2Ru(II)Pc]$ complex. Reports of Hambright *et al* [108], have shown that the spectra of the cyano complexes of ruthenium porphyrins were dependent on the pH of the solution and the behaviour was attributed to the loss of the axial cyanide ligands. It is possible then that the lack of solubility of the $[(CN)_2Os(II)Pc]^{2-}$ complex, in low pHs may also be due to the loss of the axial cyanide ligands.

The electronic absorption spectra of $[(CN)_2Os(II)Pc]^{2-}$ in water at pH 9 or in non-aqueous solvents, **Figure 12**, showed the split in the soret band which is typical of cyano complexes of the MPc species [14,17,109].

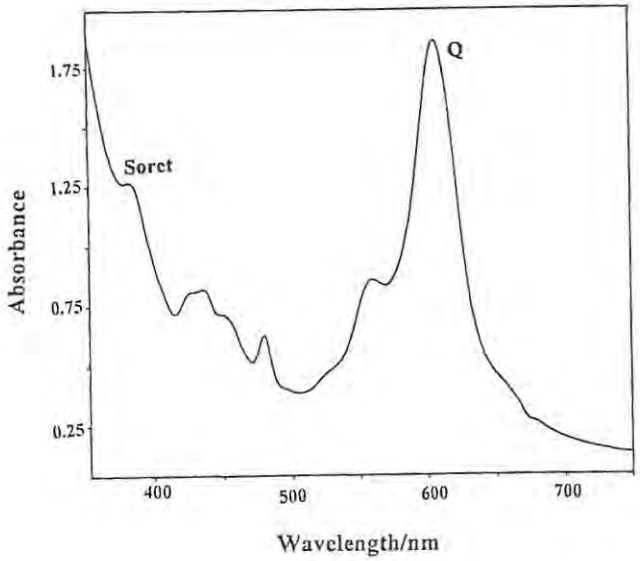

Figure 12 Electronic absorption spectra of $[(CN)_2Os(II)Pc]^{2-}$ in DMF

The Q band for this complex in acetonitrile is located at 625 nm. The Q band for $[(CN)_2Os(II)Pc]^{2-}$ in acetonitrile is blue shifted when compared with the Q band of $[(CN)_2Ru(II)Pc]^{2-}$ which is located at 630 nm in the same solvent [19]. This blue shifting of the spectra of OsPc complexes relative to the spectra of the RuPc and FePc species has been observed before by Hanack *et al* [103] and was attributed to the $d\pi$-donor ability of osmium(II). The higher energy of the $5d\pi$-orbitals of OsPc complex, compared with the $4d\pi$- of RuPc, results in significant mixing between the $5d\pi$ orbitals and the $eg(\pi)$ of the ring, the LUMO. This mixing raises the energy of the $eg(\pi)$ and increases the spacing between the a_{1u}, the highest occupied molecular orbital of the ring, resulting in the shift to higher energies of the spectra of the $[(CN)_2Os(II)Pc]^{2-}$ complexes compared with the $[(CN)_2Ru(II)Pc]^{2-}$ species.

Cyanide as an axial ligand, is known to act as a bridging ligand in some metal phthalocyanines and the bridging between two or more phthalocyanine rings results in the formation of dimeric (or polymeric) MPc species [101,109]. Dimerization in MPc complexes is normally characterized by significant broadening of the Q band [14]. Since the Q band for $[(CN)_2Os(II)Pc]^{2-}$ complex is relatively narrow, **Figure 12**, it can be concluded that the species is a monomer and is non-aggregated in solution.

The plot of concentration versus absorbance for $[(CN)_2Os(II)Pc]^{2-}$ complex dissolved in water at pH 9, within the concentration range of 10^{-6} - 10^{-4} mol^{-1} dm^3, was found to obey Beers law, thus confirming that there was no formation of dimers in aqueous solution within this concentration range. An extinction coefficient of 5×10^4 dm^3 mol^{-1} cm^{-1} was obtained in water and this value is within the range reported for the L_2RuPc complexes [19,102].

The infrared spectral data for $K_2[(CN)_2Os(II)Pc]$ were recorded as KBr disks, **Figure 13**. A weak IR band observed at 2070 cm^{-1} is due to the Os-CN stretching.

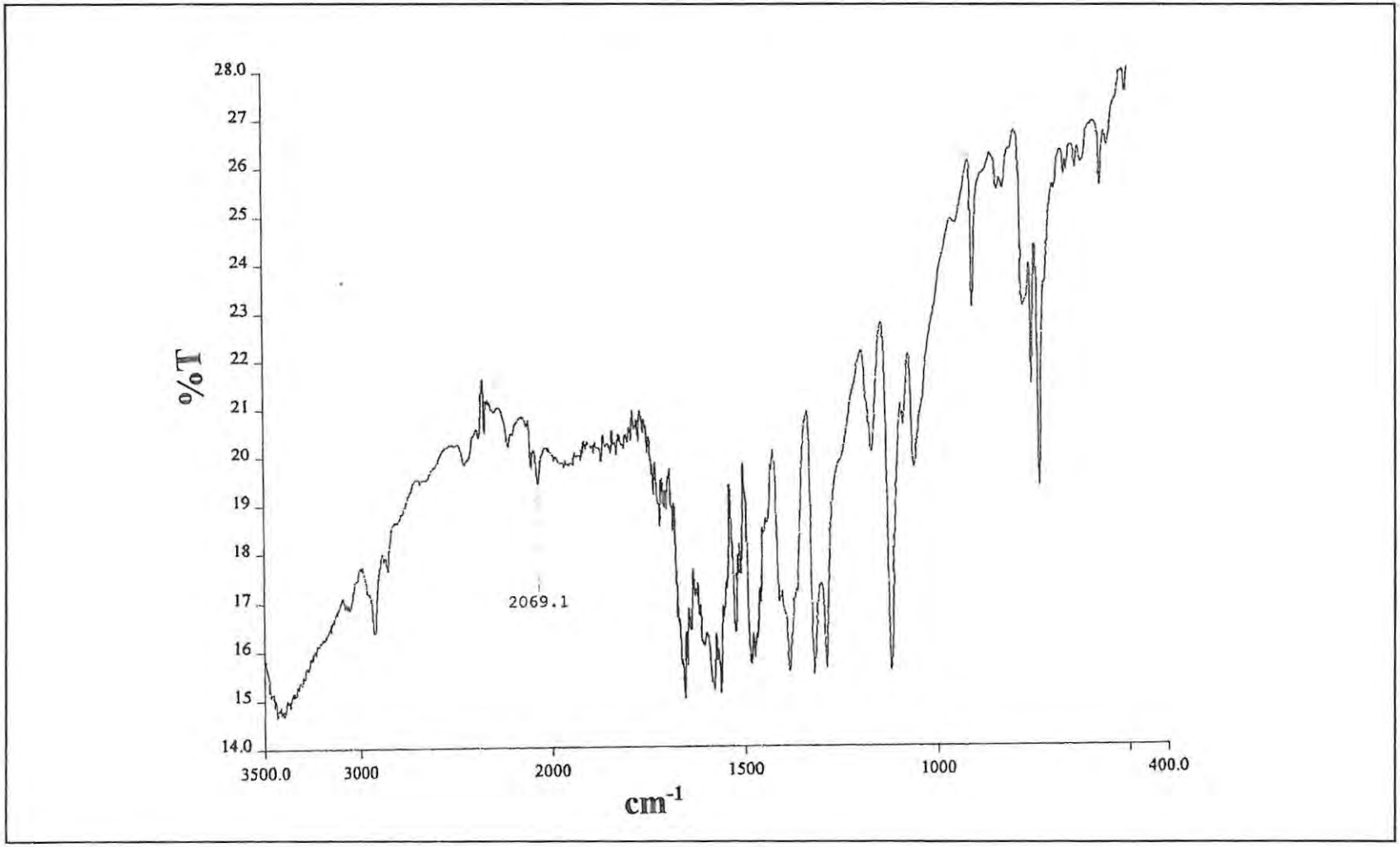

Figure 13 Infrared spectra of $K_2[(CN)_2Os(II)Pc]$ (KBr disks)

The complex seemed to be free from contamination by free CN^-, which is normally characterized by the band at approximately 2080 cm^{-1} . The M-CN vibrational frequency for $K_2[(CN)_2Os(II)Pc]$ was observed at lower frequencies than those reported for $K_2[(CN)_2Ru(II)Pc]$ at 2075 cm^{-1} [19] and for $K_2[(CN)_2Fe(II)Pc]$ at 2120 cm^{-1} [110]. A similar trend has been reported by Hanack *et al* for the M-CN vibrational frequencies in isocyanide complexes of OsPc, RuPc, and FePc and was attributed to the π back- bonding of the osmium [103].

Cyanide ion as a ligand is known to act as a σ-donor by donating electrons to the metal and also as a π-acceptor by accepting electrons from the metal. σ-donation by the cyanide ion is known to raise the M-CN vibrational frequency since electrons are tranferred from the 5σ- orbital which is weakly antibonding, while the π-backbonding tends to decrease the M-CN vibrational frequency because the electrons enter into the antibonding 2pπ*-orbital [103,111].

The other vibrational bands exhibited by $K_2[(CN)_2OsPc]$ species are characteristic of the phthalocyanine macrocycle [112,113] and are assigned as follows: the aromatic C-H stretching vibrations are observed at 3190 cm^{-1} , the C-H out-of- plane bending vibrations at 1908, 754 and 736 cm^{-1} . The C-C benzene ring skeletal stretching vibrations are characterized by the 1655 and 1475 cm^{-1} bands. The absence of the strong bands at 715 and 1000 cm^{-1} is an indication that the complex is free from contamination by metal free phthalocyanine [114].

3.1.2 Redox properties of $[(CN)_2Os(II)Pc]^{2-}$

Cyclic voltammetry of $[(CN)_2Os(II)Pc]^{2-}$ in aqueous solvents.

The cyclic voltammetry for $[(CN)_2Os(II)Pc]^{2-}$ dissolved in water at pH 9, **Figure 14**, shows one weak oxidation couple located at a half wave potential of -0.11 V versus SCE. The oxidation couple is quasi-reversible and showed a slight enhancement of the cathodic currents relative to anodic currents, behaviour that is typical of weakly adsorbed product [27]. An enhancement of the cathodic currents have been reported before in our laboratory for the cyclic voltammograms of the solutions of $[(CN)_2Ru(II)Pc]^{2-}$ in water [19] and was attributed to the weak adsorption of the oxidized products on the electrode surface [29].

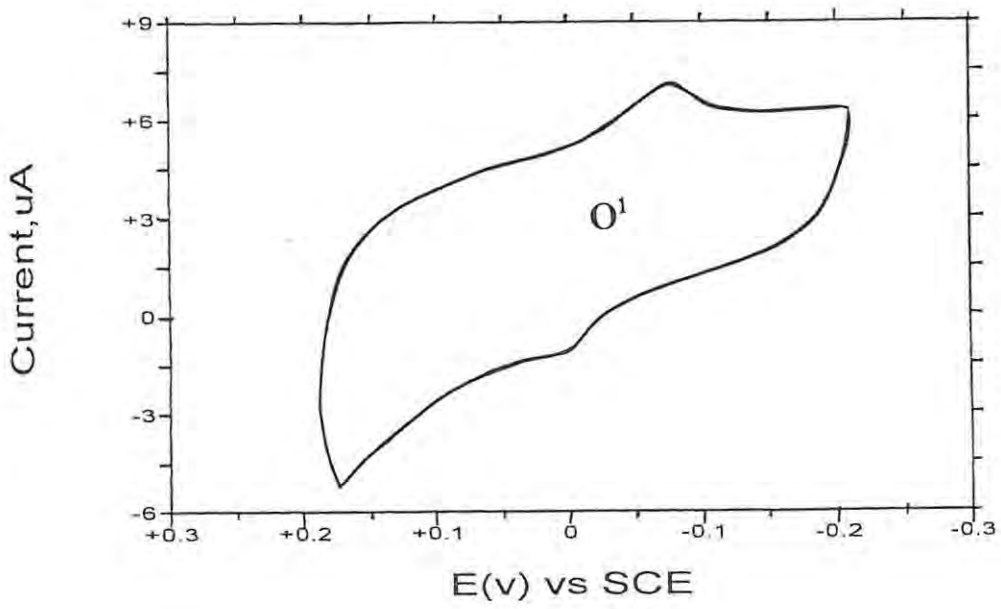

Figure 14: Cyclic voltammogram of $[(CN)_2Os(II)Pc]^{2-}$ in pH 9 buffer. Scan rate 200 mVs^{-1}.

Controlled potential electrolysis of $[(CN)_2Os(II)Pc]^{2-}$ at potential slightly more positive of the first oxidation couple, (-0.11 V), was carried out in order to determine the overall number of

electrons transferred during oxidation and to electrogenerate the oxidation products in order to determine their electronic absorption spectra which would help in confirming the site of oxidation. Exhaustive electrolysis at this potential resulted in electrocrystallization and adsorption of the product to the electrodes, implying that the oxidized products are less soluble in water than the original $[(CN)_2Os(II)Pc]^{2-}$ complex, hence it was difficult to obtain meaningful spectral changes. Chemical oxidation of $[(CN)_2Os(II)Pc]^{2-}$ in water at pH 9, using bromine, resulted in spectral changes shown in **Figure 15**.

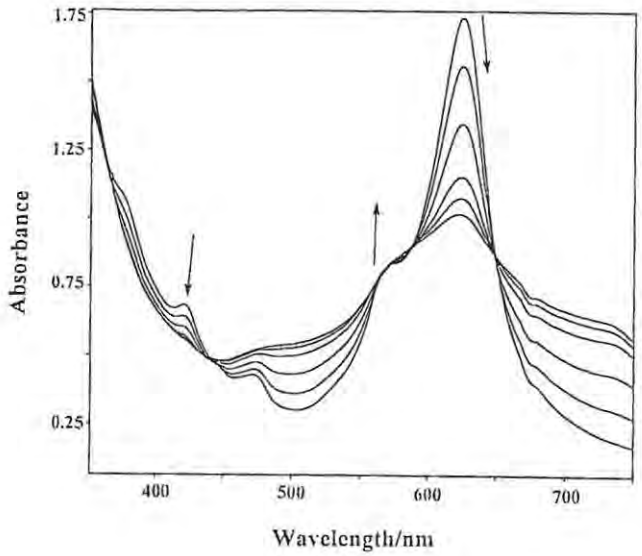

Figure 15 Spectral changes observed on chemical oxidation of $[(CN)_2Os(II)Pc]^{2-}$

The original bands located at 625 and 422 nm decreased in intensity and a new band was formed at 567 nm. The solution changed from blue to purple. The new band at 567 nm, was formed with clear isosbestic points at 648, 588, and 440 nm. Clear isosbestic points normally indicate that there are only two species in equilibrium in the solution. As mentioned in the introduction, the change of colour of the MPc solution from blue to purple, the loss of intensity of the Q band

and the formation of the new band at approximately 500 nm is normally associated with the oxidation at the phthalocyanine ring. Oxidation at the central metal is normally characterized by the shift of the Q band without significant loss of intensity. The intensity of the Q band is only affected if an electron is added or removed from the phthalocyanine ring. The spectral changes observed in Figure 15 can therefore be attributed to the oxidation of the phthalocyanine ring in $[(CN)_2Os(II)Pc]^{2-}$ and the formation of the $[(CN)_2Os(II)Pc(-1)]^{-}$ π- cation radical species. When sodium borohydride ($NaBH_4$) was added to the purple solution of $[(CN)_2Os(II)Pc(-1)]^{-}$ the original $[(CN)_2Os(II)Pc]^{2-}$ species was regenerated.

Cyclic voltammetry of $[(CN)_2Os(II)Pc]^{2-}$ in acetonitrile and in DMF

The cyclic voltammetry of $[(CN)_2Os(II)Pc]^{2-}$ was studied in DMF and in acetonitrile with TEAP employed as an electrolyte. The cyclic voltammogram of $[(CN)_2Os(II)Pc]^{2-}$ in DMF showed two oxidation couples, $\mathbf{O^1}$ and $\mathbf{O^2}$, and two reduction couples, $\mathbf{R^1}$ and $\mathbf{R^2}$, **Figure 16**.

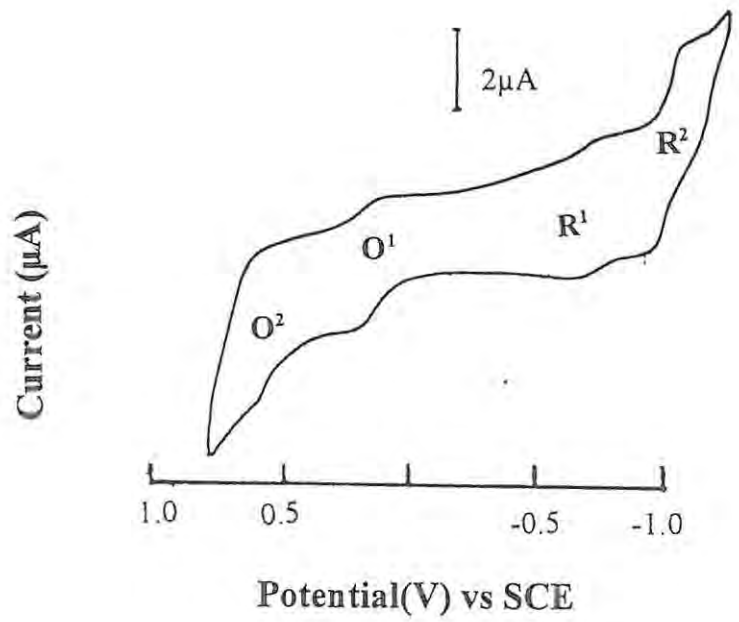

Figure 16: Cyclic voltammogram of $[(CN)_2Os(II)Pc]^{2-}$ in DMF containing TEAP. Scan rate 200 mVs^{-1}.

The half wave potential ($E_{1/2}$) for the first oxidation in DMF was observed at 0.25V versus SCE and in acetonitrile at 0.21V versus SCE, **Table 7**. The separation of anodic (E_{pa}) and cathodic (E_{pc}) peak potentials (ΔE) is approximately 60 mV, the value which is known to correspond to a reversible one electron transfer. The ratio of anodic to cathodic peak currents is close to unity, indicative of a reversible system. The reduction couples were quasi-reversible one-electron systems with ΔE values ranging from 70 to 100 mV.

Table 7: Half-wave potentials for the $M(II)PcL_2$ complexes.

M = Os and Ru.

			$E_{1/2}$ vs SCE			
Complex	**solvent**	**Electrolyte**	**O^2**	**O^1**	**R^1**	**R^2**
$[CN)_2Os(II)Pc]^{2-}$	DMF	TEAP	0.63	0.21	-0.73	-1.05
	CH_3CN	TEAP	0.67	0.25	-0.68	-0.86
	H_2O	pH 9 buffer		-.11		
$(Py)_2Os(II)Pc$	DMF	TEAP	0.80	0.62	-0.69	-1.09
	CH_3CN	TEAP	0.78	0.54	-0.69	-0.89
(DMSO)2Os(II)Pc	DMF	TEAP	0.79	0.68	-0.59	-0.81
$[(CN)_2RuPc]^{2-}$	CH_3CN	TEAP	1.15	0.45		
	H_2O	pH 9 buffer		0.29		
$(Py)_2RuPc$	DMF	TEAP	1.38	0.54		

$E_{1/2}$ values in DMF and CH_3CN were determined using ferrocene as an internal standard (section 2.5.1) and the values were calculated versus SCE as explained in section 2.5.1.

The $E_{1/2}$ values for the first oxidation of $[(CN)_2Os(II)Pc]^{2-}$ in DMF or CH_3CN are slightly higher than the reported potentials for the first oxidation of $[(CN)_2Fe(II)Pc]^{2-}$ to $[(CN)_2Fe(III)Pc]^-$, which occurs at $E_{1/2}$ = 0.14 V versus SCE in DMSO [114] but are lower than the values reported for ring oxidation of $[(CN)_2RuPc(-2)]^{2-}$ to $[(CN)_2RuPc(-1)]^-$ at 1.15 V versus SCE in

acetonitrile [19]. In fact the $E_{1/2}$ values for the first oxidation of $[(CN)_2Os(II)Pc]^{2-}$ are lower than the values reported for ring oxidation of the MPc complexes in general, in the same solvents [29,42]. In order to confirm on the site of oxidation and to determine the number of electrons transferred in each oxidation step, controlled potential electrolysis of the solution of $[(CN)_2Os(II)Pc]^{2-}$ in acetonitrile was carried out at a potential slightly positive of the first oxidation, with TEAP employed as an electrolyte. The products of electrolysis were characterized by electronic absorption spectroscopy. Before electro-oxidation, the absorption spectral bands for $[(CN)_2Os(II)Pc]^{2-}$ **Figure 17**, were observed at 607, 557, 479, 453, 435, 427 and 385 nm. As oxidation proceeded, the blue solution of $[(CN)_2Os(II)Pc]^{2-}$ turned purple. The original absorption spectra bands decreased in intensity and new bands were formed at 658, 548, and 476 nm, with clear isosbestic points at 626, 574 and 458 nm.

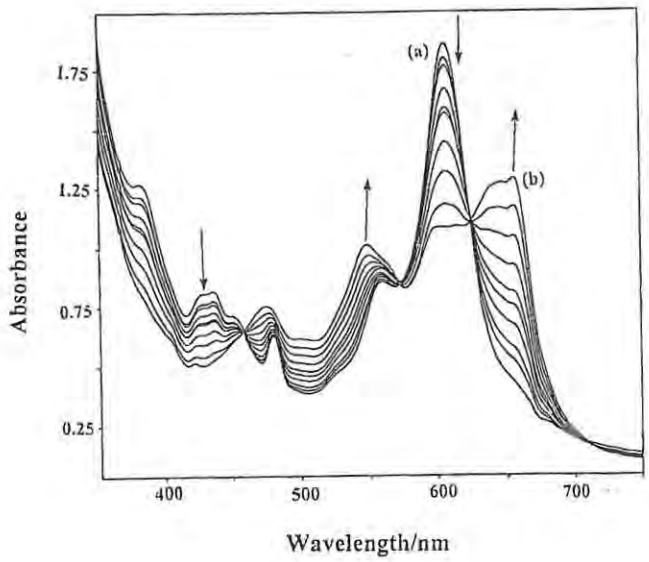

Figure 17: Electronic spectral changes observed during controlled potential electrolysis, at 0.35 V vs SCE, of $[(CN)_2Os(II)Pc]^{2-}$ in acetonitrile containing TEAP.

Where. (a) = The spectra of the original $[(CN)_2Os(II)Pc(-2)]^{2-}$.

(b) = The spectra of the oxidized $[(CN)_2Os(II)Pc(-1)]^{-}$.

As already mentioned, the change of colour from blue to purple in MPc complexes and the formation of broad band near 500 nm are characteristic of the MPc π-cation radical species. The value of n = 0.98 ± 0.02 was obtained as the number of moles of electrons transferred during oxidation potential of the first oxidation couple. The final spectra obtained on one-electron oxidation of $[(CN)_2Os(II)Pc(-2)]^{2-}$ is therefore assigned to the formation of $[(CN)_2Os(II)Pc(-1)]^{-}$ π-cation species. Generally, the presence of a broad band near 700 nm in the spectra of MPc π-cation radical species is associated with dimerization of the radical species [115]. The absorption band located at 658 nm in **Figure 17**, could be due to dimerization of the $[(CN)_2Os(II)Pc(-1)]^{-}$ π-cation radical species. The spectral changes observed in **Figure 17**, were also obtained by bromine oxidation of $[(CN)_2Os(II)Pc]^{2-}$ in acetonitrile.

When the π-cation radical species, $[(CN)_2Os(II)Pc]^{-}$ was chemically reduced with sodium borohydride ($NaBH_4$) or reduced at zero volts with controlled potential electrolysis, the original $[(CN)_2Os(II)Pc]^{2-}$ species was regenerated. The exposure of the solid $K_2[(CN)_2Os(II)Pc]$ complex to bromine fumes let to the formation of the π-cation radical species with the infrared spectra that showed bands typical of π-cation radical species near 1040 and 1440 cm^{-1} [19,116], which are observed at 1070 and 1440 cm^{-1} for $[(CN)_2Os(II)Pc]^{-}$ **Figure 18.**

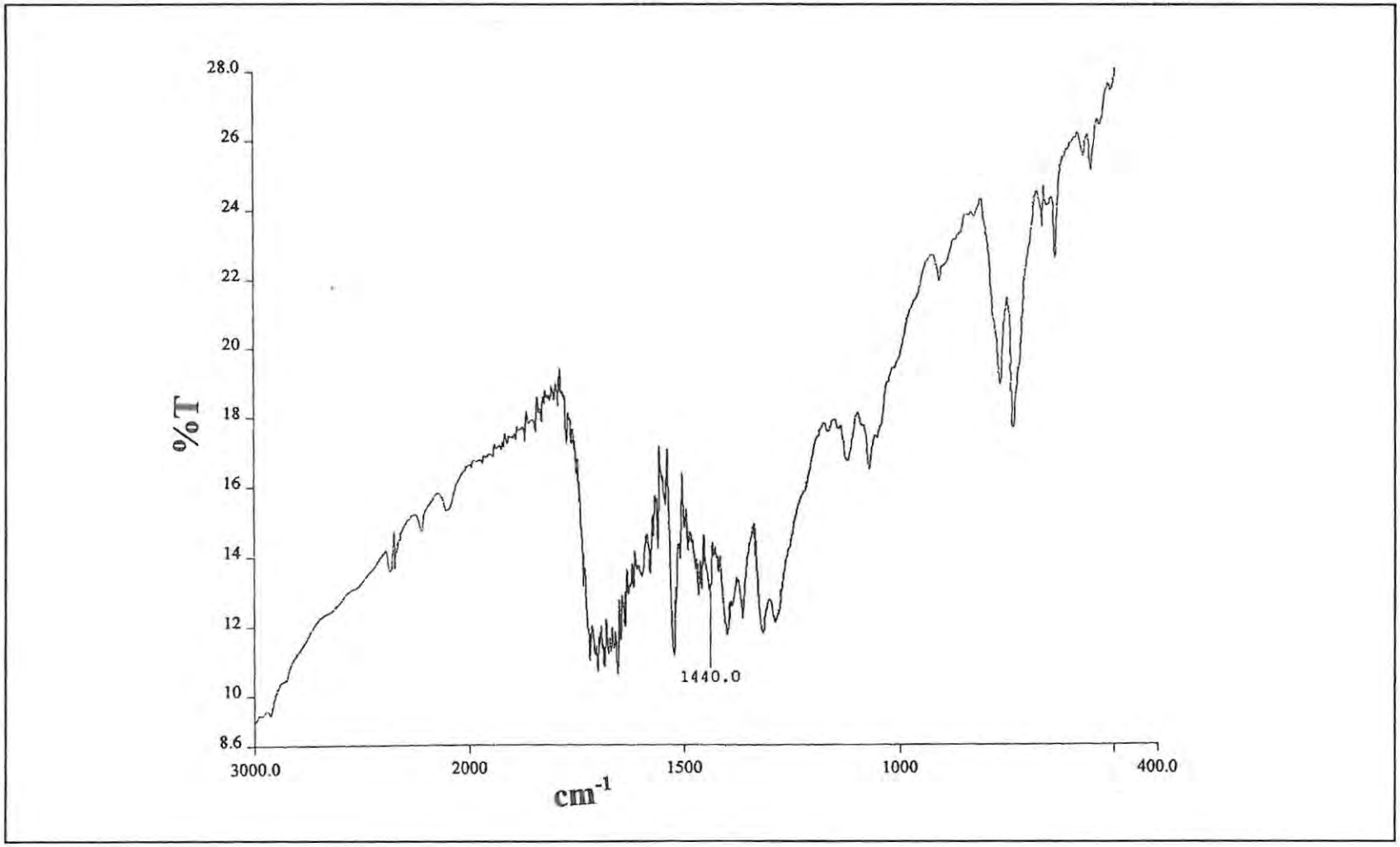

Figure 18 Infrared spectra of bromine oxidized $K_2[(CN)_2Os(II)Pc]$ recorded in KBr disks

The bromine oxidized species gave a magnetic moment of u_{eff} = 1.8 B.M (B.M = Bohr Magneton). This value is close to that expected for one unpaired electron. The diamagnetic correction of -290 x 10^{-6} c.g.s units was employed [117]. The second oxidation couple for $[(CN)_2Os(II)Pc]^{2-}$ in DMF is located at 0.63V versus SCE and at 0.67V versus SCE in acetonitrile. Controlled potential electrolysis at potentials of the second oxidation couple in acetonitrile resulted in the solution changing colour from purple to yellow and the formation of a relatively featureless absorption band observed near 450 nm, **Figure 19**.

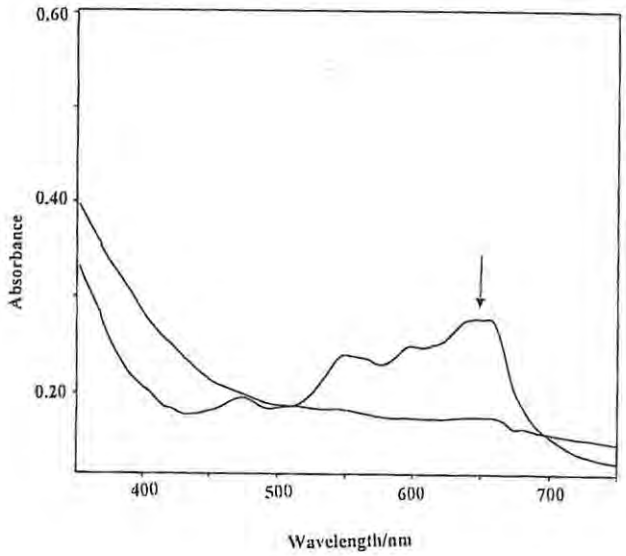

Figure 19 Electronic spectral changes observed during controlled potential electrolysis of $[(CN)_2Os(II)Pc]^{2-}$ at 0.77 V vs SCE, in acetonitrile containing TEAP.

In reported studies on $[(CN)_2Ru(II)Pc]^{2-}$ species [19], the absorption band near 450 nm was associated with the second oxidation of the phthalocyanine ring. Even though the absorption band formed for controlled potential electrolysis of $[(CN)_2Os(II)Pc(-2)]^2$ is relatively featureless, it could not be due to decomposition since it is reversible. The species formed on oxidation of

$[(CN)_2Os(II)Pc(-2)]^{2-}$ at potential of the second oxidation couple could possibly be due to the second oxidation of the ring and the formation of $(CN)_2Os(II)Pc(0)$.

The first reduction couple for $[(CN)_2Os(II)Pc]^{2-}$ in DMF, is located at $E_{1/2}$ = -0.73 V versus SCE. This value is in the range reported for ring reduction in other third-row transition metal phthalocyanines [19]. This couple is assigned to the reduction of the phthalocyanine ring in $[(CN)_2Os(II)Pc(-2)]^{2-}$ and the formation of $[(CN)_2Os(II)Pc(-3)]^{3-}$ species. Reduction at the metal to form Os(I)Pc species is unlikely, since the literature reports have shown that coordination compounds containing monovalent osmium(I) are very rare [118]. No spectral changes were observed on controlled potential electrolysis of $[(CN)_2Os(II)Pc]^{2-}$ at potentials of the first reduction couple, suggesting that the monoanion species, $[(CN)_2Os(II)(-3)]^{3-}$, is only stable on cyclic voltammetry scale.

The first reduction couple is separated from the first oxidation couple by 0.93 V. This value is very low when compared to the normal value of approximately 1.6 V for the separation between the first ring oxidation and the first ring reduction in transition metal phthalocyanine, and is reported to correspond to the magnitude of energy difference between the HOMO and the LUMO in MPc complexes [25,29,30]. This low value of $\Delta E_{1/2}$ for $[(CN)_2Os(II)Pc]^{2-}$ could be due to the relative ease of ring reduction in this species when compared with other MPc complexes. The ease of ring reduction in $[(CN)_2Os(II)Pc]^{2-}$ species might be due to the presence of the electron withdrawing axial cyanide ligands. Coordination of electron withdrawing groups, such as CN^- onto the metalloporphyrins and metallophthalocyanines is known to lead to a thermodynamically easier reduction of the complex, because the cyanide groups decrease the average electron density on the total conjugated system, which results in a lowering of the energy level of the LUMO. This increases the electron affinity of the phthalocyanine ring and thus leads to easier reductions [32]. The second reduction couple for

$[(CN)_2Os(II)Pc]^{2-}$ complex observed at -1.05 V vs SCE probably corresponds to further reduction of the ring in $[(CN)_2Os(II)Pc(-3)]^{3-}$ and the formation of $[(CN)_2Os(II)Pc(4-)]^{4-}$ species.

3.2 *Synthetic route for the preparation of bis(pyridine)(phthalocyaninato) osmium(II) $(py)_2Os(II)Pc$ and $(DMSO)_2Os(II)Pc$.*

The preparation of bis(pyridine)(phthalocyaninato)osmium(II), (py)Os(II)Pc, was carried out by refluxing crude Os(II)Pc in pyridine, **Scheme 9**. The detailed method of synthesis is described in section 2.1.3.

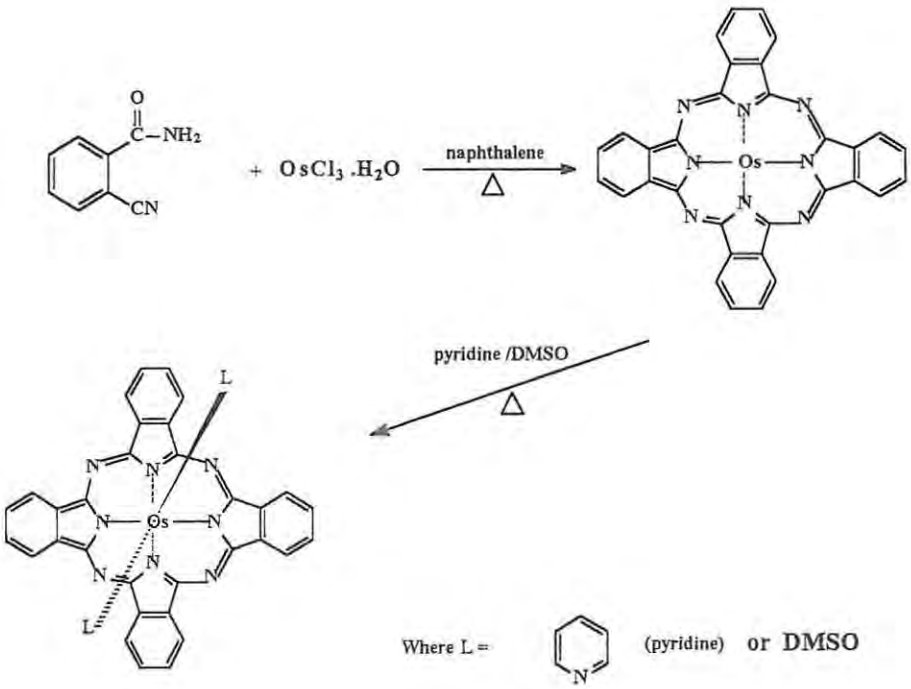

Scheme 9 Synthesis of $(py)_2Os(II)Pc$.

3.2.1 Spectroscopic characterization of $(py)_2OS(II)Pc$

Unlike $[(CN)_2Os(II)Pc]^{2-}$, $(py)_2Os(II)Pc$ was found to be insoluble in water. The electronic absorption band in acetonitrile is typical of the $(py)_2M(II)Pc$ complexes [103] with the Q band located at 612 nm and the soret band at 367 nm, **Figure 20.**

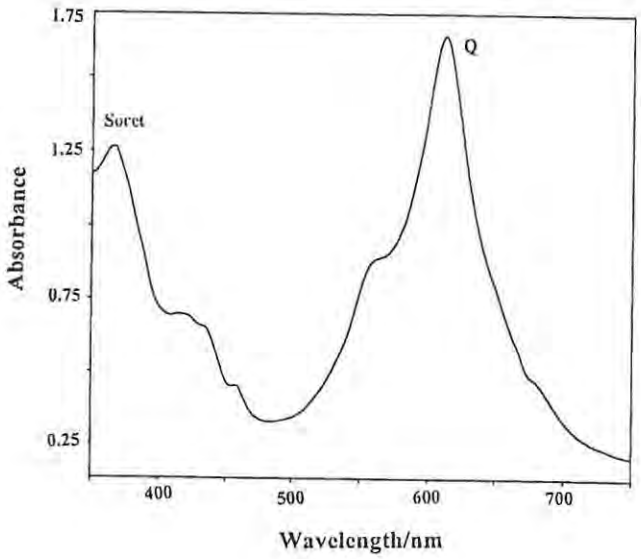

Figure 20 Electronic absorption spectra of $(py)_2Os(II)Pc$ in acetonitrile.

There are other two bands located at 434 and 420 nm. In reported studies by Hanack *et al* [103] the absorption bands in this region have been assigned to the charge transfer transitions between the metal and the ligand. Like all the Os(II)Pc complexes the Q band for $(py)_2Os(II)Pc$ is blue shifted when compared to that of $(py)_2Ru(II)Pc$ located at 625nm [103]. This behaviour has been correlated to the $d\pi$-donor ability of the central metal. **Figure 21** shows the infrared spectra of $(py)_2Os(II)Pc$ complex recorded on KBr disks. The pyridine C-H stretch are observed at 3055cm^{-1} and the C-N aromatic stretch at 1300 - 1360 cm^{-1}. The other vibrational bands exhibited by $(py)_2Os(II)Pc$ are typical of the phthalocyanine macrocycle.

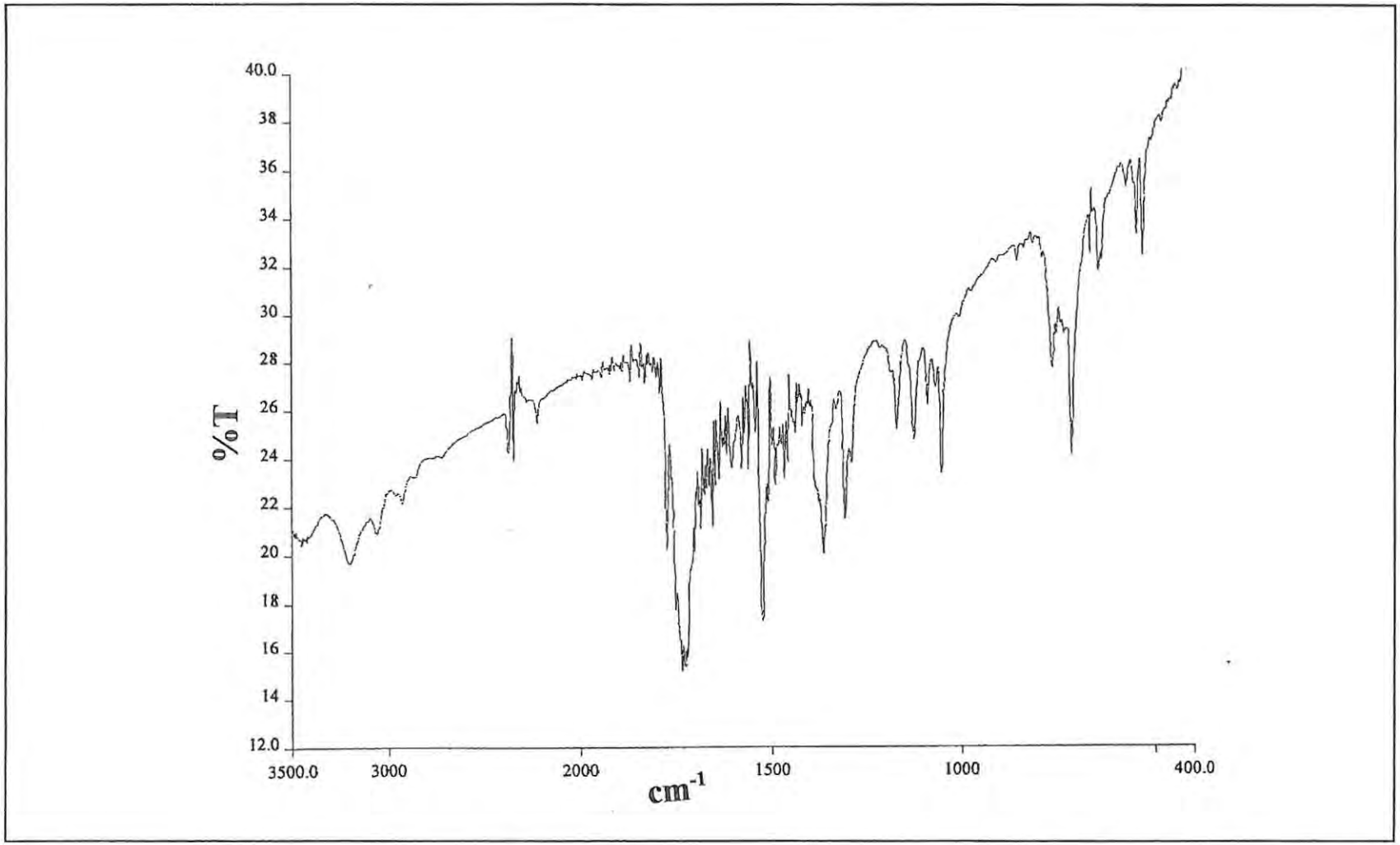

Figure 21 Infrared spectra of $(py)_2Os(II)Pc$ recorded in KBr disks

3.2.2 *Redox properties of $(py)_2Os(II)Pc$*

In this work the cyclic voltammetry for $(py)_2Os(II)Pc$ was determined in DMF and in acetonitrile using TEAP as an electrolyte. The cyclic voltammogram for this complex in acetonitrile show two oxidation couples and two reduction couples, **Figure 22**.

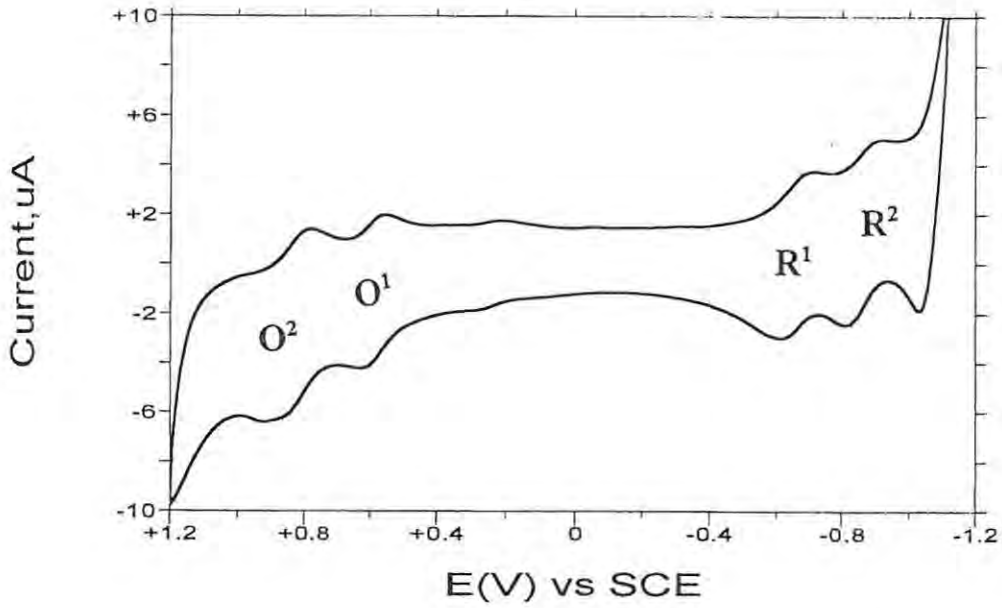

Figure 22 Cyclic Volatammogram of $(py)_2Os(II)Pc$ in acetonitrile containing TEAP. Scan rate 200 mVs^{-1}.

The oxidation couples were reversible with ΔE of 60 mV, indicative of one-electron reversible system. The first oxidation couple is located at 0.62 V versus SCE in DMF and at 0.54 V versus SCE in acetonitrile, **Table 7**. These values are within the range reported for the ring oxidation in MPc complexes. [19,29,30,99]. This suggests that the first electron in $(py)_2Os(II)Pc$ is removed from the phthalocyanine ring.

Bulk electrolysis of solutions of $(py)_2Os(II)Pc$ in acetonitrile and at potential of the first oxidation, gave the spectral changes observed in **Figure 23**.

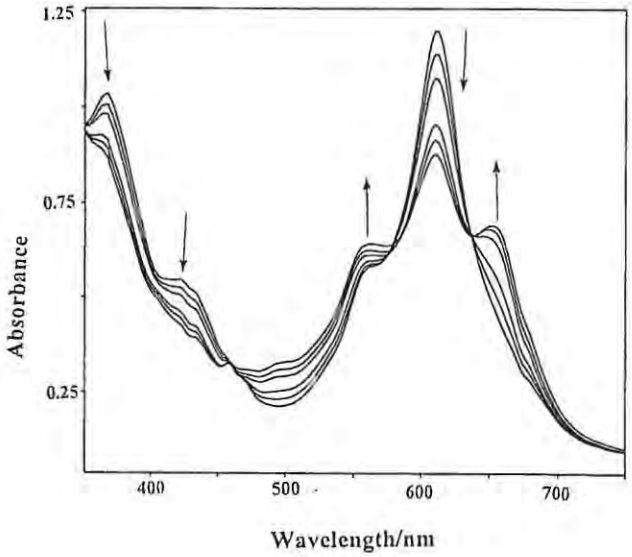

Figure 23: Electronic absorption spectral changes observed during controlled potential electrolysis at 0.65V versus SCE, of $(py)_2Os(II)Pc$ in acetonitrile.

The blue solution of $(py)_2Os(II)Pc$ changed to purple and the original bands located at 612, 433, 422 and 367 nm decreased in intensity and the new bands were formed at 562 and 657 nm with isosbestic points at 637 and 462 nm. It has been mentioned above for $(CN)_2Os(II)Pc$ that the change of colour from blue to purple and the formation of new band around 550 nm are characteristic of the formation of the MPc π-cation radical species. The value of $n = 0.89 \pm 0.05$ was obtained. The final spectra obtained on one-electron oxidation in $(py)_2Os(II)Pc(-2)$ may be assigned to the formation of $[(py)_2Os(II)Pc(-1)]^+$.

The second oxidation couple was observed at 0.80 V versus SCE in DMF and in acetonitrile

at 0.78V versus SCE. This couple is assigned for further oxidation of the ring and the formation of $[(py)_2Os(II)Pc(0)]^{2+}$.

3.2.3 Spectral and electrochemical characterization of Bis(dimethylsulphoxide)(phthalocyaninato)osmium(II), $(DMSO)_2Os(II)Pc$

Bis(dimethylsulphoxide)(phthalocyaninato)osmium(II) was synthesized by refluxing crude Os(II)Pc in dimethyl sulphoxide. The preparative scheme is the same as Scheme 9 except that DMSO was used for refluxing instead of DMF. The detailed method of preparation is described in section 2.1.3. $(DMSO)_2Os(II)Pc$ does not dissolve in water. The electronic absorption spectra is very similar to that of the other $(DMSO)_2M(II)Pc$ complexes, **Figure 24**.

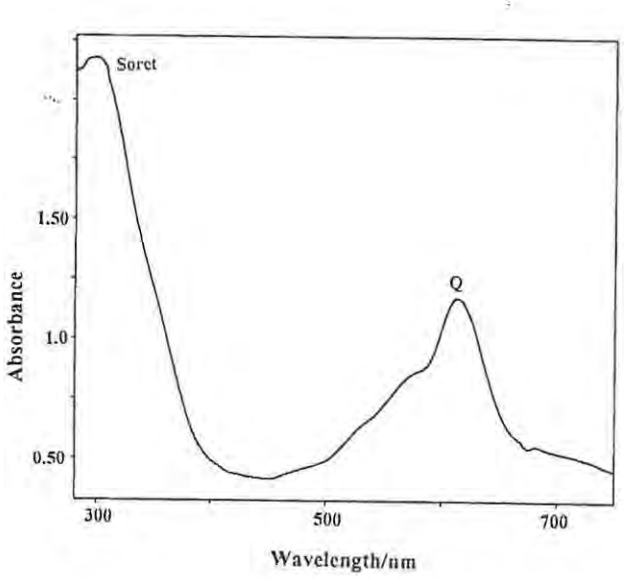

Figure 24 Electronic absorption spectra of $(DMSO)_2Os(II)Pc$ in DMF.

The Q band in DMF is located at 612 nm and the soret band at 297 nm. Unlike in $(py)_2Os(II)Pc$ there are no clear bands indicating the presence of charge transfer transitions, but the broadness

of the Q band implies the presence of underlying charge transfer transitions. The infrared spectral data for this complex is presented in experimental section and shown in Figure 25. The S=O stretch band is observed at 1124 - 1169 cm^{-1} indicative of S bonded DMSO. There are no bands in the 950 cm^{-1} region, which would be characteristic of oxygen bonded DMSO. C-H stretch of the methyl groups are observed at 2847 - 2922 cm^{-1}.

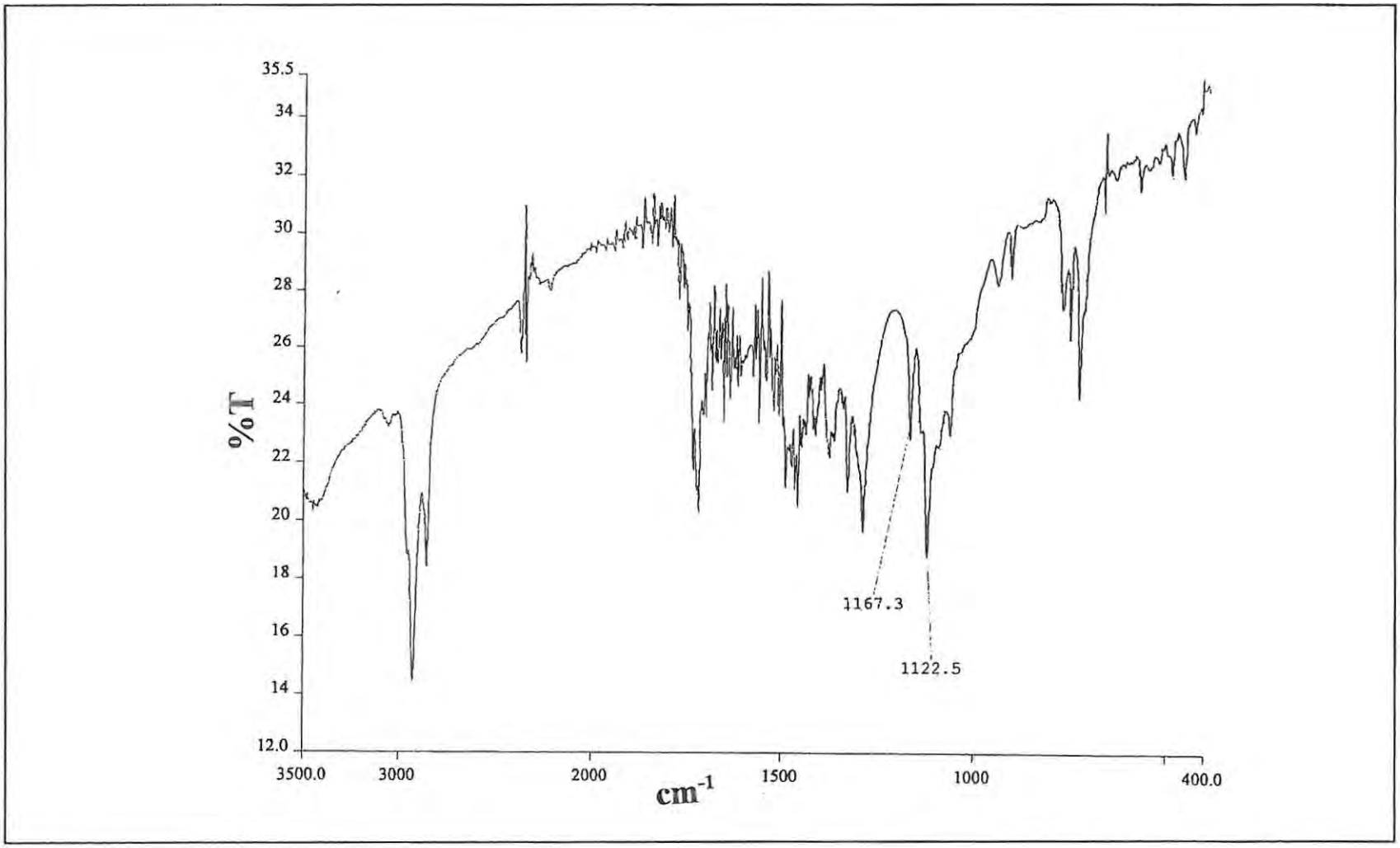

Figure 25 Infrared spectra of Os(II)Pc(DMSO)$_2$.DMSO recorded in KBr disks

The cyclic voltammogram of $(DMSO)_2Os(II)Pc$ in DMF showed two oxidation couples, **Figure 26.** The $E_{1/2}$ value for the first oxidation of $(DMSO)_2Os(II)Pc$ was observed at higher potentials than the values observed for $[(CN)_2Os(II)Pc]^{2-}$, $(py)_2Os(II)Pc$, $[(CN)_2Ru(II)Pc]^{2-}$ and $(py)_2Ru(II)Pc$, **Table 7**.

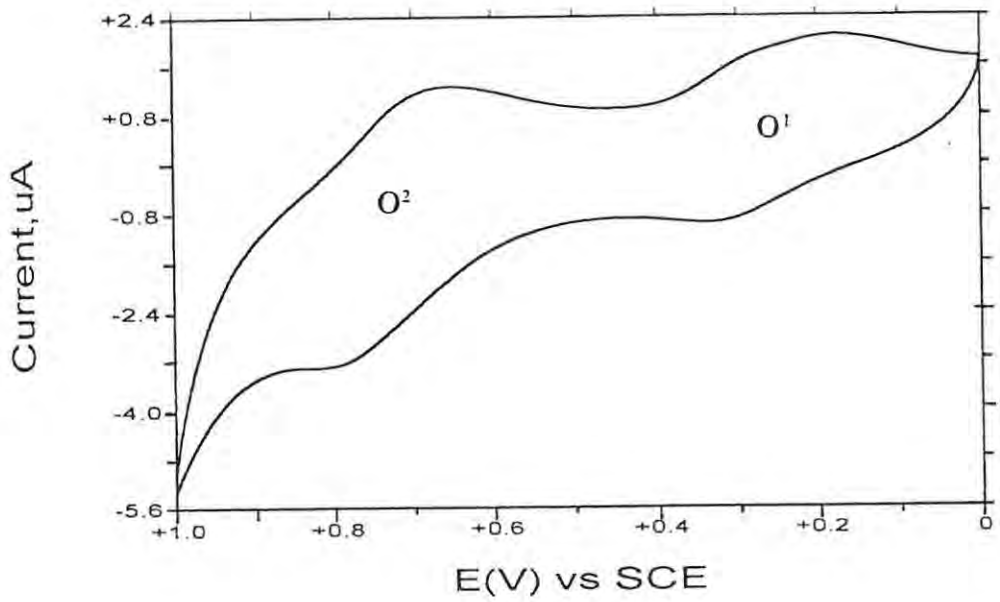

Figure 26 cyclic voltammogram of $(DMSO)_2Os(II)Pc$ in DMF containing TEAP. Scan rate: 50 mVs^{-1}.

Dolphin *et al* [20] have shown that the $E_{1/2}$ values for the first oxidation of L_2RuPc complexes (L = py, imid, DMF, DMSO, and CH_3CN) decrease in accordance with the increasing electron donor strength of the axial ligand. Electron donating ligands such as pyridine tend to decrease the electron density of the MPc complex, thus making the ring easier to oxidize. CN^- is known to act both as an electron donor and also as an electron acceptor. The low values for the first oxidation potential of $[(CN)_2Os(II)Pc]^{2-}$ and $[(CN)_2Ru(II)Pc]^{2-}$ as compared to that of $(DMSO)_2Os(II)Pc$ may be attributed to the strong σ-donating ability of the cyanide ligand when

compared with DMSO.

3.3 Tetramethyltetrapyridinoporphyrazine complexes of palladium(II) and platinum (II)

The tetramethyltetrapyridinoporphyrazine complexes of palladium(II) and platinum(II) were synthesized by reacting the tetrapyridinoporphyrazine derivatives with dimethyl sulphate in refluxing DMF under nitrogen atmosphere. **Scheme 10** shows the synthetic route for the NN'N"N'"-tetramethyltetra-2,3-pyridinoporphyrazines for (a) palladium(II) and (b) platinum(II), while **Scheme 11** shows the preparative route for the NN'N"N'"-tetramethyltetra-3,4-pyridinoporphyrazines of (a) palladium(II) and (b) platinum(II). The detailed procedures for the synthesis are outlined in sections 2.1.4 and 2.1.5 respectively.

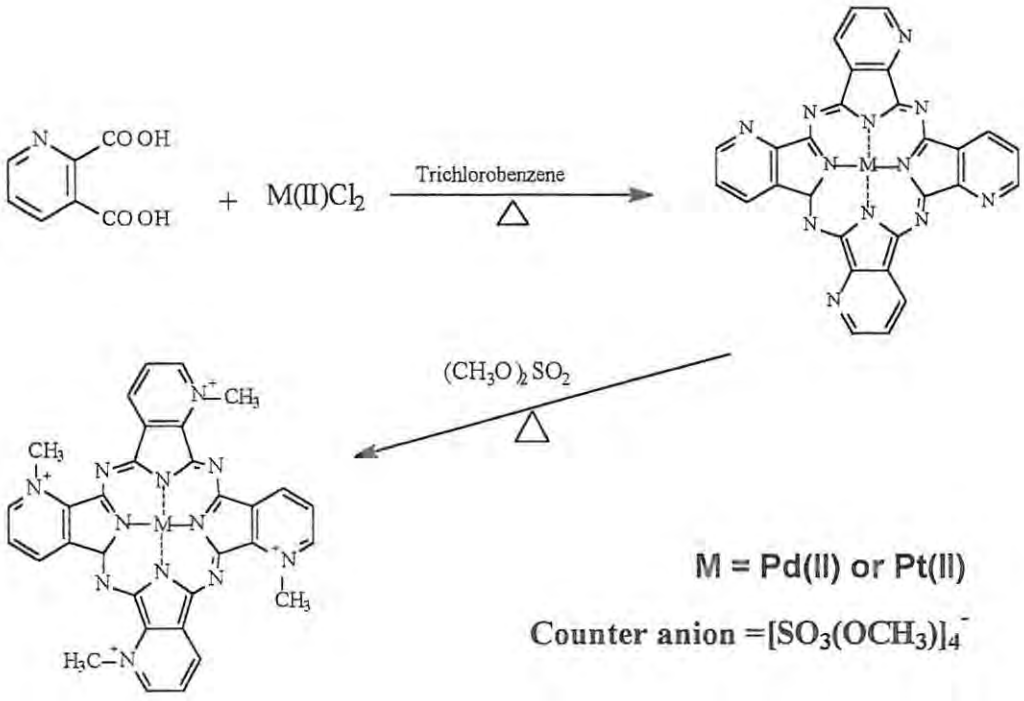

Scheme 10 Synthetic route for the preparation of the tetramethyltetra-2,3-pyrdinoporphyrazine complexes of palladium and platinum(II).

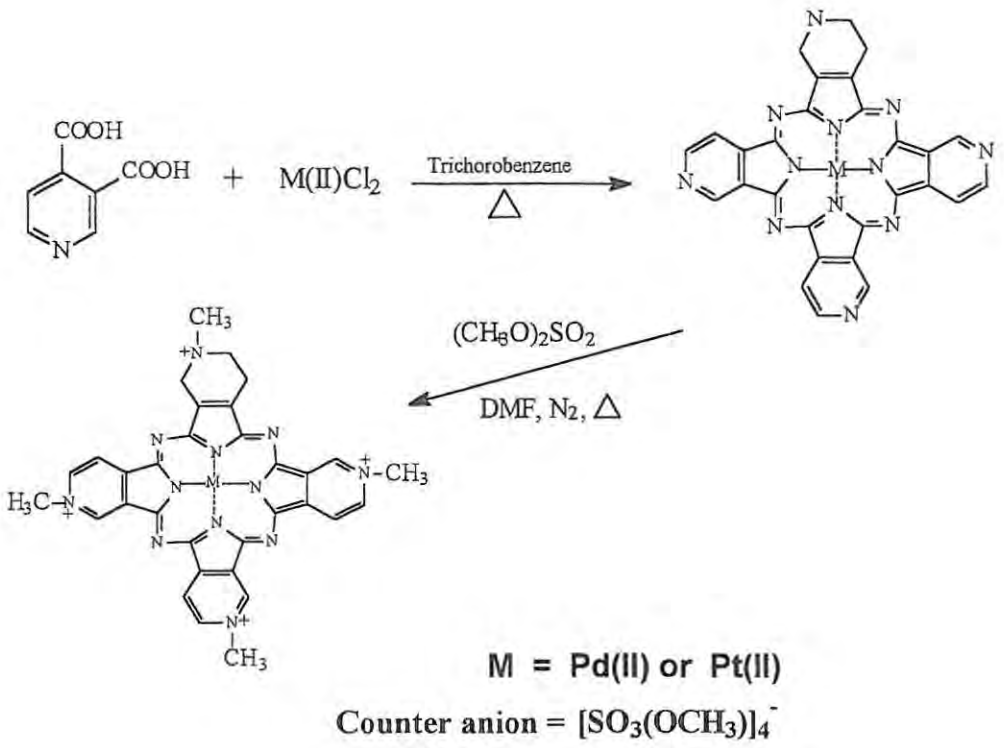

Scheme 11 Synthetic route for tetramethyltetra-3,4-pyridinoporphyrazine complexes of palladium(II) and platinum(II).

3.3.1 Spectroscopic characterization of palladium(II) and platinum(II) tetramethyltetrapyridinoporphyrazine complexe

The 2,3 and 3,4 tetramethyltetrapyridinoporphyrazine complexes of palladium(II) and platinum(II): $[Pd(II)2,3Tmtppa]^{4+}$, $[Pd(II)3,4Tmtppa]^{4+}$, $[Pt(II)2,3Tmtppa]^{4+}$ and $[Pt(II)3,4Tmtppa]^{4+}$ are highly soluble in water. These compounds have very similar electronic absorption spectra. The spectra resemble that of the metallophthalocyanine species, except that for the tetramethyltetrapyridinoporphyrazine (Tmtppa) complexes the Q

band is split, **Figure 27**.

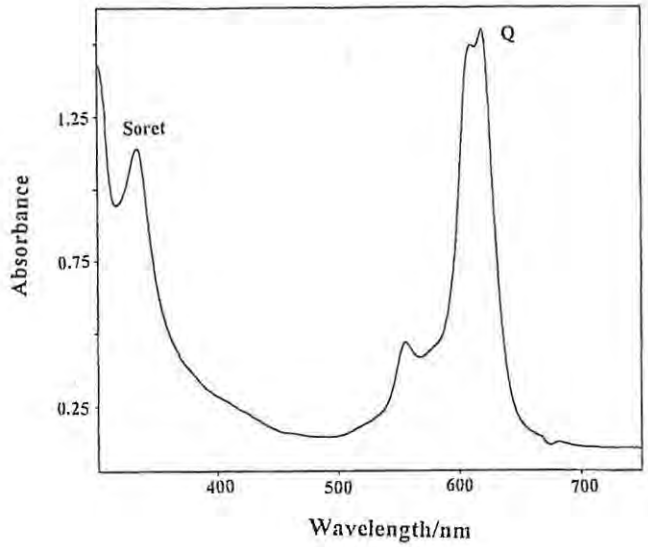

Figure 27 Electronic absorption spectra for $[Pd(II)Tmtppa]^{4+}$ in distilled water.

The split Q band has been observed before for DMF insoluble Zn and Cu Tmtppa complexes [59]. The electronic absorption data for these complexes are presented under experimental in sections 2.1.3 and 2.1.4, respectively. The Q band exhibited by the Pd(II) and Pt(II) Tmtppa complexes is quite sharp, even though it is split, indicating that there were no formation of dimmers in aqueous solution. This observation is in agreement with the literature reports which have shown that the $[M(II)Tmtppa]^{4+}$ species have advantage over the tetrasulphonated metallophthalocyanines, in that the $[M(II)Tmtppa]^{4+}$ do not aggregate in aqueous solution [58], a one criteria for photosensitization reactions.

The Mtmtppa complexes dissolve in water to form a blue to greenish solutions at low pHs. In alkaline pHs the blue colour of the solution changes to purple and goes colourless at highly

alkaline pHs. Reports by Smith *et al* [58] have shown that $[Co(II)Tmtppa]^{4+}$ complex is stable in acidic to neutral pHs but tend to decompose in slightly alkaline solutions. Chemical reduction of $[Pd(II)2,3Tmtppa]^{4+}$ with sodium borohydride in distilled water resulted in the change of blue colour of the solution to purple. The absorption spectral changes observed during the reduction are shown in Figure 28. The original bands located at 619, 610, 555, and 334 nm decreased in intensity and a new band was formed at approximately 525nm. Similar absorption spectral changes were obtained when the $[Pd(II)3,4Tmtppa]^{4+}$, $[Pt(II)2,3Tmtppa]^{4+}$, and $[Pt(II)3,4Tmtppa]^{4+}$ were chemically reduced with sodium borohydride.

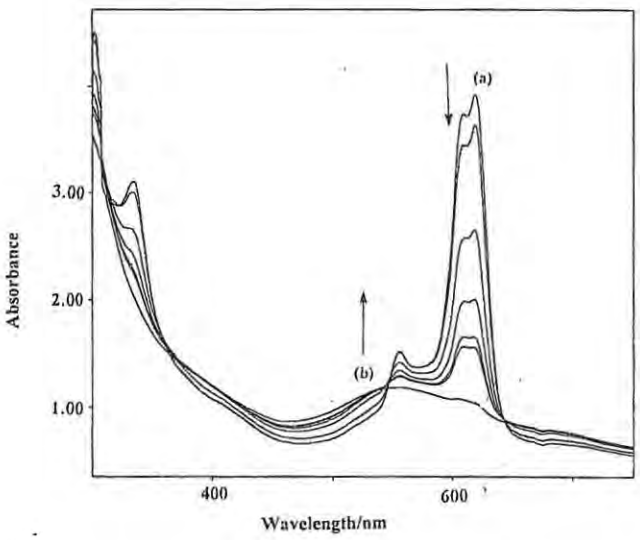

Figure 28 Spectral changes observed on chemical reduction of $[Pd(II)Tmtppa]^{4+}$ with $NaBH_4$.

The formation of a new band at 525 nm and the change of colour from blue to purple during the reduction of $[Co(II)2,3Tmtppa]^{4+}$ complex with ascorbic acid, have been associated with one electron reduction, with the formation of $[Co(I)2,3Tmtppa]^{3+}$ complex [58]. It has been reported that the exposure of the purple solution formed on reduction of $[Co(II)2,3Tmppa]^{4+}$ to molecular oxygen resulted in rapid colour change to the original blue colour. The rapid

colour change was however not observed when the purple solution of the reduced $[Pd(II)Tmtppa]^{4+}$ or $[Pt(II)Tmtppa]^{4+}$ complex was exposed to air but the original blue colour was observed when bromine was added to the purple solution. This may suggest that the site of reduction in these species is different from that of $[Co(II)2,3Tmtppa]^{4+}$. It is likely that reduction on Pd(II) and Pt(II) Tmtppa occurs on the ring and not on the central metal as in $[Co(II)Tmtppa]^{4+}$. In Pd(II) and Pt(II) phthalocyanine complexes reduction have been reported to occur exclusively on the phthalocyanine ring [29].

Chemical oxidation with bromine in these $[M(II)Tmtppa]^{4+}$ complexes in water resulted in the colour of the solution changing from blue to bright green. The absorption spectra, **Figure 29**, showed a decrease in intensity of the Q band and the formation of the new band at near 700 nm.

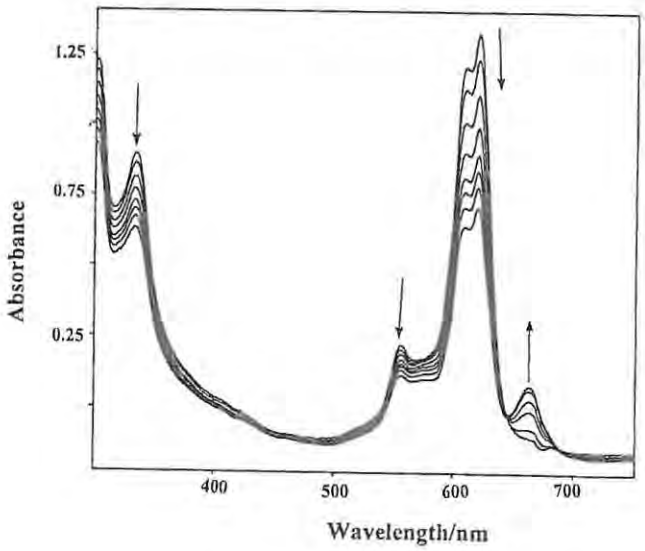

Figure 29 Spectral changes observed on chemical oxidation of $[Pd(II)Tmtppa]^{4+}$ with bromine

In some MPc species, for example $[(CN)_2Ru(II)Pc]^{2-}$, the formation of the new band near 700 nm on oxidation of the species, normally indicate the dimerization of the $[(CN)_2Ru(II)Pc(-1)]^{-}$ π-cation radical. There was no new band formed near 550 nm upon oxidation of $[Pt(II)Tmtppa]^{4+}$ and $[Pd(II)Tmtppa]^{4+}$ complexes as would be expected for the formation of π cation radical species. The colour change also show that π cation radical was not formed. Due to the presence of the positive charges, the oxidation of these complexes is expected to occur with great difficulty, hence the incomplete oxidation observed in Figure 29 is not surprising. When sodium borohydride was added to the bright green solution, the original blue colour of the solution was regenerated, thus indicating that the oxidation was reversible.

The infrared data for the $[Pd(II)2,3Tmtppa]^{4+}$, $[Pd(II)3,4Tmtppa]^{4+}$, $Pt(II)2,3Tmtppa]^{4+}$, and $[Pt(II)3,4Tmtppa]^{4+}$ were recorded in KBr disks, **Figure 30**, and the results are presented in Table 4. The infrared spectra of these $[M(II)Tmtppa]^{4+}$ complexes are very similar and seem to be independent of the central metal ion. This behaviour has been reported in the literature for the infrared of the metallophthalocyanine complexes [49]. Two weak absorption bands at 3033 - 3400 cm^{-1} are observed in all the spectra of the $[M(II)Tmtppa]^{4+}$ complexes. These absorption bands are assigned to the C-H stretching vibrations of the pyridine groups of the macrocyle. Bands around 1218 - 1300 cm^{-1} indicate the presence of the C-N aromatic stretching. The symmetrical and asymmetrical C-H bending vibrations of the methyl groups are observed at 1384 - 1463 cm^{-1}. All other vibrational bands exhibited by the $[M(II)Tmtppa]^{4+}$ complexes can be assigned similarly to those of the phthalocyanine skeletal.

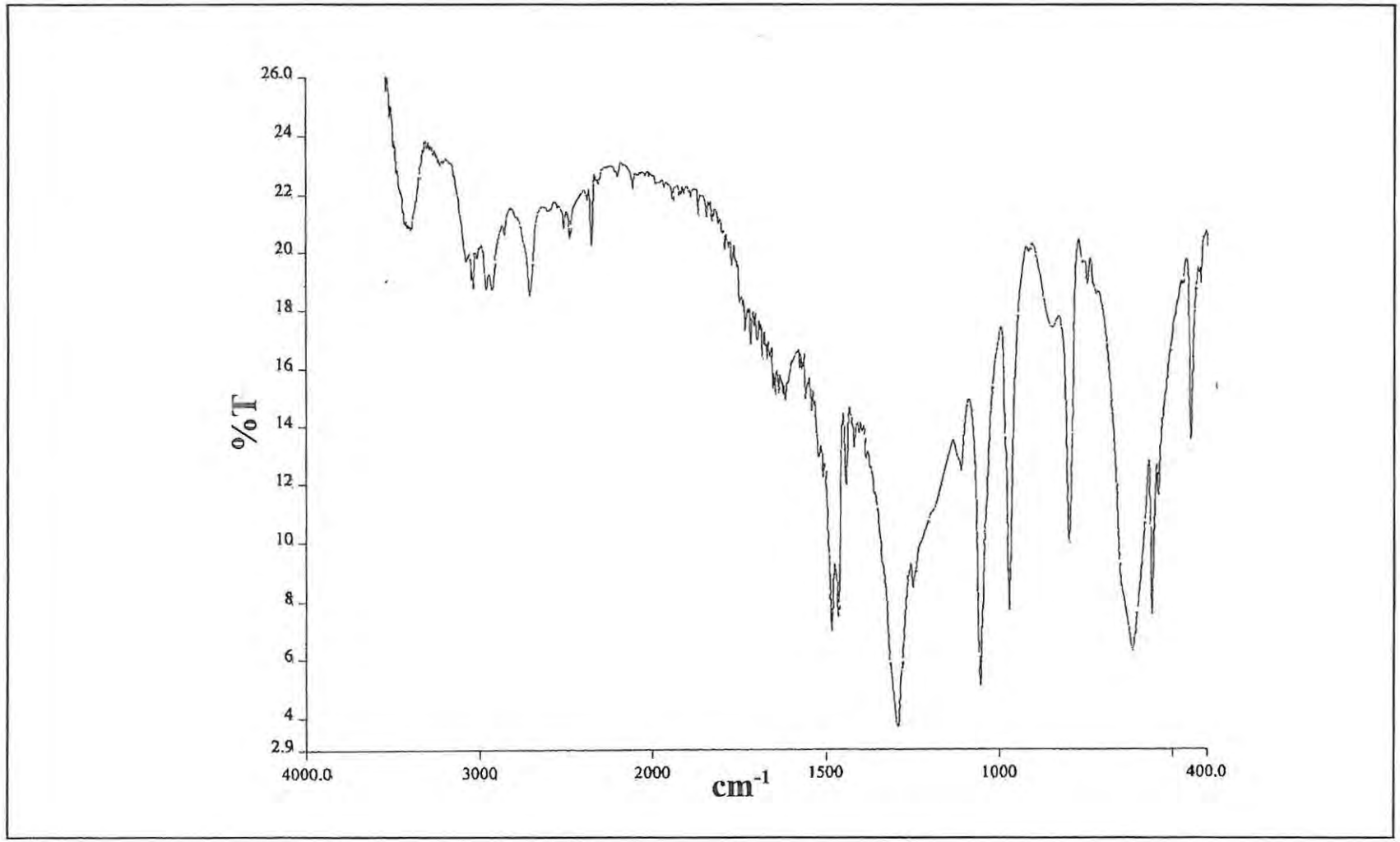

Figure 30 Infrared spectra of $[Pd(II)2,3Tmtppa]^{4+}$ recorded in KBr disks

3.3.2 Redox properties of $[Pd(II)Tmtppa]^{4+}$ and $[Pt(II)Tmtppa]^{4+}$ complexes

Figure 31 shows the cyclic voltammograms for $[Pd(II)2,4Tmtppa]^{4+}$ in water containing Na_2SO_4 on (a) carbon fibre microelectrode and (b) on Pt disc electrode.

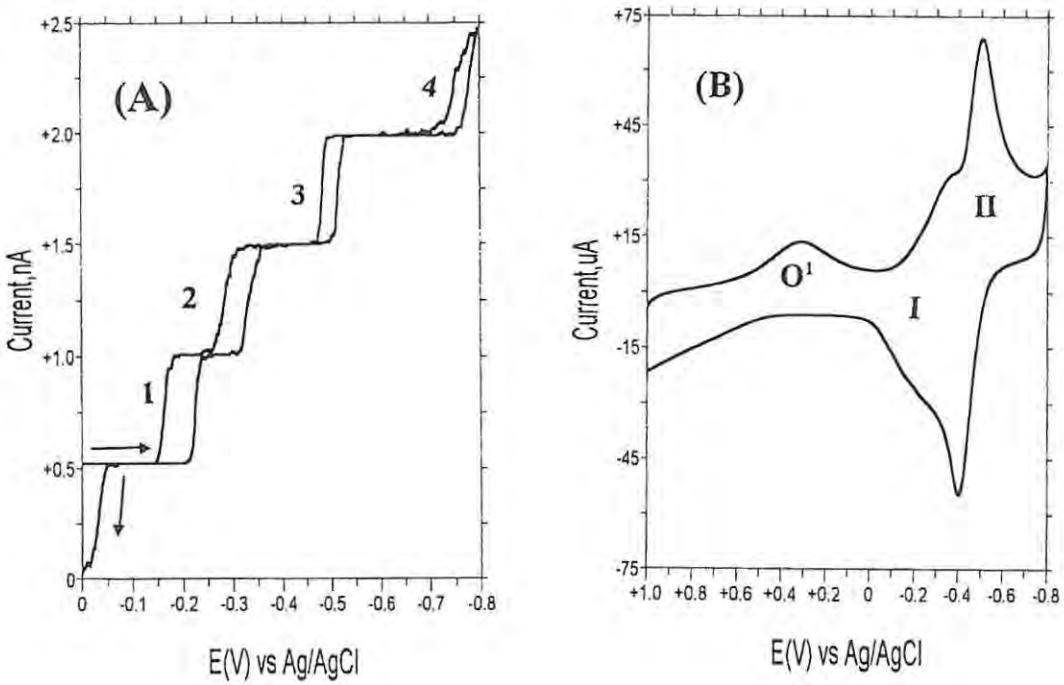

Figure 31 Cyclic voltammogram for $[Pd(II)2,4Tmtppa]^{4+}$ on (a)carbon fibre microelectrode. Scan rate : $5mVs^{-1}$. (b) on platinum disk electrode. Scan rate $100mVs^{-1}$.

At low scan rates (5 mVs^{-1} or less) the cyclic voltammogram for Pd(II)2,3Tmtppa of carbon fibre microelectrode, **Figure 31(a)**, exhibit four reduction processes (1 to 4) of equal height. The equal heights show that the same number of electrons are transferred in each step. Comparing the first and the subsequent scans showed no difference in the nature of the voltammogram showed in **Figure 31(a)**. The cyclic voltammogram of the Pd(II) and the Pt(II) Tmtppa complexes on platinum disc electrode Figure 31 (b) showed two reduction couples, **I** and **II**. An irreversible oxidation peak, O^1, was observed at 0.32 V vs Ag/AgCl. The two reduction couples in **Figure 31(b)** showed a significant overlap. The reduction peaks were observed at more negative potentials on the platinum disc electrode when compared to the

potentials on the carbon fibre electrode. On platinum disc electrode, the reduction potentials for couple (I) for the NN'N"N"'-tetrmethyltetra-2,3-pyridinoporphyrazine metal complexes, were observed near -0.3 V vs Ag/AgCl, and near -0.2 V for the NN'N'N"'-tetramethyltetra-3,4-pyridinoporphyrazine metal complexes. The potentials for the second reduction couple were observed at -0.46 V vs Ag/AgCl on platinum disc electrode for all the complexes.

The $[Pd(II)Tmtppa]^{4+}$ and $[Pt(II)Tmtppa]^{4+}$ complexes studied in this thesis showed very similar cyclic voltammograms. There are no significant differences in the reduction potentials of the corresponding Pt(II) and Pd(II) complexes. For both reduction processes and for the oxidation process there was no change in the nature of the peaks with the successive cyclic voltammogram scans.

There is very little reported data available on the solution chemistry of PdPc and PtPc complexes and this is the first report on the synthesis, spectroscopic and electrochemical properties of Pd(II) and Pt(II) tetrapyridinoporphyrazine complexes. Earlier studies on the polarography of NN'N"N"'-tetramethyltetrapyridinoporphyrazine complexes of Cu(II) and Ni(II) in water showed that these complexes exhibit two reduction waves at -0.55 V and -1.20 V vs SCE [58]. The first reduction wave was associated with the addition of one electron to the porphyrazine complex, and the second wave at -1.20 V was associated with a multi-electron transfer reduction process. Multi-electron transfer have also been reported by Araullo-McAdams *et al* [120] in structurally similar (meso-tetrakis(1-methylpyridinium-4-yl)porphyranato)cobalt, $[CoTmtpp]^{4+}$. Janda *et al* [60] have shown that $[Co(II)Tmtppa(-2)]^{4+}$ get reduced to $[Co(I)Tmtppa(-2)]^{3+}$ in the presence of *l*-ascorbic acid when $[Co(II)Tmtppa(-2)]^{4+}$ was used to coat a carbon microfiber electrode. The same behaviour has been reported by Tse *et al* [68] for $Co(II)Tmtppa(-2)]^{4+}$ when this complex was deposited on highly oriented pyrolytic graphite (HOPG) electrode for the determination

of sulphide concentration by direct potentiometry. In comparison with other $[M(II)Tmtppa]^{4+}$ and the $[CoTmtpp]^{4+}$ complexes, the first reduction in $[Pd(II)Tmtppa]^{4+}$ and $[Pt(II)Tmtppa]^{4+}$ complexes is tentatively assigned to the one electron reduction of the porphyrazine complex with the formation of the monoanion species. Reduction at the central metal is quite unlikely. The second multi-electron process in Figure 31(b) is probably due to the reduction of the methylpyridinium substituents which would require a total of four electrons. For couple **I** the peak currents were found to be proportional to the square root of scan rate ($V^{1/2}$), **Figure 32(a)**, suggesting a reversible diffusion controlled electron transfer process.

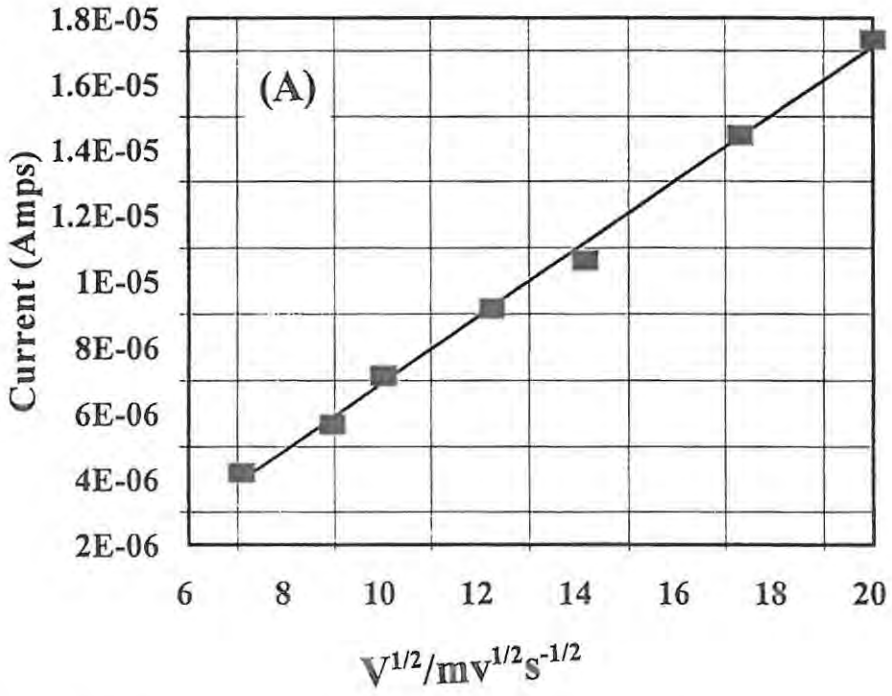

Figure 32(a) Plot of peak current *vs* squareroot of scan rate for couple **I**.

The peak currents for couple **II**, were found to be linear with scan rates only at scan rates less than 200 mV/s, **Figure 32(b)**.

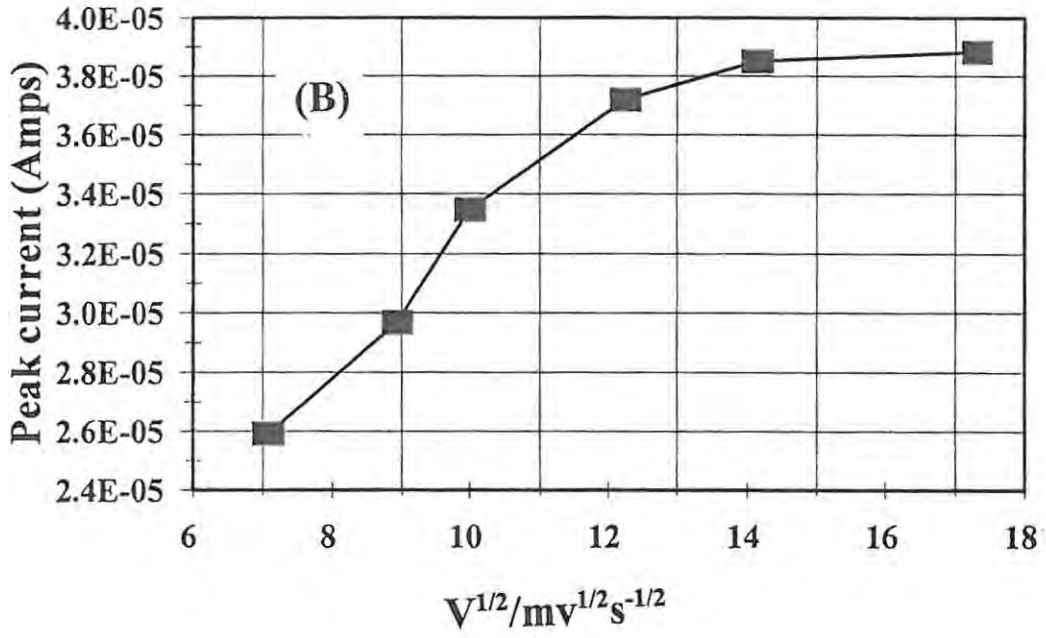

Figure 32(b) Plot of peak current *vs* squareroot of scan rate for couple **II.**

The deviations from linearity suggests that the electron transfer is not governed only by diffussion. When compared with the 4,4',4",4"'-tetraaminophthalocyanine (PdTAPc) it was found that the first reduction in $[Pd(II)Tmtppa]^{4+}$ complexes occurs at more positive potentials than the first reduction in PdTAPc, which has been reported at -0.95V vs SCE in DMSO [55].

The difference in potential may be due to the fact that the $[M(II)Tmtppa]^{4+}$ complexes are expected to be more easily reduced than the corresponding phthalocyanine complexes due to the positive charges.

The number of electrons and the nature of the reduction and oxidation products were confirmed by controlled potential electrolysis and by spectroelectrochemisty. Figure 33 shows the spectral changes observed on controlled potential electolysis of $[Pd(II)Tmtppa]^{4+}$ at potentials of couple (I) (-0.2 to -0.3V), in water containing sodium sulphate.

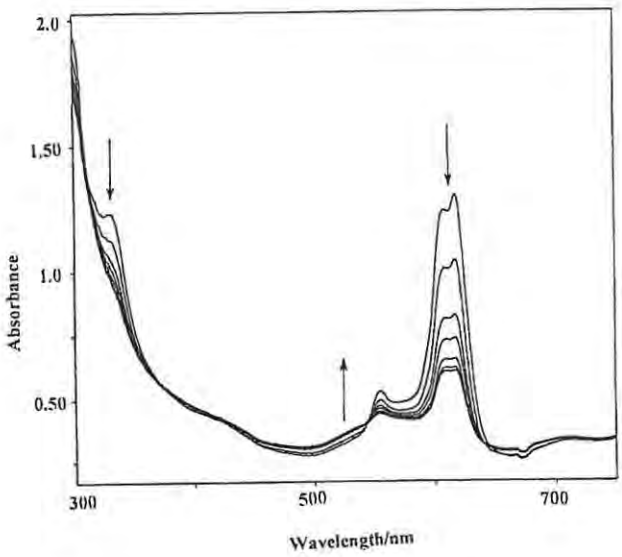

Figure 33 Spectral changes observed on controlled potential elecrolysis of $[Pd(II)Tmtppa]^{4+}$ in distilled water containing Na_2SO_4, at -0.3 V.

On controlled potential electrolysis, the blue colour of the solution $[Pd(II)Tmtppa]^{4+}$ changed to purplish blue. As Figure 33 shows, the Q band decreased in intensity and a new broad band was formed near 525 nm. The new band was formed with the isosbestic points at 641, 545 and 368 nm. The drastic decrease in intensity of the Q-band is normally associated with ring based redox process in metallophthalocyanine complex [59]. These observations are in agreement with those of Worhle *et al* [59] for the photoreduction of $[Zn(II)Tmtppa]^{4+}$ in the presence cysteine. Worhle *et al* attributed the absorption band formed at 570 nm to the product formed on one electron reduction of $[ZnTmtppa]^{4+}$. The spectral changes observed in Figure 33 are assigned to the formation of the monoanion species formed on one electron reduction of $[Pd(II)Tmtppa]^{4+}$ and $[Pt(II)Tmtppa]^{4+}$ complexes. The colour change to purple has been associated with the formation of the monoanion species before [59]. The spectral changes observed in Figure 33 were observed for all the tetramethyltetrapyridinoporphyrazine complexes being discussed in this thesis.

The differences in the wavelength at which the reduction product of $[Zn(II)Tmtppa]^{4+}$ (570 nm) and that of the $[Pd(II)Tmtppa]^{4+}$ or $[Pt(II)Tmtppa]^{4+}$ (525 nm), are probably due to the effects of the central metal ion. Controlled potential electrolysis gave the number of moles of electrons transferred as $n = 1.0 \pm 0.1$, thus confirming a one electron reduction at couple **I.** Couple **I** is therefore assigned to the reduction of $[Pd(II)Tmtppa]^{4+}$ or $[Pt(II)Tmtppa]^{4+}$ and the formation of $[Pd(II)Tmtppa(-3)]^{3+}$ and $[Pt(II)Tmtppa(-3)]^{3+}$ monoanions respectively. The formation of the monoaninon species was reversible since the reoxidation of the reduced species at zero volts, resulted in the regeneration of the original species.

Bulk electrolysis at couple II (-0.46 V) showed no new spectral changes . However at this potential the total number of moles of electrons transferred were more than three. The fact that no new spectral changes were observed suggest that there was no formation of the dianion species which would be characterized by the formation of new absorption band at shorter wave length as reported by Worhle *et al* [59]. The second reduction couple is therefore probably due to the reduction on the methylpyridinium substituents.

Controlled potential electrolysis at the oxidation potential resulted with no change in colour of the solution of $[Pd(II)Tmtppa]^{4+}$ and $[Pt(II)Tmtppa]^{4+}$ complexes. There were no observable spectral changes and therefore the nature of the oxidation product could not be identified. The observation of the oxidation peak may be due to the adsorption of the $[M(II)Tmppa]^{4+}$ species of the electrode.

4. Electrocatalytic Reactions

4.1 *L*-Cysteine*

4.1.1 Heterogeneous catalysis with rhodium phthalocyanine complexes

The cyclic voltammetry of cysteine was determined on glassy carbon electrode (GCE) modified with the following rhodium phthalocyanine complexes: (DMSO)(Cl)Rh(III)Pc, (py)(Cl)Rh(III)Pc and $[(CN)_2Rh(III)Pc]^-$. On unmodified GCE electrode, the cyclic voltammetry peak due to cysteine was not observed. The cyclic voltammetry of blank solution (pH 7.2 phosphate buffer) on GCE modified with (DMSO)(Cl)Rh(III)Pc, **Figure 34(a)**, was featureless..

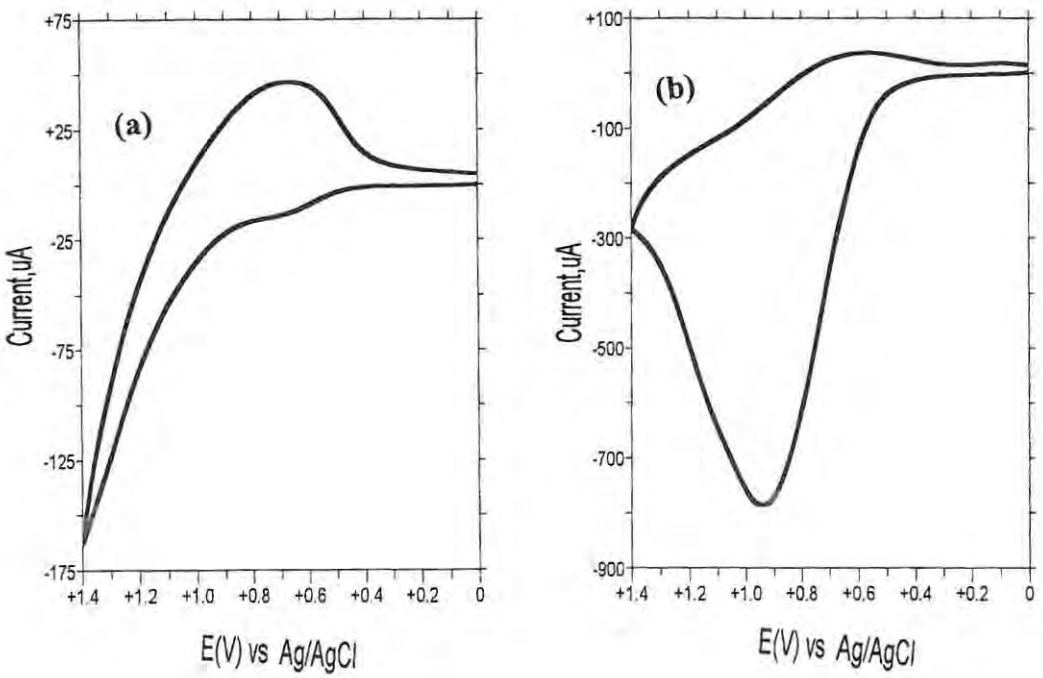

Figure 34 Cyclic voltammetry of, (a) blank (pH 7.2 buffer) and (b) 0.10 mol dm^{-3} cysteine on GCE modified with (DMSO)(Cl)Rh(III)Pc.
Scan rate: $100mVs^{-1}$

*The following paper has resulted from the research work presented in this chapter and for the sake of briefty it is not referenced further: *Electroanalysis* 1997, **9(6)**, 1257.

On addition of 0.001 mol dm^{-3} of cysteine to the buffer solution, there was a significant enhancement of the anodic peak current and the peak due to oxidation of cysteine was observed at 0.94 V (vs Ag/AgCl) **Figure 34(b)**

The enhancement of anodic peak current upon addition of cysteine (0.001 mol dm^{-3}) to buffer solution was also observed on cyclic voltammograms run on GCE modified with (py)(Cl)Rh(III)Pc and $[(CN)_2Rh(III)Pc$ complexes. On GCE electrodes modified with (DMSO)(Cl)Rh(III)Pc and $[(CN)_2Rh(III)Pc]^-$, it was observed that on repetitive scanning at 100 mVs^{-1}, the peak current increased with scan number, **Figure 35(a)**. Plots of the variations of peak current for cysteine oxidation with scan number are shown on **Figure 35(b)**.

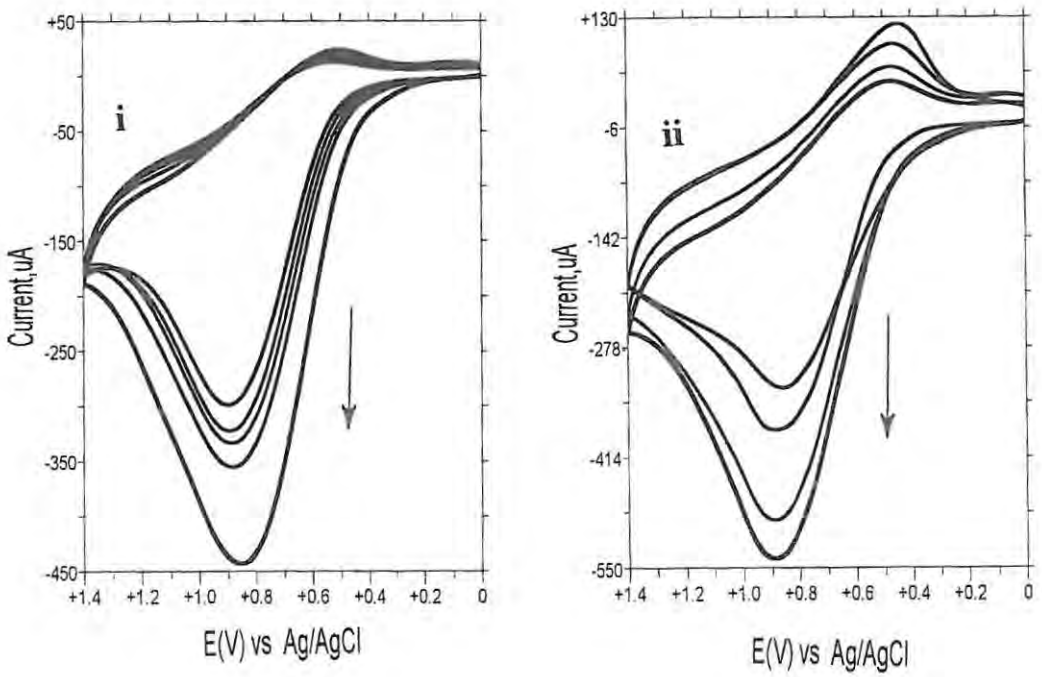

Figure 35(a) Cyclic voltammograms of 0.03 mol dm^{-3} of cysteine on GCE modified with (i)$[(CN)_2)Rh(III)Pc]^-$ and (ii) (DMSO)(Cl)Rh(II)Pc upon repetitive scanning at 100mVs^{-1}.

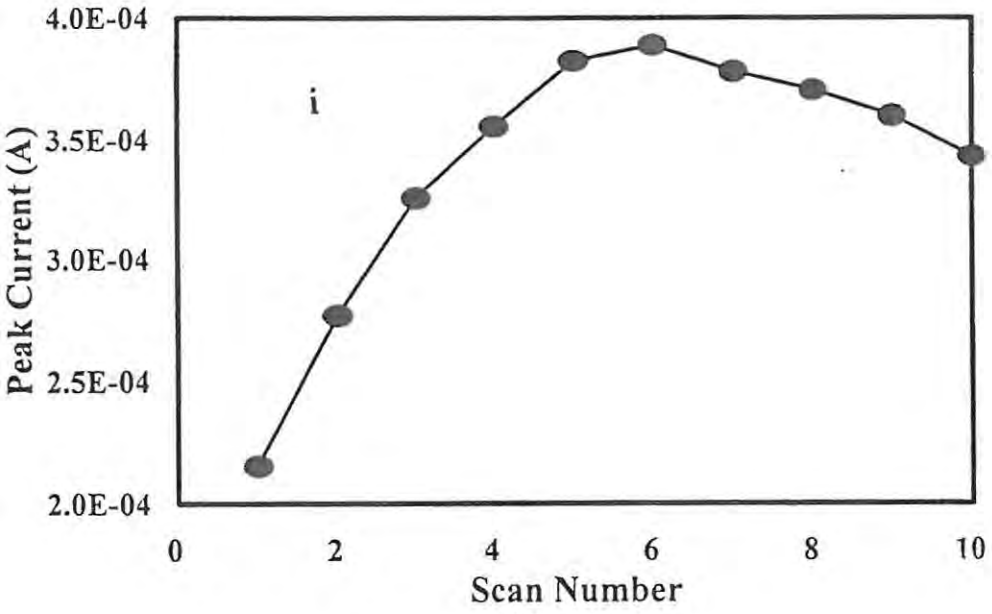

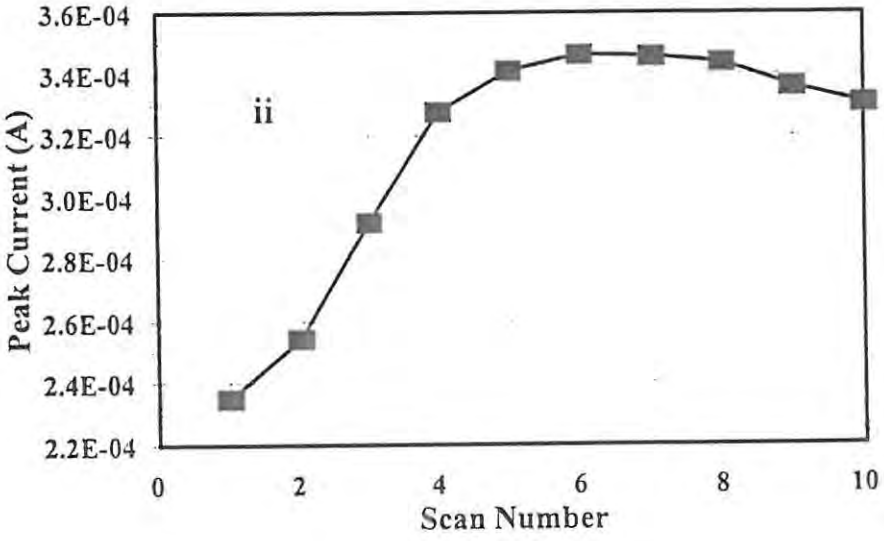

Figure 35(b) Plot of the variations of peak currents for cysteine oxidation with scan number on GCE modified with (i)$[(CN)_2Rh(III)Pc]^-$ and (ii) (DMSO)(Cl)Rh(III)Pc. Scan rate: 100 mVs^{-1}.

The increase in peak current with scan number was observed for the first few scans after which a slow decrease in current was observed. The current, however did not decrease to the level of the current observed during the first scan, even after 20 repetitive scans. This increase in current with scan number was not observed on cyclic voltammogram run on GCE modified with (py)(Cl)Rh(III)Pc.

The plots of the square root of scan rate versus cysteine oxidation peak current, on GCE modified with $[(CN)_2Rh(II)Pc]^{2-}$ or (DMSO)(Cl)Rh(III)Pc, were linear only at low scan rates (< 100 mVs^{-1}), **Figure 36(a)**. Deviations from linearity indicates that the mass movement of cysteine to the surface of the electrode is not necessarily diffusion controlled, there might be other factors, such as adsorption of the substrate on to the electrode, which complicate the movement. On GCE modified with $(py)_2Rh(III)Pc$, plot of the square root of scan rate versus cystine was linear even at scan rates greater than 100 mVs^{-1}, **Figure 36(b)**. The linearity of the plot indicates that the mass movement of cysteine to the surface of the electrode in this case is diffusion controlled.

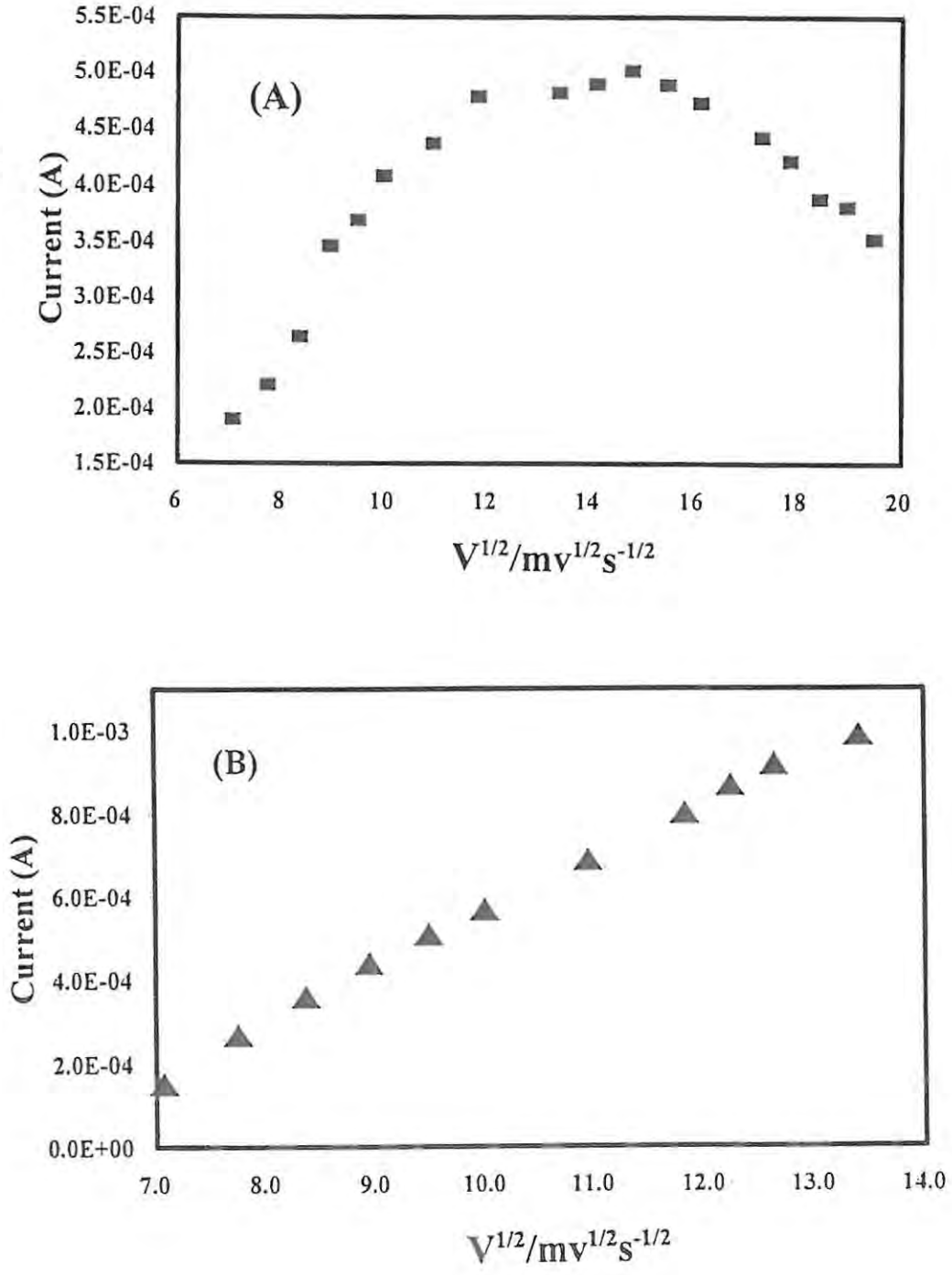

Figure 36 Variations of peak currents for cysteine oxidation with the square root of scan rate on GCE modified with (a) $[(CN)_2Rh(III)Pc]^-$ and (b) $(py)_2Rh(III)Pc$. Cysteine concentration 0.03 mol dm^{-3}.

4.1.2 Heterogeneous catalysis with ruthenium and osmium phthalocyanine complexes

The cyclic voltammetry of cysteine on GCE modified with $(py)_2Ru(II)Pc$, $[(DMSO)_2Ru(II)Pc].2DMSO$, $(py)_2Os(II)Pc$ and $[(DMSO)_2Os(II)Pc].DMSO$ was determined in pH 7.2 phosphate buffer. When unmodified electrode was employed, the cysteine oxidation peak was not observed. **Figure 37** shows the cyclic voltammogram of the blank solution (pH 7.2 phosphate buffer) on GCE modified with $[(DMSO)_2Ru(II)Pc].2DMSO$.

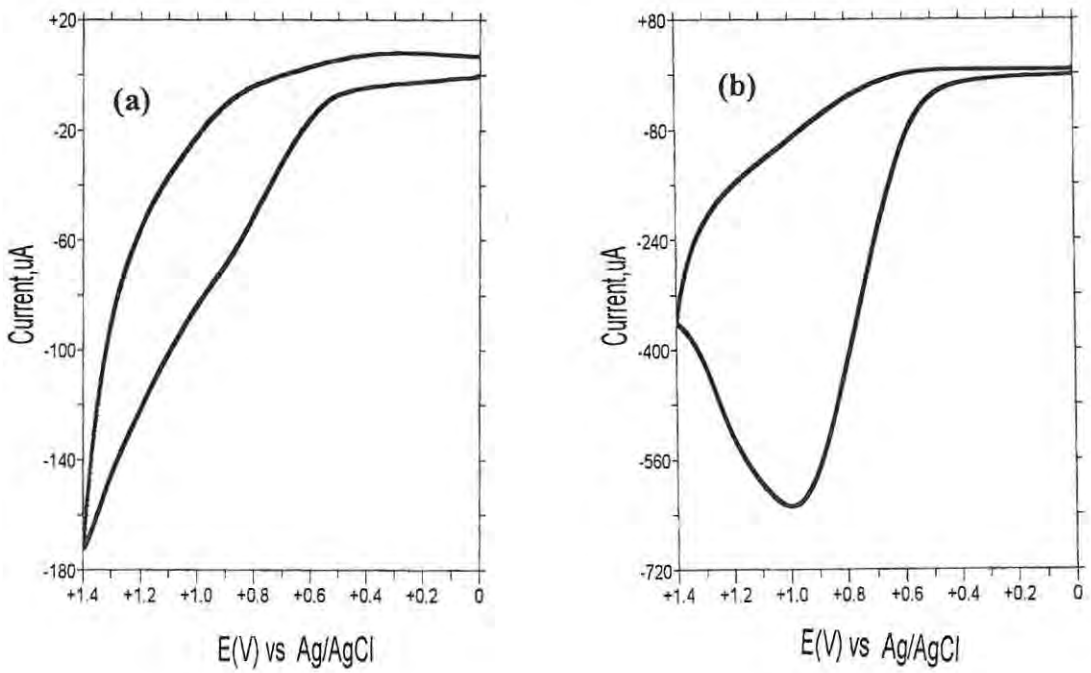

Figure 37 (a) Cyclic voltammogram of blank (pH 7.2 buffer) on GCE modified with $[(DMSO)_2Ru(II)Pc].2DMSO$, (b) Cyclic voltammogram of cysteine (0.01 mol dm^{-3}) on GCE modified with $[(DMSO)_2Ru(II)Pc].2DMSO$. Scan rate: 100 mVs^{-1}.

The cyclic voltammogram of blank shows a featureless cyclic voltammogram, **Figure 37(a)**. On addition of 0.01 mol dm^{-3} of cysteine to the buffer solution, there was a significant increase in anodic peak current due to the oxidation of cysteine, **Figure 37(b)**.

The enhancement of anodic peak current upon addition of cysteine to the buffer solution was also observed on GCE modified with $(py)_2RuPc$, $(py)_2Os(II)Pc$, and $(DMSO)_2Os(II)Pc$, **Figure 38**. The increase of peak current with the scan number upon repetitive scan for [(DMSO)RuPc].2DMSO and $[(DMSO)_2Os(II)Pc]$.DMSO but not for $(py)_2Ru(II)Pc$ and $(py)_2Os(II)Pc$.

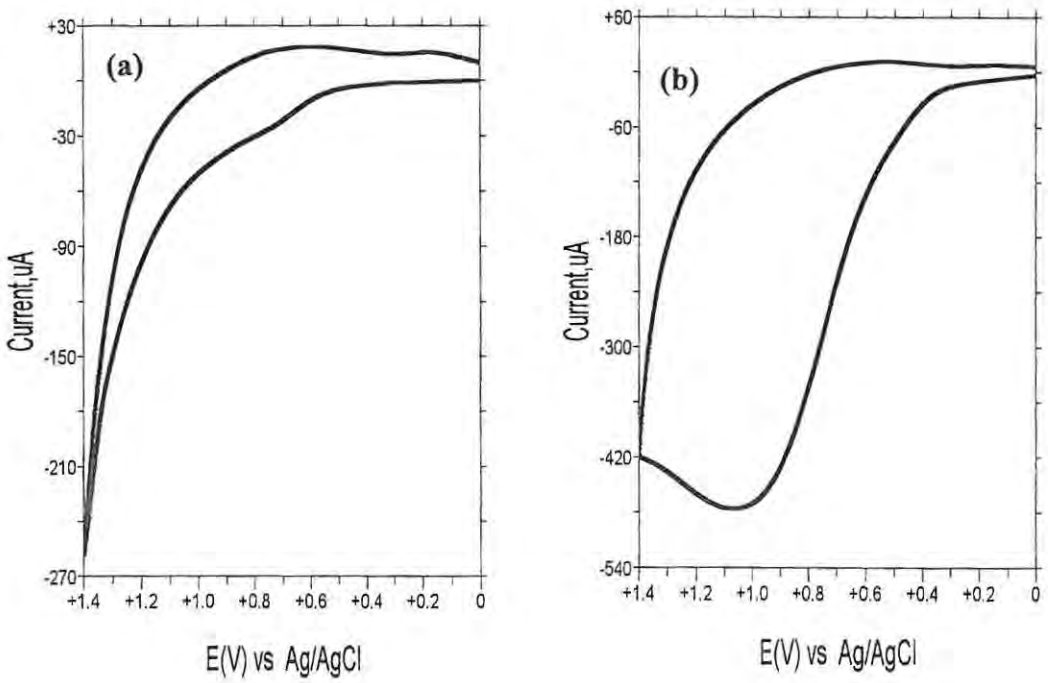

Figure 38 Cyclic voltammogram of blank (pH 7.2 buffer) and (b) 0.1 mol dm^{-3} cysteine on GCE modified with $(DMSO)_2Os(II)Pc$. Scan rate: 100 mVs^{-1}.

4.1.3 Discussion on the voltametric behaviour of cysteine on GCE modified with Rh, Ru, and Os phthalocyanines

The observation of the increase of peak current with the scan number when (DMSO)(Cl)Rh(III)Pc, $[(CN)_2Rh(III)Pc]^-$, $(DMSO)_2Ru(II)Pc$ and $(DMSO)_2Os(II)Pc$ were employed for electrode modification, suggests that these complexes exhibit the autocatalytic behaviour towards the oxidation of cysteine. When cysteine is oxidized, the oxidation product is known to be cystine. At pH's greater than 4 but less than 9, cystine formed during oxidation of cysteine is known to precipitate out and adsorbs onto the electrode surface resulting in inhibition of the electrode activity. Limson *et al* [121] have shown that oxidation of cysteine on GCE modified with $[Co(II)TSPc]^{4-}$ at pH 8.4 resulted in decrease in cysteine peak currents after the first scan. This decrease was attributed to the poisoning of the electrode by cystine.

When CoPc was employed for electrode modification, at pH's less than 4, the oxidation currents for cysteine oxidation were reported to be reproducible [6], since at low pH's cystine redissolves into the solution and the electrode surface is not poisoned. Even though the oxidation currents were reproducible in the case of CoPc-CME, they were not reported to show the increase with the scan number as observed for Rh, Ru and Os phthalocyanine complexes mentioned above, also no reproducibility in currents has been reported for pH's > 4.

The increase of cysteine peak currents with scan number observed for (DMSO)(Cl)Rh(III)Pc, $[(CN)_2Rh(III)Pc]^-$, $[(DMSO)_2Ru(II)Pc].2DMSO$ and $[(DMSO)_2Os(II)Pc].DMSO$, indicates that there is a formation of a new catalytic surface on the electrode after each scan. The catalytic activity of the electrode increases to a certain maximum and then starts to decrease slowly as shown in **Figure 35(b)**. This decrease in catalytic activity of the electrode indicate that the

electrode surface is slowly being poisoned by the oxidation product, thus there is no more new catalytic surface bing formed on the electrode.

The generally accepted mechanism for the catalytic oxidation of cysteine on MPc chemically modified electrodes (CMEs), is believed to be a two step electrocatalytic process. The process is initiated by the oxidation of the MPc complex at the central metal, followed by oxidation of cysteine by the oxidized MPc species, the formation of cystine and regeneration of the original MPc complex, **Equations 7 and 9**.

This mechanism applies to those MPc complexes containing an electroactive central metal, such as CoPc. Rhodium and ruthenium phthalocyanine complexes discussed in this work have been reported to show oxidation on the phthalocyanine ring and not on the central metal [13,19]. It has been shown in sections 3.1.2, 3.2.2 and 3.2.3 that $[(CN)_2Os(II)Pc$, $(py)_2Os(II)Pc$ and $(DMSO)_2Os(II)Pc$ show oxidation at the phthalocyanine ring. The mechanism shown in **Equations 7** to **9** for the electrocatalytic oxidation of cysteine cannot apply for these Rh, Ru, and Os phthalocyanine complexes. It is therefore, suggested that the mechanism involved in the catalytic oxidation of cysteine by these complexes is different from that shown in Equations 7 to 9 since it would not involve the central metal. The π-cation radicals of the MPc complexes formed by one electron oxidation, are known to form dimeric species in solution in equilibrium with monomeric MPc species [115].

Based on this fact, the following mechanism is suggested for cysteine oxidation on GCE modified with (DMSO)(Cl)Rh(III)Pc, $[(CN)_2Rh(II)Pc]^-$, $(DMSO)_2Ru(II)Pc$ and $(DMSO)_2Os(II)Pc$:

$MPc(-2) \rightarrow [MPc(-1)]^{+} + e^{-}$ Equation 24

$2[MPc(-1)]^{+} \rightarrow ([MPc(-1)]^{+})_2$ Equation 25

$([MPc(-1)]^{+})_2 + 2RSH \rightarrow 2MPc(-2) + RSSR + 2H^{+}$ Equation 26

Based on this suggested mechanism, it is proposed that the dimeric π-cation radical species formed by **Equation 25** oxidizes the cysteine according to **Equation 26.** Maroie *et al* [122] have reported that polymeric MPc complexes show better catalytic activity than the monomeric MPc complexes. Considering this observation then, it is believed that the observed autocatalytic behaviour exhibited by (DMSO)(Cl)Rh(III)Pc, $[(CN)_2Rh(III)Pc]^{-}$, $(DMSO)_2Ru(II)Pc$ and $(DMSO)_2Os(II)Pc$ complexes towards the oxidation of cysteine may be explained by the fact that the π-cation radical species of these complexes form dimeric species which are responsible for the oxidation of cysteine.

The observed increase in peak currents with scan number, as shown in **Figure 39**, shows the improvement of the electrode surface as the dimeric π-cation species forms on the electrode. The complete coverage of the electrode by dimeric species is reflected by the peaking of the current response after few scans. The decrease in electrode activity due to poisoning by cystine is indicated by the decrease in current response.

The effect of axial ligands on the catalytic behaviour of Rh, Ru, and Os phthalocyanine complexes toward oxidation of cysteine.

No peaks due to oxidation of cysteine were observed when non-axially substituted MPcs were employed as electrode modifiers. Cysteine oxidation peaks were observed only when axially substituted $(L)_2$MPc complexes were used for electrode modification.

The autocatalytic behaviour for oxidation of cysteine, was observed only when the GCE was modified with (DMSO)(Cl)Rh(III)Pc, $[(CN)_2Rh(III)Pc]^{-1}$, $[(DMSO)_2Ru(II)Pc].2DMSO$ and $(DMSO)_2Os(II)Pc$ where the axial ligands were cyanide or DMSO. When the GCE was modified with (py)(Cl)Rh(III)Pc , $(py)_2Ru(II)Pc$ and $(py)_2Os(II)Pc$ where the axial ligands were pyridines, the autocatalytic behaviour was not observed. These observations may indicate the difference in ability of the axially ligated MPc complexes in forming the dimeric π-cation radical species. $(CN)_2$MPc complexes have been reported to form cyano bridged polymeric species [99,101,123].

The π-cation radical species formed by one electron oxidation of $(CN)_2$MPc are then expected to easily form dimeric π-cation radicals species. Capobianchi *et al* [124] have shown that $[(DMSO)_2Ru(II)Pc].2DMSO$ readily loses the axial DMSO ligands to form $(RuPc)_2$ species. The fact that $(RuPc)_2$ can easily form the dimeric $([RuPc(-1)]^{+\cdot})_2$ π-cation radical species then explains the autocatalytic behaviour observed for $[(DMSO)_2Ru(II)Pc].2DMSO$. The autocatalytic behaviour for (DMSO)(Cl)RhPc may be explained in the same manner since $(RhPc)_2$, have been reported before [27].

The lack of autocatalytic behaviour for $(py)_2Ru(II)Pc$, $(py)_2Os(II)Pc$ and (py)(Cl)Rh(III)Pc may be due to the inability of these complexes to form dimeric π-cation radical species following

one electron oxidation. In this case then it is suggested that cysteine is oxidized by the monomeric π-cation radical species, as shown by the suggested mechanism in **Equations 27** and **28**.

$$MPc(-2) \rightarrow [MPc(-1)]^{+} + e^{-} \qquad \text{Equation 27}$$

$$2MPc(-1)]^{+} + 2RSH \rightarrow 2MPc(-2) + RSSR + 2H^{+} \qquad \text{Equation 28}$$

The electrocatalytic efficiencies of the MPc complex with respect to the axial ligand towards the oxidation of cysteine, was investigated by comparing the peak currents of the first scan rate for oxidation of 0.03 mol dm^{-3} of cysteine on GCE modified with $[(DMSO)_2Ru(II)Pc].2DMSO$, $[(CN)_2Ru(II)Pc]^{2-}$ and $(py)_2Ru(II)Pc$ complexes at the scan rate of 100 mVs^{-1}. The catalytic efficiency was found to decrease with the axial ligand in the following order: CN^{-} > DMSO > py. This order is propably reflecting the ease of formation of the dimeric π-cation radical species by the MPc complexes under discussion.

The effect of solvent on the catalytic behaviour of Rh, Ru and Os phthalocyanine complexes on the oxidation of cysteine on GCE.

The autocatalytic behaviour exhibited by Rh, Ru and Os phthalocyanine complexes was observed only when DMF and not pyridine was used for dissolving the MPc complexes before depositing onto the electrode surface. When pyridine was employed as a solvent for the deposition of the MPc complexes onto the GCE, rapid decrease of the anodic peak currents were observed after the first scan. When acetonitrile was used to dissolve the MPc complexes,

the peak currents for cysteine oxidation increased only for the first two scans and then decreased drastically. DMF, pyridine and acetonitrile are known as aprotic solvents and they are normally classified as Lewis base solvents (also called coordinating solvents). It has been reported that oxidation of organic compounds in DMF results in formation of radicals that dimerize [27]. This may explain the pronounced autocatalytic behaviour of the MPc complexes when dissolved in DMF and not in pyridine. The nitrogen atoms that serve as donors in acetonitrile and pyridine are known to be softer bases than the oxygen donors in DMF. This is known to affect the specific solubilities in these solvents and this may be the reason why organic compounds form radicals that dimerize more readily when DMF is employed as a solvent.

The effect of the central metal towards the catalytic activity of Rh, Ru and Os phthalocyanine complexes

The catalytic efficiencies of the MPc complexes with respect to the central metal towards the oxidation of cysteine were investigated by comparing the peak currents of the first scan (at 100 mVs^{-1}) for the oxidation of 0.03 mol dm^{-3} for cysteine on GCE modified with $[(CN)_2Rh(III)Pc]^-$, $[(CN)_2Ru(II)Pc]^{2-}$ and $[(CN)_2Os(II)Pc]^{2-}$. The catalytic efficiencies vary as follows: Rh > Ru > Os. For all these complexes, the first oxidation occurs on the phthalocyanine ring. The half wave potentials ($E_{1/2}$) for the first ring oxidation of $[(CN)_2Rh(III)Pc]^-$, $[(CN)_2Ru(II)Pc]^{2-}$ and $[(CN)_2Os(II)Pc]^{2-}$ in acetonitrile varies as follows: Os < Ru < Rh. If the catalytic efficiency of the complex is compared with its oxidation potential, it appears that the easily oxidized MPc complex has lower catalytic efficiency.

The detection limits of Rh, Ru and Os phthalocyanine complexes for the determination of Cysteine.

When cysteine is oxidized on MPc modified GCE, it is desirable to both lower the potential at which cysteine gets oxidized, and also to increase the sensitivity of cysteine detection. The lowest potential reported for cysteine oxidation (0.33 V) was observed before for carbon paste electrodes modified with OMo(IV)(OH)Pc [6]. As already mentioned before (section 1.6.1) even though OMo(IV)(OH)Pc lowers the potential for cysteine oxidation quite considerably, its sensitivity for cysteine detection is rather poor (1×10^{-3} mol dm^{-3}) when compared with the detection limit (1×10^{-7} mol dm^{-3}) reported for CoPc modified carbon paste electrodes [6].

If we consider only the current response during the first scan, the lowest concentration of cysteine that can be determined on GCE modified with (DMSO)(Cl)Rh(III)Pc, $[(CN)_2Rh(II)Pc]^-$ $[(DMSO)_2Ru(II)Pc].2DMSO$, and $(DMSO)_2Os(II)Pc$ was of the order of 1×10^{-3} mol dm^{-3}. Hence the detection limit of CoPc modified electrode is much better than observed for Rh, Ru and Os phthalocyanine complexes under discussion.

The plot of peak current versus cysteine concentration was linear only at low concentrations of cysteine, (< 0.02 mol dm^{-3}) , when Rh, Ru and Os phthalocyanine complexes were used to modify GCE, **Figure 39**. Deviations from linearity that were observed at high concentration, have been reported before [6] and were attributed to the loss of activity of the electrode at high concentrations of cysteine due to the competition for active sites on the electrode surface.

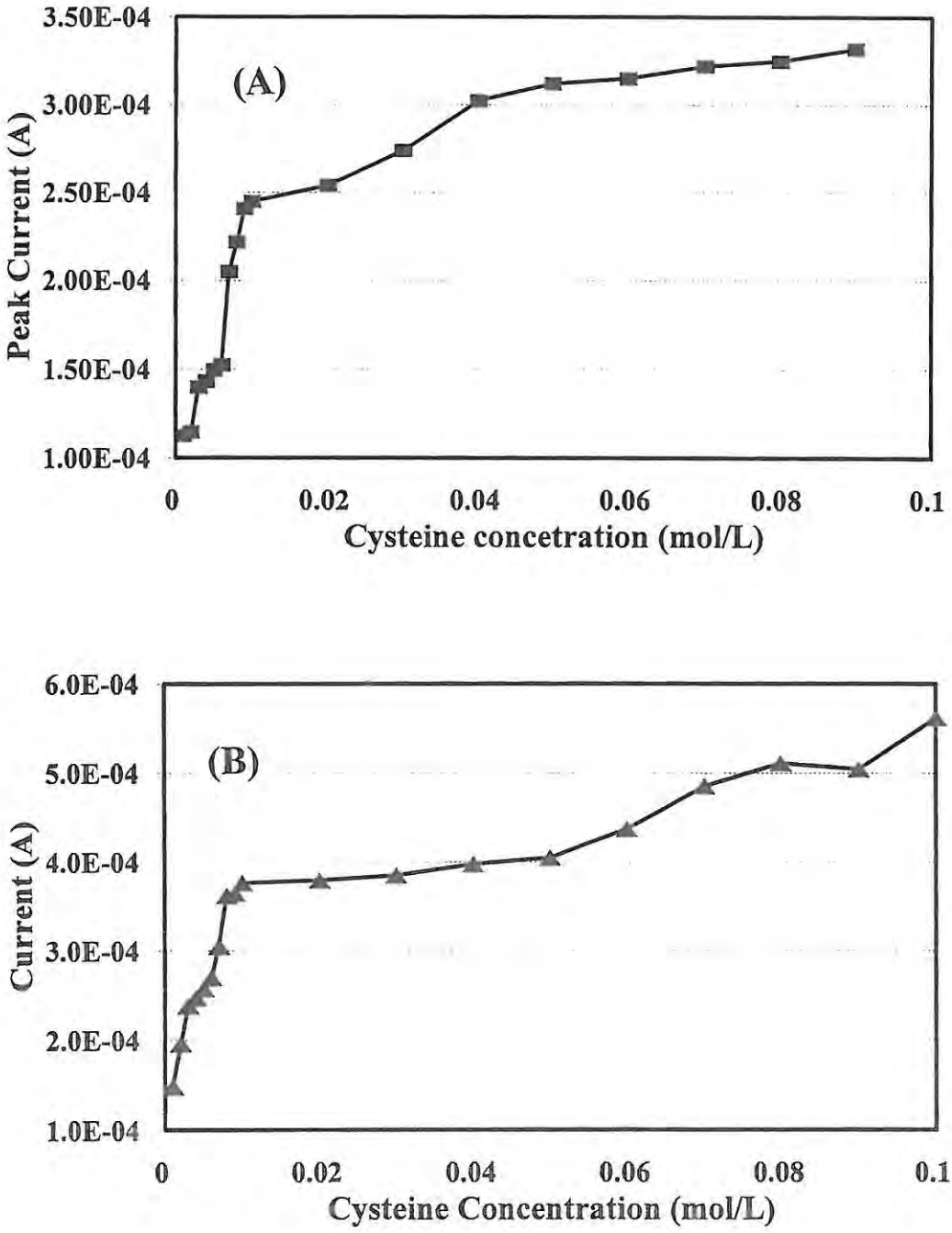

Figure 39: Variations of peak currents for cysteine oxidation with the concentration of cysteine.

Electrode: GCE modified with (a)$[(CN)_2RhPc]^-$ and (b) $(py)_2Ru(II)Pc$. Scan rate: 100 mVs^{-1}

4.1.4 Solution phase catalysis of cysteine oxidation with $[(CN)_2Ru(II)Pc]^{2-}$ and $[(CN)_2Os(II)Pc]^{2-}$ complexes

The $[(CN)_2Ru(II)Pc]^{2-}$ and $[(CN)_2Os(II)Pc]^{2-}$ complexes are water soluble and are therefore not easy to use as electrode modifiers since they tend to leach from the electrode surface. These complexes were used for solution phase catalysis of cysteine oxidation. **Figure 40(a)** shows the cyclic voltammogram of the solution of $[(CN)_2Ru(II)Pc]^{2-}$ in pH 9 phosphate buffer. The CV is different from the reported [19] since GCE instead of Pt was employed as working electrode for electrocatalytic studies.

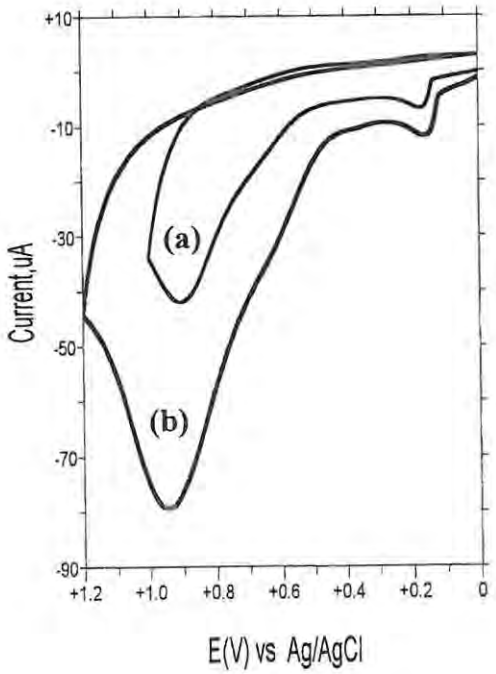

Figure 40 (a) Cyclic voltammogram of $[(CN)_2Ru(II)Pc]^{2-}$ in blank (pH 9 buffer). Scan rate 100 mVs^{-1}.
(b) Cyclic voltammogram of $[(CN)_2Ru(II)Pc]^{2-}$ in the presence of cysteine, (0.01 mol dm^{-3}). Scan rate 100 mVs^{-1}

The cyclic voltammogram of $[(CN)_2Ru(II)Pc]^{2-}$ in pH 9 buffer on GCE shows two anodic peaks,

Figure 40(a). The sharp peak observed at 0.16 V vs Ag/AgCl may be due to the adsorption of oxidation products on the electrode. When cysteine (0.01 mol dm^{-3}) was added to the buffer, the anodic peak at 0.95 V increase due to the catalytic oxidation of cysteine, **Figure 40 (b)**. The same behaviour was observed when cysteine was added to the solution of $[(CN)_2Os(II)Pc]^{2-}$ in pH 9 buffer, **Figure 41**. The cysteine oxidation peak decreased very rapidly after the first scan. The CV of $[(CN)_2Os(II)Pc]^{2-}$ is different from that shown in **Figure 14** since GCE was employed as working electrode instead of Pt electrode.

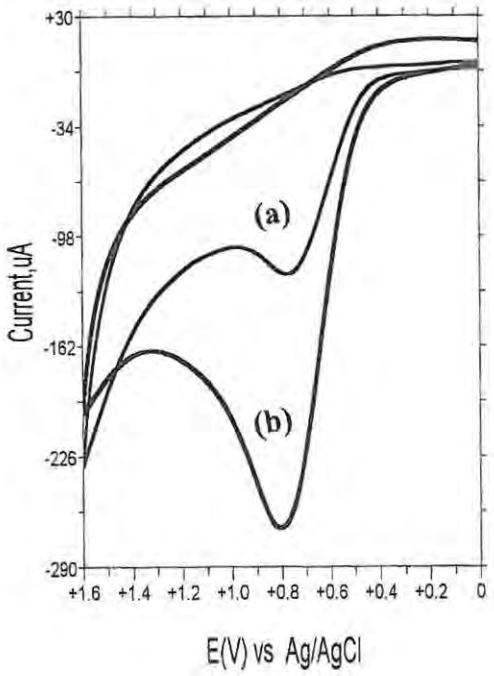

Figure 41 Cyclic voltammogram of $[(CN)_2Os(II)Pc]^{2-}$ in blank (pH 9 buffer). (b) Cyclic voltammogram of $[(CN)_2Os(II)Pc]^{2-}$ after addition of cysteine (0.01 mole dm^{-3}).

The behaviour observed for the adsorbed $[(CN)_2Rh(III)Pc]^{-}$, where the cysteine oxidation peak increased with the scan number was not observed for solution catalysis $[(CN)_2Ru(II)Pc]^{2-}$ and

$[(CN)_2Os(II)Pc]^{2-}$. The rapid decrease of cysteine oxidation peak after the first scan indicates that the electrode is poisoned by the oxidation product and the autocatalytic behaviour described above for the adsorbed Rh, Ru and Os phthalocyanine complexes is lacking in the case of $[(CN)_2Ru(II)Pc]^{2-}$ and $[(CN)_2Os(II)Pc]^{2-}$ in solution.

As already mentioned, $(CN)_2MPc$ complexes are known to form cyano bridged polymeric species and are therefore expected to form dimeric π-cation radical species quite easily. The lack of autocatalytic behaviour for $[(CN)_2Ru(II)Pc]^{2-}$ and $[(CN)_2Os(II)Pc]^{2-}$ suggests that the dimeric π-cation radical species that are likely to be formed by $[(CN)_2Ru(II)Pc(-1)]^{+}$ and $[(CN)_2Os(II)Pc(-1)]^{+}$ do not provide the new catalytic surface on the electrode. The surface seem to be formed when the catalyst is adsorbed onto the electrode.

4.2 *Electrooxidation of methionine on GCE modified with Rh, Os and Ru phthalocyanines*

The catalytic behaviour of the Rh, Ru and Os phthalocyanine complexes towards the oxidation of methionine was investigated. **Figure 42** shows the cyclic voltammogram obtained for blank solution (pH 7.2) on GCE modified with $[(CN)_2Rh(III)Pc]^-$. The cyclic voltammogram shows very well defined cathodic and anodic peaks, due to the ring oxidation of $[(CN)_2Rh(III)Pc(-2)]^-$ to form $(CN)_2Rh(III)Pc(-1)$.

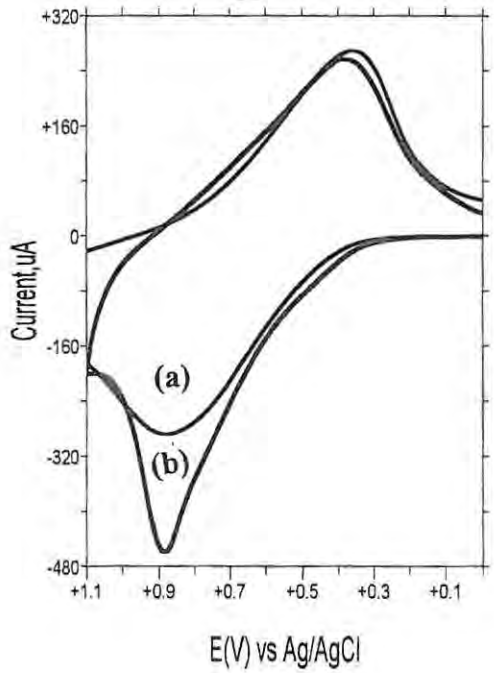

Figure 42 (a) Cyclic voltammogram of blank (pH 7.2 buffer) on GCE modified with $[(CN)_2Rh(III)Pc]^-$. Scan rate: 100 mVs^{-1}. (b) Cyclic voltammogram of 0.01 mol dm^{-3} methionine on GCE modified with $[(CN)_2Rh(III)Pc]^-$. Scan rate: 100 mVs^{-1}.

On addition of 0.01 mol dm^{-3} of methionine to the buffer solution, the anodic peak current

increased and the peak due to oxidation of methionine was observed at 0.88 V vs Ag/AgCl. The autocatalytic behaviour observed for oxidation of cysteine when $[(CN)_2Rh(III)Pc]^-$ was employed for electrode modification was not observed in the case of methionine oxidation. The fast decrease of methionine oxidation peak currents indicated the rapid deactivation of the electrode activity by the oxidation products.

4.3 Electrooxidation of hydrazine and hydroxylamine on GCE modified with Rh, Ru and Os phthalocyanine complexes

On bare GCE (unmodified) the cyclic voltammograms of both hydrazine and hydroxylamine did not show any observable cathodic or anodic peaks. **Figure 43(a)** shows the cyclic voltammograms of hydrazine on unmodified GCE and **Figure 43(b)** shows the cyclic voltammogram of hydrazine on GCE modified with $[(CN)_2Rh(III)Pc]^-$.

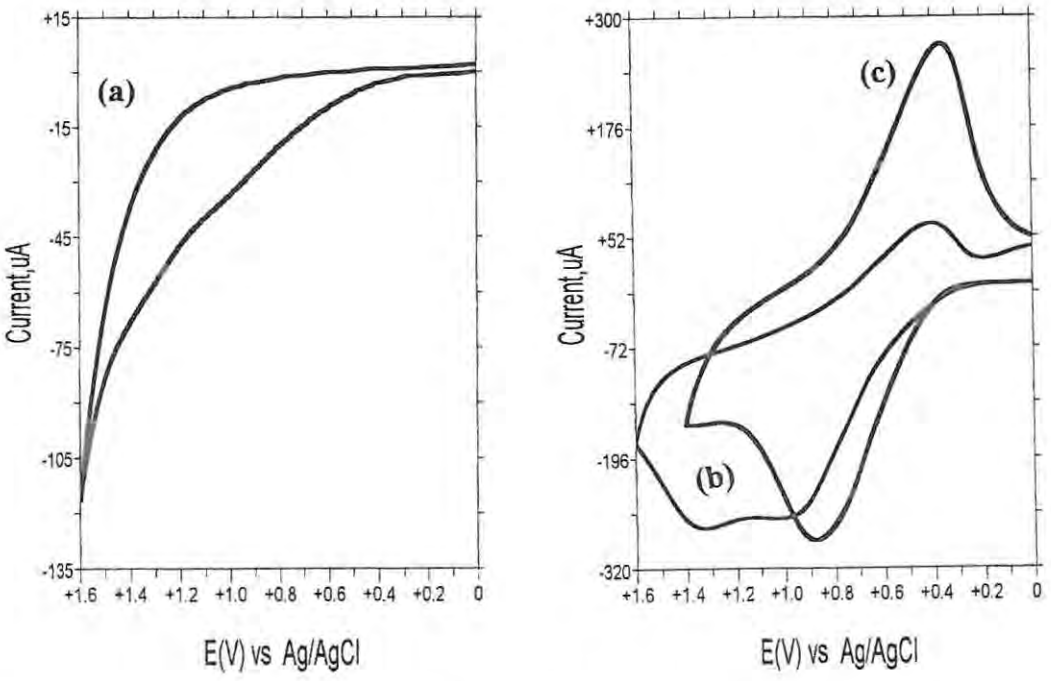

Figure 43 Cyclic voltammogram of hydrazine (a) on unmodified GCE and (b) on GCE modified with $[(CN)_2Rh(III)Pc]^-$. (c) Cyclic volatammogram of $[(CN)_2Rh(III)Pc]^-$ in pH 7.2 buffer.

When GCE modified with $[(CN)_2Rh(III)Pc]^-$ was employed, there was no enhancement of the anodic peak current in the presence of hydrazine but two anodic peaks were observed, as shown in **Figure 43(b)**. The peak at 0.9V vs Ag/AgCl is near the peak observed on the cyclic voltammogram of blank solution' (pH 7.2 buffer) on GCE modified with $[(CN)_2Rh(III)Pc]^-$ before the addition of hydrazine to the buffer solution, **Figure 43(c)**. On addition of hydrazine to the buffer solution, a new peak was formed at 1.34 V which we believe is probably due to the oxidation of hydrazine, since this peak increased with hydrazine concentration. **Figure 44(a)** shows the cyclic voltammogram of hydroxylamine on bare GCE, while **Figure 44(b)** shows cyclic voltammogram of hydroxylamine on GCE modified with $[(CN)_2Rh(III)Pc]^-$ complex.

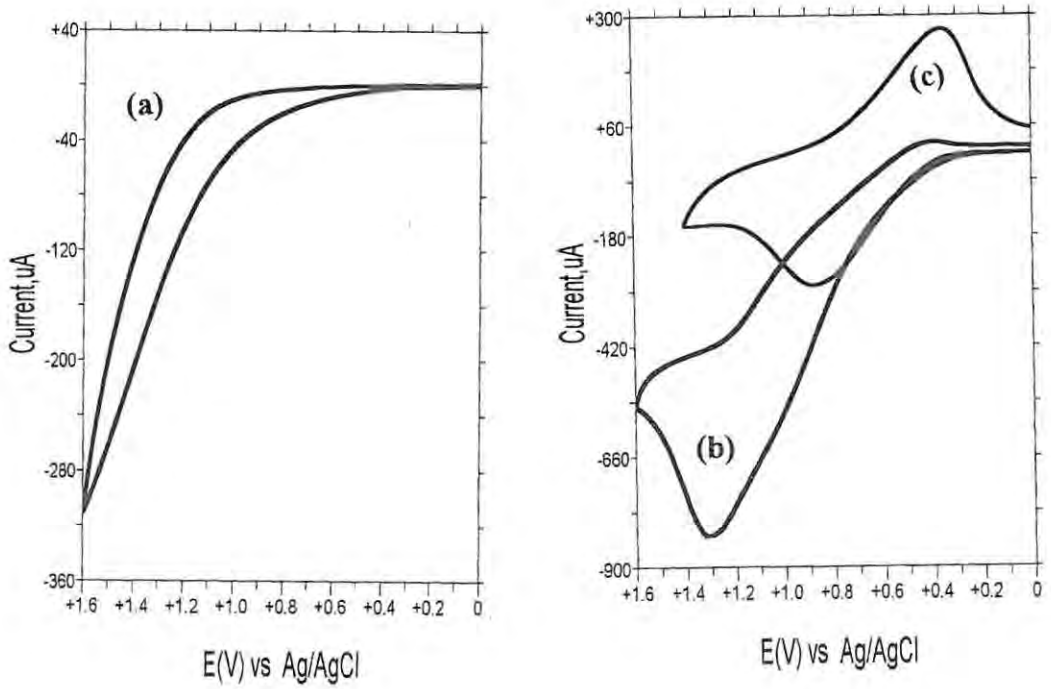

Figure 44 Cyclic voltammogram of hydroxylamine (a) on unmodified GCE, (b) on GCE modified with $[(CN)_2Rh(III)Pc]^-$ and (c) $[(CN)_2Rh(III)Pc$ in blank (pH 7.2 buffer). Scan rate 100 mVs^{-1}.

The peak due to the oxidation of hydroxylamine was observed at 1.30 V, and it increased with increase in hydroxylamine concentration. Unlike in the case of hydrazine oxidation only one anodic peak was observed when hydroxylamine was added to the buffer solution. For both hydrazine and hydroxylamine, we observed a fast decrease of the oxidation currents after the first scan on GCE modified with either $[(CN)_2Rh(III)Pc]^-$, (DMSO)(Cl)Rh(III)Pc, $(DMSO)_2RuPc$ or $(DMSO)_2Os(II)Pc$. The fast decrease of the oxidation currents for the oxidation of hydrazine, hydroxylamine and methionine suggested that the autocatalytic behaviour observed for Ru, Rh and Os complexes for the oxidation of cysteine depend on the nature of the oxidation products and the extent to which the products adsorb onto the electrode surface. An extensive adsorption of the oxidation products onto the electrode would inhibit the activity of the dimeric π-cation radicals formed by the relevant Ru, Rh and Os phthalocyanine complexes, resulting in rapid poisoning of the electrode.

4.4 Voltammetric behaviour of metallothionein on $[(CN)_2Rh(III)Pc]^-$ modified electrode

Metallothionein (MT) is a cystine containing protein known to bind a variety of heavy metal such as Zn(II), Cd(II), Hg(II) and Cu(I). The electrochemical determination of this protein relies heavily on its cysteine content. One third of MT residues is known to consist of cysteine [125,126]. $[Co(II)TSPc]^{4+}$ chemically modified glassy carbon electrode (CoTSPc-CMGCE), has been employed [121] for the determination of metallothionein. The problem encountered in using CoTSPc-CMGCE is that the activity of the electrode decreased after the first scan due to the poisoning of the electrode by adsorption of the oxidation products. In this work the electrochemical determination of MT on glassy carbon electrode modified with $[(CN)_2Rh(III)Pc]^-$ was attempted in order to find out if the electrode activity can be improved particularly since this complex showed autocatalytic behaviour towards oxidation of cysteine.

The cyclic voltammogram of $[(CN)_2Rh(III)Pc]^-$ in blank (pH 7.2 buffer) exhibit one reversible couple with the anodic peak observed at approximately 0.9 V vs Ag/AgCl, **Figure 45 (a)**.

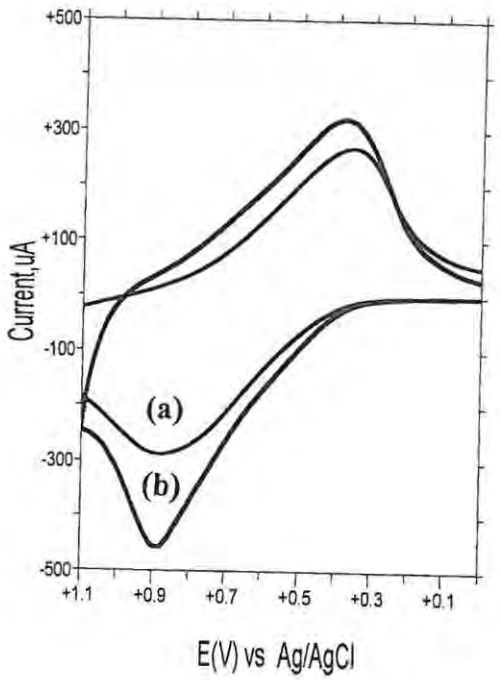

Figure 45 Cyclic voltammogram of $[(CN)_2Rh(III)Pc]^-$ in a) blank (pH 7.2 buffer) and (b) in the presence of 0.01 mol dm^{-3} metallothionein. Scan rate: 100 mVs^{-1}.

On addition of metallothionein to the buffer solution, the enhancement of the anodic peak current was observed. It is possible that this enhancement was due to the oxidation of MT since the peak current increased with increasing concentration of metallothionein. However, the peak due to oxidation of MT decreased drastically after the first scan, suggesting the poisoning of the electrode by oxidation products also the cathodic peak was relatively intense, uncharacteristic of catalytic behaviour. The autocatalytic behaviour observed for $[(CN)_2Rh(III)Pc]^-$ on electrooxidation of cysteine was not observed in the case of

metallothionein.

5. Interactions with Amino Acids

*5.1 Interactions of cobalt(II)tetrasulphophthalocyanines with l-histidine**

As mentioned in the introduction, metal tetrasulphophthalocyanines species $[(M(II)TSPc]^{4-}$ exists as dimmers in aqueous solutions. Their electronic absorption spectra is normally described in terms of equilibria between the dimeric and monomeric species, **Figure 46(a)**. Generally the high energy peak near 620 nm is associated with the dimeric species while the peak near 670 nm is associated with the monomer [127,128].

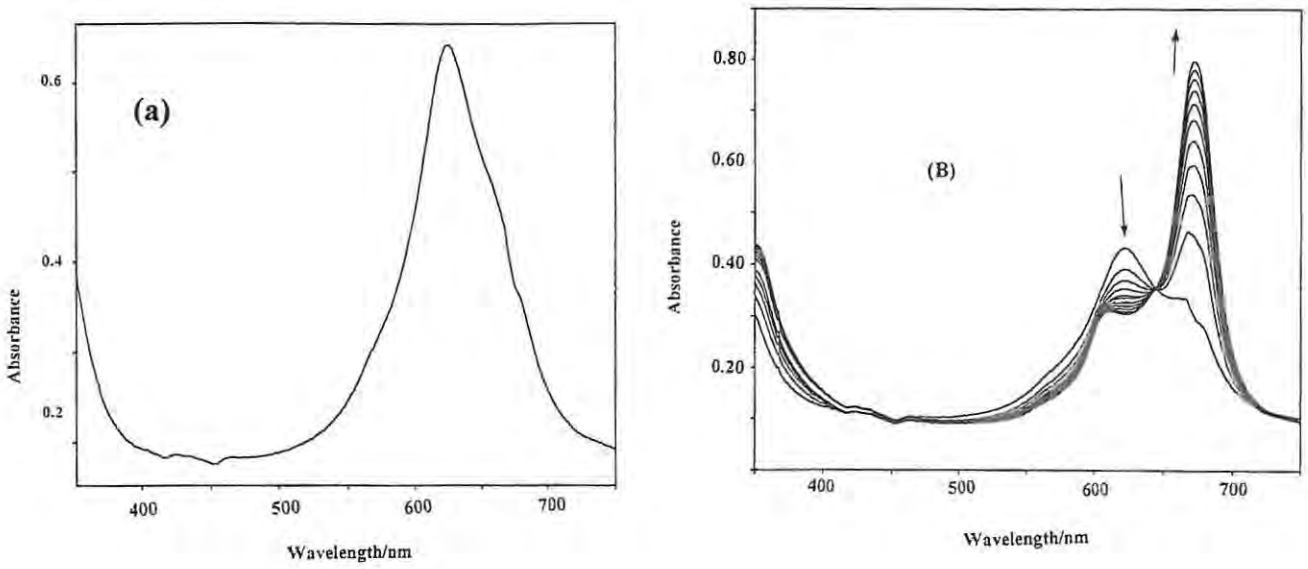

Figure 46: a) Absorption spectra of $[Co(II)TSPc]^{4-}$ in phosphate buffer (pH 7.2). b) spectral changes on addition of *l*-histidine (0.085 mole dm^{-3}) to the solution of $[Co(II)TSPc]^{4-}$ (8.0×10^{-6} mole dm^{-3}) in pH 7.2 buffer.

*The following paper has resulted from research work on "the interactions of Co(II)TSPc with cysteine and histidine", and is not referenced in this thesis: *Polyhedron*, 1997, **16(19)**, 3279-3289.

The interactions between *l*- histidine and $[Co(II)TSPc]^{4-}$ are known to promote the oxidation of $[Co(II)TSPc]^{4-}$ species to $[Co(III)TSPc]^{3-}$ in the presence of air [78]. **Figure 46(b)** shows the spectral changes observed when solutions of *l*-histidine (0.085 mol dm^{-3}) was added to solutions of $[(Co(II)TSPc]^{4-}$ in phosphate buffer (pH 7.2).

On addition of *l*-histidine to the $[Co(II)TSPc]^{4-}$ solution, the peak which is associated with the dimeric species, on the electronic spectra of $[Co(II)TSPc]^{4-}$ at 624 nm, decreased in intensity with time, while the peak due to monomeric species at 666 nm increased. The increase of the monomeric peak was also accompanied by the slight shifts to 672 nm. The spectral changes occurred with the isosbestic point at 645 nm. The fact that the peak in the region of the spectra associated with the monomeric species increased when histidine was added to the solution of $[Co(II)TSPc]^{4-}$, suggests that the presence of histidine favours the formation of the monomeric $[Co(II)TSPc]^{4-}$.

The final spectra with the peak at 672 nm in **Figure 32(b)**, is similar to the spectra obtained by Cookson *et al* [78] on oxidation of $[Co(II)TSPc]^{4-}$ to $[Co(III)TSPc]^{3-}$. Similar spectra on chemical oxidation of $[Co(II)TSPc]^{4-}$ with bromine have been observed. The final spectra obtained on addition of *l*-histidine to $[Co(II)TSPc]^{4-}$, **Figure 46**, is therefore attributed to the oxidation of $[Co(II)TSPc]^{4-}$ to $[Co(III)TSPc]^{3-}$. When a reducing agent like sodium borohydride ($NaBH_4$) was added to the solution of $[Co(II)TSPc]^{4-}$ in which histidine has been added, and at the end of the reaction between $[Co(II)TSPc]^{4-}$ and histidine, the original spectra due to $[Co(II)TSPc]^{4-}$ was regenerated. This confirmed that the spectral changes we observed were due to the formation of an oxidized species.

The involvement of oxygen in the reaction was investigated by deliberately excluding oxygen from the solutions of histidine and that of $[Co(II)TSPc]^{4-}$. This was achieved by bubbling

nitrogen to both solutions before mixing. The stoppered spectrophotometric cell was used in order to avoid the interference of atmospheric oxygen during the cause of the reaction. When oxygen was excluded from the reaction the spectral changes shown in **Figure 46** were not observed. This confirmed the earlier reports by Weber *et al* [129] which suggested that *l*-histidine and other imidazole ligands facilitated the oxidation of $[Co(II)TSPc]^{4-}$ to $[Co(III)TSPc]^{3-}$ by atmospheric oxygen. The actual role of *l*- histidine has however not been determined. To determine whether the oxidation of $[Co(II)TSPc]^{4-}$ to $[Co(III)TSPc]^{3-}$ would occur in the presence of atmospheric oxygen in the absence of histidine, histidine was not added to the solution of $[Co(II)TSPc]^{4-}$ in phosphate buffer and the stoppered spectrophotometric cell was used in order to avoid the variations in the oxygen dissolved in the solution of $[Co(II)TSPc]^{4-}$. In the absence of histidine, there were no changes observed over a period of twenty four hours, when the solution of $[Co(II)TSPc]^{4-}$ in pH 7.2 phosphate buffer was monitored with time, showing that the oxygen available in the solution is not enough to oxidize the $[Co(II)TSPc]^{4-}$ species without the facilitatory role of *l*-histidine. This observation then confirmed that *l*-histidine plays an important role in the oxidation of $[Co(II)TSPc]^{4-}$.

When phosphate buffer (pH = 6) was employed, the spectral changes shown in **Figure 32** were not observed. The changes were only observed for phosphate buffer at pHs varying from 7.2 to 10. These observations are in agreement with those of Gruen *et al* [127] which showed that an increase in the absorption due to the monomeric species followed by a further shift to lower energy has been observed when oxygen was bubbled through an alkaline solution of $[Co(II)TSPc]^{4-}$ and the final spectra in this reaction was attributed to the formation of an adduct between oxygen and $[Co(II)TSPc]^{4-}$. In neutral media these spectral changes were not observed [127]

Reports by Sundberg *et al* [130] have shown that the rate of autooxidation of $[Co(II)TSPc]^{4-}$

to $[Co(III)TSPc]^{3-}$ depends strongly on the nature of the axial ligand attached to the $[Co(II)TSPc]^{4-}$ complex. Electron withdrawing ligands tend to favour oxidation, while electron donating ligands stabilise $[Co(II)TSPc]^{4-}$ species. The differences in the ability of histidine to influence the oxidation of $[Co(II)TSPc]^{4-}$ at different pH values could be attributed to the differences in the electron donor ability of this amino acid at various pHs. Reports have shown that addition of histidine to the solutions of $[Co(II)TSPc]^{4-}$ results in axial ligation of histidine to the $[Co(II)TSPc]^{4-}$ species, [129,130] with the resulting complex undergoing oxidation to the $[Co(III)TSPc]^{3-}$ species. Since $[Co(II)TSPc]^{4-}$ is known to be coordinated to two water molecules in aqueous solution [115], it is suggested that during the reaction between histidine and $[(H_2O)_2Co(II)TSPc]^{4-}$, *l*- histidine replaces at least one of the water molecules from $[(H_2O)_2Co(II)TSPc]^{4-}$ to form $[(His)(H_2O)Co(II)TSPc]^{4-}$ complex (where His = histidine). The $[(His)(H_2O)Co(II)TSPc]^{4-}$ complex thus formed then undergoes oxidation as shown in **Equations 29** and **30**.

$$\mathbf{[(H_2O)_2Co(II)TSPc]^{4-} + His \rightarrow [(His)(H_2O)Co(II)TSPc]^{4-} + H_2O} \qquad \text{Equation 29}$$

$$\mathbf{[(His)(H_2O)Co(II)TSPc]^{4-} + O_2 \rightarrow [(His)(H_2O)Co(III)TSPc]^{3-}} \qquad \text{Equation 30}$$

In MPc complexes, axial substitution reactions are known to be stepwise reaction. The coordination of the first ligand normally occurs much faster than that of the second ligand [110,131,132]. The substitution of each ligand often occurs with distinct spectroscopic changes. The initial increase in the peak at 666 nm, **Figure 46(b)**, is associated with the monomeric $[(His)(H_2O)Co(II)TSPc]^{4-}$ species formed by the axial ligation of histidine to the $[(H_2O)_2Co(II)TSPc]^{4-}$ species before the electron transfer reactions shown in **Equation 30.** The final spectra, which is accompanied by the shift of 6 nm from spectra of the monomeric

$[Co(II)TSPc]^{4-}$ species , is then due to the oxidized $[Co(III)TSPc]^{3-}$ species.

As already mentioned, reduction of the $[(His)(H_2O)Co(III)TSPc]^{3-}$ species with the $NaBH_4$ resulted in regeneration of the original $[(H_2O)_2Co(II)TSPc]^{4-}$ species without any shift in the absorption maxima. This observation suggests that the histidine molecules are reversibly bound to the $[Co(II)TSPc]^{4-}$ complex and that the histidine ligands are lost on reduction of the oxidized $[(His)(H_2O)Co(III)TSPc]^{3-}$ species. If there was a change in axial ligands after the reduction of $[His(H_2O)_2Co(II)TSPc]^{4-}$ species, there would be a small shift in the original spectra of $[(H_2O)_2Co(II)TSPc]^{4-}$ regenerated upon chemical reduction of $[(His)(H_2O)Co(III)TSPc]^{4-}$.

Kinetic studies for the interactions of [Co(II)TSPc]$^{4-}$ with l-histidine.

In order to study the kinetics of the reaction between histidine and [Co(II)TSPc]$^{4-}$ complex, the formation of the [(His)(H_2O)Co(III)TSPc]$^{3-}$ species at 672 nm was followed by recording the absorbance at regular time intervals. The concentrations of histidine ranged from 0.001 to 0.3 mol dm^{-3} and the concentration of [Co(II)TSPc]$^{4-}$ complex was kept constant at 8.0 x 10^{-6} mol dm^{-3}. Since excess amounts of histidine were used, pseudo first order conditions were assumed in the determination of the rate constant for the oxidation of [Co(II)TSPc]$^{4-}$ in the presence of histidine. Plots of the logarithm of absorbance against time, **Figure 47**, were linear for the formation of the [(His)(H_2O)Co(III)TSPc]$^{3-}$ species. The linearity of these plots is the confirmation that the reaction between histidine and [(H_2O)$_2$Co(II)TSPc]$^{4-}$, is first order with respect to the later species.

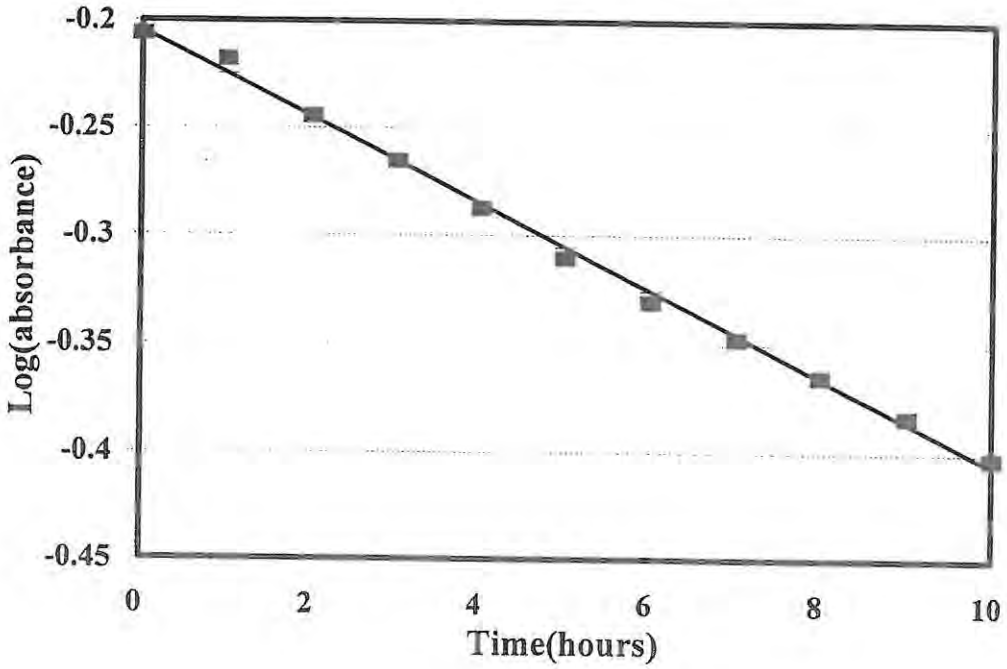

Figure 47 Plot of the logarithm of absorbance versus time for the reaction of histidine (0.085 mol dm^{-3}) with [Co(II)TSPc]$^{4-}$ (8.0 x 10^{-6} mol dm^{-3}).

The observed rate constant, k_{obs}, is given by the slope of the plot of the logarithm of absorbance against time. The observed rate constant was obtained for various concentrations of *l*-histidine. Plots of k_{obs} against concentration of histidine were also linear, **Figure 48**, and the linearity of this plots showed the first order dependence of the reaction on *l*-histidine.

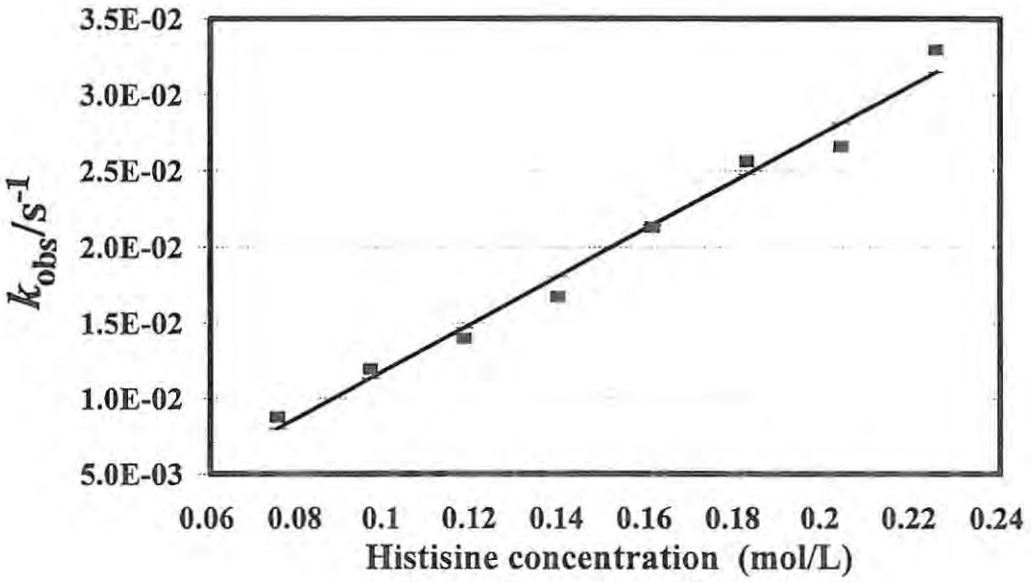

Figure 48 The plot of the observed rate constant, k_{obs} (s^{-1}) versus the concentration of histidine.

The slope of the plot of k_{obs} versus concentration of histidine gave the rate constant, $k_2 = 0.16 \pm 0.01$ mol^{-1} dm^3 s^{-1} . The increase of the observed rate constant with increase in the concentration of histidine implies that the rate law followed by the oxidation of $[(H_2O)_2Co(II)TSPc]^{4-}$ in the presence of histidine is given by **Equation 31**.

$$\frac{d[Co(III)TSPc]^{3-}}{dt} = k_{obs}[Co(III)TSPc]^{3-} \qquad \text{Equation 31}$$

Where $k_{obs} = k_2$[Histidine]

Since the exchange of the ligand for at least one water molecule is assumed to occur during oxidation, as discussed above, the coordination of histidine to the $[Co(II)TSPc]^{4-}$ species is therefore expected to show a larger rate constant than the oxidation process. As already mentioned, the role of histidine in the oxidation process has not been determined. Histidine itself is not known to be an oxidizing agent. Even in the oxidation of $[Co(II)TSPc]^{4-}$ to $[Co(III)TSPc]^{3-}$ it is clear that histidine is not an oxidizing agent, since in oxygen free solutions, in the presence of histidine, the oxidized $[Co(III)TSPc]^{3-}$ species is not formed.

Sundberg *et al* [130] have shown that during oxidation of Cu(II) histidine complexes by molecular oxygen, histidine gets oxidized. They proposed that electron transport in cytochrome is mediated by the oxygen oxidation of the imidazole ring of histidine leading to the suggestion that both Fe(II) cytochrome and histidine act as one-electron donor to oxygen. The observed linear dependence of the rate of formation of $[Co(III)TSPc]^{3-}$ on the concentration of histidine may be explained by proposing that both histidine and $[Co(II)TSPc]^{4-}$ transfer one electron to oxygen as was suggested for the electron transfer reaction in cytochromes. This proposal would explain the increase in the rate with increase in histidine concentration, and hence may lead to the understanding of the role of histidine and other ligands in the oxidation of the $[Co(II)TSPc]^{4-}$ species.

5.2 *Interaction of [Co(II)TSPc]$^{4-}$ with* L-*cysteine*

The interaction of cysteine with the [Co(II)TSPc]$^{4-}$ species is known to result in the oxidation of cysteine to cystine and the reduction of [Co(II)TSPc]$^{4-}$ to [Co(I)TSPc]$^{5-}$ at pHs greater than 4 [37,78]. It has been suggested that cysteine coordinate to MPc or metalloporphyrin complexes before the electron transfer [6,134]. **Figure 49** shows the spectral changes observed when cysteine (0.0069 mol dm^{-3}) was added to the solution of [Co(II)TSPc]$^{4-}$ in phosphate buffer (pH 7.2).

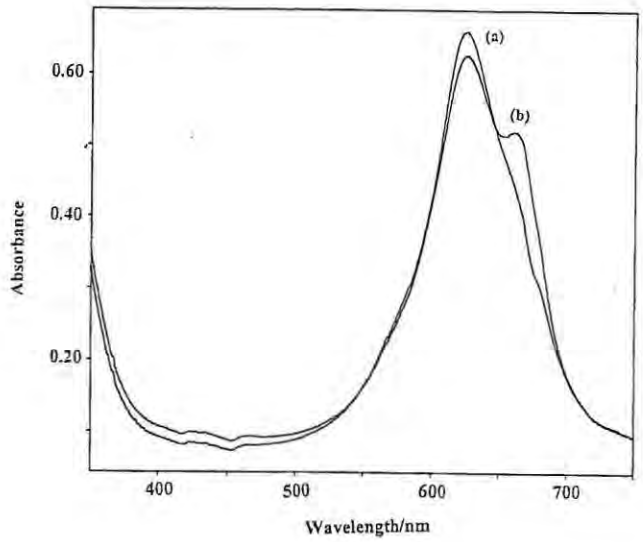

Figure 49 Spectral changes observed when cysteine (0.0069 mol dm^{-3}) was added to solutions containing 8.0 x 10^{-6} mol dm^{-3} of [Co(II)TSPc]$^{4-}$ dissolved in pH 7.2 phosphate buffer. Spectra (a) before addition of cysteine. (b) 1 min after addition of cysteine.

The spectral changes in Figure 49 above show an increase in the absorption at 660 nm, in the region of the spectra associated with the monomeric [Co(II)TSPc]$^{4-}$ species, **Figure 49(b)**. These spectral changes are associated with the coordination of cysteine to the [Co(II)TSPc]$^{4-}$

species. Assuming again that the axial positions in $[M(II)TSPc]^{4-}$ complexes are occupied by the water molecules, it is then suggested that the coordination of cysteine occurs by **Equation 32.**

$$\mathbf{[(H_2O)_2Co(II)TSPc]^{4-} + RSH \rightarrow [(RSH)(H_2O)Co(II)Pc]^{4-} + H_2O} \quad \text{Equation 32}$$

Where RSH = cysteine

The fact that the peak due to the monomeric $[Co(II)TSPc]^{4-}$ species is observed at 666 nm in the presence of histidine and at 660 nm in the presence of cysteine, is a good indication that these amino acids form slightly different species with $[Co(II)TSPc]^{4-}$. This observation is in agreement with the proposed occurrence of axial ligand exchanges on addition of histidine or cysteine to solution of $[Co(II)TSPc]^{4-}$. The small differences in the spectra are expected on changing ligands in axial positions in MPc complexes. The monomeric $[(RSH)(H_2O)Co(II)TSPc]^{4-}$ species is expected to show a slightly different Q band maxima than the $[(His)(H_2O)Co(II)TSPc]^{4-}$ species.

Spectral changes shown in **Figure 50** were observed when a solution containing Co(II)TSPc and cysteine was monitored with time. Both the dimeric peak at 624 nm and the peak at 660nm, **Figure 50(a)** decreased in intensity. While the peaks associated with the $[Co(I)TSPc]^{5-}$ species were formed, **Figure 50(b)**. The formation of Co(I)TSPc is known to be accompanied by the formation of peaks in the 400 - 500 nm region [133], due to charge transfer transitions.

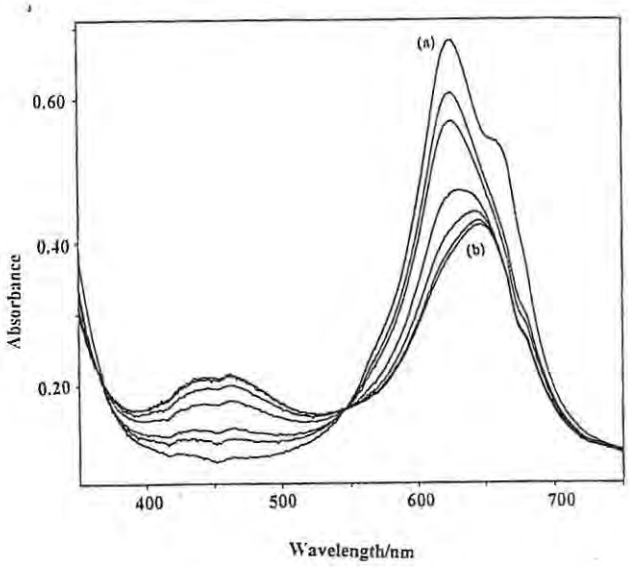

Figure 50: Spectral changes observed when cysteine (0.0069 mol dm^{-3}) was added to solutions containing 8.0 x 10^{-6} mol dm^{-3} of $[Co(II)TSPc]^{4-}$ dissolved in pH 7.2 phosphate buffer. Spectra (a) 1min after addition of cysteine. (b) 16 min after addition of cysteine.

The peaks associated with the $[Co(I)TSPc]^{5-}$ species in **Figure 50(b)** above were formed with the isosbestic points at 546 and 369 nm and show two broad peaks at 646 nm and near 450 nm The broad peak at 450 nm is due to charge transfer involving Co(I) species. The final spectra in **Figure 50(b)** is typical of the spectra of the $[Co(I)TSPc]^{5-}$ species [133].

Kinetic studies for the interaction of $[Co(II)TSPc]^{4-}$ with l-cysteine.

The peak associated with the coordination of cysteine to the $[Co(II)TSPc]^{4-}$ formed and then disappeared too fast to be followed with time. The disappearance of the spectra due to $[Co(II)TSPc]^{4-}$ species at 624 nm was followed with time and linear plots of the logarithm of

absorbance versus time were obtained, thus confirming a first order dependence of the reaction of the $[Co(II)TSPc]^{4-}$ species as was observed above for the interaction of histidine. The plots of k_{obs} versus the concentration of cysteine was linear, **Figure 51**, and the slope of the plot gave a rate constant of $k_2 = 2.2 \pm 0.2$ mol^{-1} dm^3 s^{-1}.

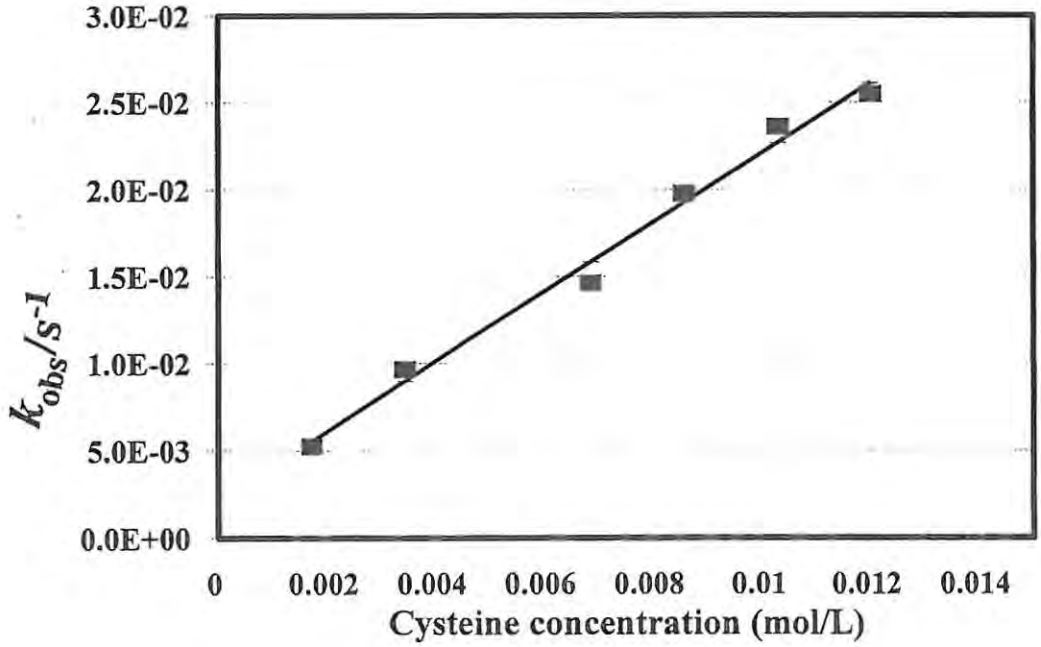

Figure 51 The plot of the observed rate constant, k_{obs} (s^{-1}) versus the concentration of cysteine.

Since the concentration of cysteine was much larger than the concentration of the $[Co(II)TSPc]^{4-}$ species, pseudo first order conditions were assumed. The observed linear dependence of k_{obs} on the concentration of cysteine again suggests that the reaction follow the rate law given by **Equation 33**.

$$\frac{-d[Co(II)TSPc]^{4-}}{dt} = k_{obs}[Co(II)TSPc]^{4-} \qquad \text{Equation 33}$$

Where $k_{obs} = k_2[RSH]$

This rate law is similar to that suggested in **Equation 31** for the oxidation of $[Co(II)TSPc]^{4-}$ in the presence of histidine except that in **Equation 31**, the formation of the oxidized $[Co(III)TSPc]^{3-}$ species was followed kineticaly. It is proposed that in the presence of cysteine, the equilibrium between the monomeric and the dimeric $[Co(II)TSPc]^{4-}$ species is shifted towards the monomeric species. The evidence for this is given by the spectral changes shown in **Figure 49**, which are due to the formation of the monomeric species on addition of cysteine to the solutions containing the $[Co(II)TSPc]^{4-}$. **Equations 34** and **35** show the possible mechanism for electron transfer reactions involving the $[(RSH)(H_2O)Co(II)TSPc]^{4-}$ species formed by **Equation 32.**

$$\mathbf{[(RSH)(H_2O)Co(II)TSPc]^{4-} \rightarrow [(RS^{\cdot})(H_2O)Co(I)TSPc]^{5-} + H^{+}} \qquad \text{Equation 34}$$

$$\mathbf{2[(RS^{\cdot})(H_2O)Co(I)TSPc]^{5-} \rightarrow 2[(H_2O)(Co(I)TSPc]^{5-} + RSSR} \qquad \text{Equation 35}$$

The transfer of an electron from cysteine to the central Co(II) metal in $[(RSH)(H_2O)Co(II)TSPc]^{4-}$ results in the formation of the $[Co(I)TSPc]^{5-}$ species. Two moles of the oxidized $RS^{\cdot}$ species, lost from the axial positions, react to form cystine (RSSR). It is believed that cysteine, like histidine, is reversibly bound to axial position in $[(RSH)(H_2O)Co(II)TSPc]^{4-}$ since the solutions of $[Co(I)TSPc]^{5-}$ could be chemically oxidized with bromine back to the starting $[Co(II)TSPc]^{4-}$ species without any changes in the spectra of $[Co(II)TSPc]^{4-}$.

5.3 Interactions of [Ni(II)TSPc]$^{4-}$ and [Pd(II)TSPc]$^{4-}$ with l-histidine and l-cysteine

On attempting the reactions between either [Ni(II)TSPc]$^{4-}$and [Pd(II)TSPc]$^{4-}$ with histidine and cysteine, we did not observe the spectral changes similar to those observed for reactions of histidine with [Co(II)TSPc]$^{4-}$. On addition of either histidine or cysteine to the solution of [Ni(II)TSPc]$^{4-}$ or [Pd(II)TSPc]$^{4-}$ in pH 7.2 phosphate buffer there was no change to the electronic spectra of the M(II)TSPc complexes (M = Ni or Pd). This was an implication that the reactions that took place between histidine or cysteine with [Co(II)TSPc]$^{4-}$ were not occurring in the case of [Ni(II)TSPc]$^{4-}$ and [Pd(II)TSPc]$^{4-}$ in phosphate buffer (pH 7.2).

Nickel(II) and palladium(II) metals are known to form four coordinate complexes. Hence the tetrasuphophthalocyanine complexes of these metals may not have the axially coordinated water molecules which are assumed to be coordinated to [Co(II)TSPc]$^{4-}$ species. Coordination of cysteine or histidine could not be possible in the case of [Ni(II)TSPc]$^{4-}$ or [Pd(II)TSPc]$^{4-}$. It is also known that for [Ni(II)TSPc]$^{4-}$ and [Pd(II)TSPc]$^{4-}$ oxidation or reduction occurs at the phthalocyanine ring and not at the central metal [115], unlike in [Co(II)TSPc]$^{4-}$ where oxidation occurs at the central metal. This could explain the lack of reactivity between these complexes, and cysteine or histidine.

5.4 Interaction of [Pd(II)Tmtppa]$^{4+}$ and [Pt(II)Tmtppa]$^{4+}$ complexes with *l*-cysteine and *l*-histidine

On addition of 0.01 mol dm^{-3} of *l*-histidine to solutions of NN'N"N'"-tetramethyltetra-2,3-pyridinoporphyrazine palladium(II), the spectral changes shown in **Figure 52** were observed. The Q band decreased in intensity and a new band was formed at approximately 525 nm with isosbestic points at 645, 545, and 368 nm. The change in colour of the solution from blue to purplish-blue was also observed.

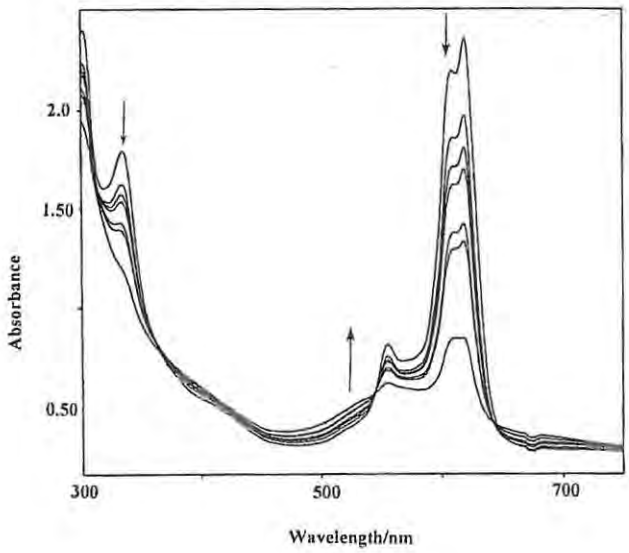

Figure 52 Spectral changes observed on addition of histidine (0.01 mol dm^{-3}) to solutions of [Pd(II)2,3Tmtppa]$^{4+}$ in distilled water. (a) before addition of histidine
(b) 1 hour after addition of histidine

The spectral changes observed in **Figure 52**, were also observed when *l*-histidine was added to the solutions of NN'N"N'"-tetramethyltetra-3,4-pyridinoporphyrazine palladium(II), NN'N"N'"-tetramethyltetra-2,3-pyridinoporphyrazine platinum(II) and NN'N"N'"-

tetramethyltetra-3,4-pyridinoporphyrazine platinum(II).

When the solution of *l*-cysteine in water was added to the solutions of the $[M(II)Tmtppa]^{4+}$ (M = Pd or Pt) complexes mentioned above, spectral changes very similar to those shown in **Figure 52** were observed only for the $[Pt(II)Tmtppa(-2)]^{4+}$ complexes. The reactions between the $[Pd(II)Tmtppa(-2)]^{4+}$ complexes with cysteine were too fast to follow accurately under the present experimental conditions. Spectral changes very similar to those shown in **Figure 52** were also observed on controlled potential electrolysis of $[M(II)Tmtppa(-2)]^{4+}$at potentials of the first reduction couple, see **Figure 33**, which were associated with the formation of $[M(II)Tmtppa(-3)]^{3+}$ species. The fact that the spectral changes observed on interaction of either histidine or cysteine with the $[Pd(II)Tmtppa]^{4+}$ and $[Pt(II)Tmtppa]^{4+}$ are very similar to those observed on controlled potential electrolysis of these complexes is an implication that the interaction between these amino acids with $[Pd(II)Tmtppa(-2)]^{4+}$ and $[Pt(II)Tmtppa]^{4+}$ result in reduction of these complexes and the formation of their monoaninon species. Thus the spectral changes observed in **Figure 52** are assigned to the reduction of the monoanions species, $[Pd(II)Tmtppa(-3)]^{3+}$ and $[Pt(II)Tmtppa(-3)]^{3+}$ formed upon reduction of $[Pd(II)Tmtppa(-2)]^{4+}$ and $[Pt(II)Tmtppa(-2)]^{4+}$ respectively. The reduction of $[Pd(II)Tmtppa(-2)]^{4+}$ by *l*-histidine and of $[Pt(II)Tmtppa(-2)]^{4+}$ by either *l*-histidine or *l*-cysteine was reversible since the addition of chemical oxidants such as bromine to the solution obtained after the formation of the final spectra shown in **Figure 52**, resulted in regeneration of the original spectra. The formation of a monoanion of $[Zn(II)Tmtppa(-3)]^{3+}$ complex has been reported before by Worhle *et al* [59] on photolysis of $[Zn(II)Tmtppa(-2)]^{4+}$ in the presence of cysteine. The spectral changes shown in Figure 52 were observed without photolysis of the solution containing $[Pd(II)Tmtppa(-2)]^{4+}$ or $[Pt(II)Tmtppa(-2)]^{4+}$ complexes and the appropriate amino acid. However, it was observed that irradiation of the solution containing the tetramethyl-

tetrapyridinoporphyrazine complex and histidine or cysteine with a 50 W tungsten lamp, resulted with a faster reduction of the complexes. Considering the same concentration of the $[Pd(II)Tmtppa(-2)]^{4+}$ or $[Pt(II)Tmtppa(-2)]^{4+}$ complexes and the amino acid, the time taken for the completeness of the reduction (as judged by the electronic absorption spectral changes) was decreased by a factor of 5 on irradiation.

Worhle *et al* [59] have shown that irradiation of the solution containing $[Zn(II)Tmtppa(-2)]^{4+}$ species resulted with the formation of the monoanion and finally with the formation of the dianion species, with λ_{max} at 500 nm, and the final reduction product consisted of a fine precipitate. However, there was no formation of a precipitate upon addition of cysteine or histidine to the solutions of $[Pd(II)Tmtppa(-2)]^{4+}$ and $[Pt(II)Tmtppa(-2)]^{4+}$ thus showing that the dianion species was not formed.

In section 5.1 and 5.2 it was shown that $[Co(II)TSPc]^{4-}$ species is oxidized in the presence of histidine and reduced in the presence of cysteine. For the $[M(II)Tmtppa(-2)]^{4+}$ complexes studied in this thesis, both histidine and cysteine acted as reducing agents. Since cysteine is a one electron reducing agent, the following mechanism is suggested for the reduction of the $[Pd(II)Tmtppa(-2)]^{4+}$ and $[Pt(II)Tmtppa(-2)]^{4+}$ complexes in the presence of the cysteine.

$$\mathbf{[M(II)Tmtppa(-2)]^{4+} + RSH \rightarrow [M(II)Tmtppa(-3)]^{3+} + RS^{\cdot} + H^{+}} \quad \text{Equation 36}$$

$$\mathbf{2RS^{\cdot} \rightarrow 2RSSR} \quad \text{Equation 37}$$

Where M(II) = Pd(II) or Pt(II)

RSH = cysteine

RSSR = cystine

Since [M(II)Tmtppa(-3)]$^{3+}$ species is also formed in the presence of histidine, it is believed that **Equation 36** may also apply for the reduction of [Pd(II)Tmtppa(-2)]$^{4+}$ and [Pt(II)Tmtppa(-2)]$^{4+}$ in the presence of histidine. It was proposed in sections 5.1 and 5.2 that addition of histidine or cysteine to solutions of [Co(II)TSPc]$^{4-}$ result in axial ligation of the amino acid to the MPc complex. Coordination of ligands on the axial positions in MPc complexes is normally characterized by small shifts of the Q band in the absorption spectra of the MPc complex. Spectral changes which would suggest the coordination of either histidine or cysteine to the [Pd(II)Tmtppa(-2)]$^{4+}$ and [Pt(II)Tmtppa(-2)]$^{4+}$ complexes were not observed.

Kinetic studies for the interaction of [Pd(II)Tmtppa(-2)]$^{4+}$ and [Pt(II)Tmtppa(-2)]$^{4+}$ complexes with l-histidine and l-cysteine.

The disappearance of [M(II)Tmtppa(-2)]$^{4+}$ species in the presence of *l*-histidine and *l*-cysteine, was followed with time. Since the concentration of the histidine and that of cysteine were much greater than the concentration of the [M(II)Tmtppa(-2)]$^{4+}$, again first order conditions were assumed in the determination of the rate constants for the reduction of the [M(II)Tmtppa(-2)]$^{4+}$ complexes.

Plots of the logarithm of absorbance of [M(II)Tmtppa]$^{4+}$ against time were linear for at least 70% conversion of [M(II)Tmtppa(-2)]$^{4+}$ to [M(II)Tmtppa(-3)]$^{3+}$ species, **Figure 53**. The linearity of the plots is the confirmation that the reaction is first order with respect to the [M(II)Tmtppa(-2)]$^{4+}$ species. The slopes of these plots give the observed rate constant. Plots of observed rate constant against the concentration of histidine or cysteine were also linear , thus showing the first order dependence of the reaction on histidine or cysteine.

Figure 54 shows the plots of k_{obs} against the concentration of cysteine or histidine for [Pt(II)3,4-Tmtppa(-2]$^{4+}$. Similar plots were obtained for the reaction of cysteine or

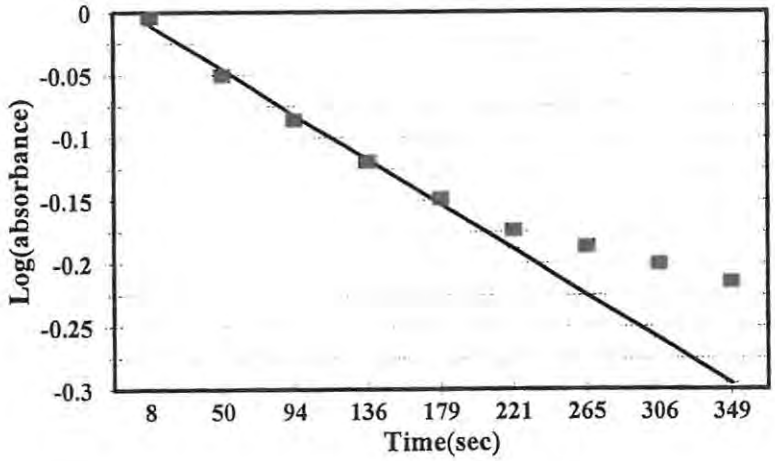

Figure 53 Plot of absorbance of Pd(II)3,4Tmtppa]$^{4+}$ against time, for the reduction of [Pd(II)3,4Tmtppa]$^{4+}$ in the presence of histidine.

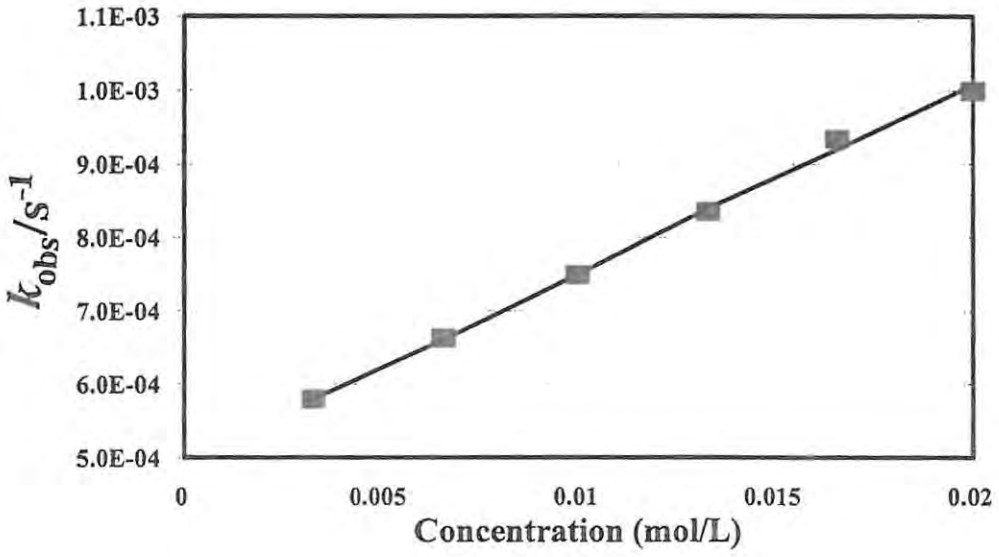

Figure 54 Plot of the observed rate constant, k_{obs} (s^{-1}) versus concentration of (a) histidine for the reduction of [Pt(II)3,4Tmtppa(-2)]$^{4+}$.

histidine with other $[M(II)Tmtppa(-2)]^{4+}$ complexes. The specific rate constant, k_2, for the $[M(II)Tmtppa(-2)]^{4+}$ complex is given by the slope of the plot of k_{obs} versus concentration histidine or cysteine.

Table 8 lists the values of specific rate constants for the various $[M(II)Tmtppa(-2)]^{4+}$ studied in this thesis. The increase of the observed rate constant with the increase in concentration of histidine or cysteine suggests that the rate law followed by the reduction of $[M(II)Tmtppa(-2)]^{4+}$ in the presence of either histidine or cysteine is given by **Equation 38.**

$$\frac{\mathbf{d[M(II)Tmtppa(-2)]^{4+}}}{\mathbf{dt}} = \mathbf{k_{obs}[M(II)Tmtppa(-2)]^{4+}} \qquad \text{Equation 38}$$

Where $k_{obs} = k_2$[histidine] or $= k_2$[cysteine]

It is observed from Table 8 that the rate constant for the interaction of cysteine with $[Pt(II)2,3Tmtppa(-2)]^{4+}$ is higher than the rate constant observed for cysteine interaction with $[Pt(II)3,4Tmtppa(-2)]^{4+}$. A similar trend is observed for the interaction of histidine with $[Pd(II)2,3Tmtppa(-2)]^{4+}$ and $[Pd(II)3,4Tmtppa(-2)]^{4+}$. This observation suggests that the position of the pyridine ring somehow affects the interaction of the amino acids with the tetramethyltetrapyridinoporphyrazine complexes.

Table 8 Rate constants for the interaction of cysteine or histidine with the $[M(II)Tmtppa]^{4+}$ complexes in water.

Complex	Amino acid	$k_2/dm^3\ mol^{-1}\ s^{-1}$
$[Pt(II)2,3Tmtppa(-2)]^{4+}$	Cysteine	0.26 ± 0.01
$[Pt(II)2,3Tmtppa(-2)]^{4+}$	Histidine	0.12 ± 0.01
$[Pt(II)3,4Tmtppa(-2)]^{4+}$	Cysteine	0.088 ± 0.007
$[Pt(II)3,4Tmtppa(-2)]^{4+}$	Histidine	0.0019 ± 0.0001
$[Pd(II)2,3Tmtppa(-2)]^{4+}$	Histidine	0.056 ± 0.005
$Pd(II)3,4Tmtppa(-2)]^{4+}$	Histidine	0.0026 ± 0.006

Comparing the corresponding Pt(II) and Pd(II) complexes, a faster rate constant was obtained for the histidine reduction of the $[Pd(II)3,4Tmtppa(-2)]^{4+}$ than for the corresponding $[Pt(II)3,4Tmtppa(-2)]^{4+}$ complex. In general, the Pd complexes showed the faster rate of reduction in the presence of cysteine than the Pt complexes, since the reaction between cysteine and the Pd complexes was too fast to follow under our experimental conditions, whereas these reactions were observed for the Pt complexes. However, the rate constant for the reaction of the $[Pd(II)2,3Tmtppa(-2)]^{4+}$ with histidine was lower than for the reduction of $[Pt(II)2,3Tmtppa(-2)]^{4+}$ with histidine. It is observed in Table 8 that the rate constants for the interaction $[M(II)Tmtppa(-2)]^{4+}$ complexes with cysteine are higher than the corresponding rate constants for the interaction with histidine. However, the rate constants for the reduction of $[M(II)Tmtppa(-2)]^{4+}$ complexes in the presence of cysteine are lower than the rate constant (2.2 $dm^3\ mol^{-1}\ s^{-1}$) we have obtained (section 5.2) for the reduction of $[Co(II)TSPc]^{4-}$ to $[Co(I)TSPc]^{3-}$ in the presence of cysteine. This could be due to the fact that the site of reduction is the central metal in Co(II)TSPc, whereas ring based reductions occur in Pd and Pt complexes.

In attempts to react the MPc complexes or the $[MTmtppa]^{4+}$ complexes with proteins such as Bovine Serum Albumen (BSA) or metallothionein, we observed no change in the absorption spectra of MPc or $[MTmtppa]^{4+}$ complexes, thus indicating that there was no interaction between these complexes and the proteins. The solution of the MPc complex, in phosphate buffer pH 7.2, became cloudy after few minutes of adding the protein indicating that the protein precipitates.

6. Photosensitization Reactions of MPcs

6.1 Determination of quantum yield for singlet oxygen production by Os(II) and Ru(II) phthalocyanine complexes

As discussed in the introduction, phthalocyanine complexes act as photosensitizers for the generation of singlet oxygen, an important step for Type II mechanism in PDT. We tested the Os(II) and Ru(II) phthalocyanine complexes for their efficiency in generating singlet oxygen. DPBF was employed as a convenient quencher for singlet oxygen. The spectra of DPBF can easily be monitored since the peak is at a region where most MPc complexes do not absorb.

The quantum yield (Q_Δ) for singlet oxygen production by $[(CN)_2Ru(II)Pc]^{2-}$ and $[(CN)_2Os(II)Pc]^{2-}$ complexes in this work was determined using DPBF as a chemical quencher. DPBF is soluble in DMF and in other organic solvents such as DMSO and acetonitrile. However this compound does not dissolve in water and therefore we used DMF as a solvent for the photolysis of $[(CN)_2Ru(II)Pc]^{2-}$ and $[(CN)_2Os(II)Pc]^{2-}$. The detailed method of photolysis is outlined in section 2.8.

The singlet oxygen, $O_2(^1\Delta_g)$, generated by photolysis of MPc complexes in the visible region and in the presence of triplet molecular oxygen, $O_2(^3\Sigma_g)$, is known to decay according to the following decay pathways [135,136].

$$O_2(^1\Delta_g) \xrightarrow{K_d} O_2(^3\sum_g) \quad \text{(natural decay)} \qquad \text{Equation 39}$$

$$\mathbf{DPBF} + O_2(^1\Delta_g) \xrightarrow{K_c} \mathbf{Oxidation\ products} \quad \text{(chemical quenching)} \qquad \text{Equation 40}$$

$$\mathbf{MPc} + \mathbf{O_2(^1\Delta_g)} \xrightarrow{K_p} \mathbf{O_2(^3\Delta_g)} + \mathbf{MPc} \quad \text{(physical quenching)} \qquad \text{Equation 41}$$

Physical quenching by DPBF is not expected to be significant since DPBF in known to be a pure chemical quencher for singlet oxygen in many solvents including DMF [135]. From **Equations 39** to **40**, the rate of disappearance of DPBF in the presence of $O_2(^1\Delta_g)$ is given by **Equation 42**.

$$\frac{-[\mathbf{DPBF}]}{\mathbf{dt}} = k_c[\mathbf{DPBF}][\mathbf{O_2(^1\Delta_g)}] \qquad \text{Equation 42}$$

Applying steady state gives:

$$[\mathbf{O_2(\Delta_g)}] = \frac{\mathbf{Q_\Delta I_o}}{K_d + K_c[\mathbf{DPBF}] + K_p[\mathbf{MPc}]} \qquad \text{Equation 43}$$

$\mathbf{I_o}$ is the rate of photon absorption by MPc photosensitizer. Combination of **Equation 42** and **43**, gives the modified Stern-Volmer plot, **Equation 44**.

$$\frac{-\mathbf{d[DPBF]}}{\mathbf{dt}} = \frac{\mathbf{I_o Q_\Delta Kc[DPBF]}}{\mathbf{Kc[DPBF]} + K'} \qquad \text{Equation 44}$$

Where $K' = K_d + K_p[\mathrm{MPc}]$

The inverse of Equation 44 gives Equation 45.

$$\frac{-dt}{d[DPBF]} = \frac{K'}{I_o Q_\Delta K_c [DPBF]} + \frac{1}{I_o Q_\Delta}$$ Equation 45

From the plots of the inverse of the disappearance of DPBF versus the inverse of the concentration of DPBF, the quantum yield, Q_Δ, may be determined. **Figure 55** shows the spectral changes observed when solutions of $[(CN)_2 Ru(II)Pc]^{2-}$ in DMF saturated with oxygen and in the presence of DBF (1.1×10^{-4} mol dm^{-3}) were photolysed with a 50 W tungsten lamp fitted with a 600 nm radiation filter.

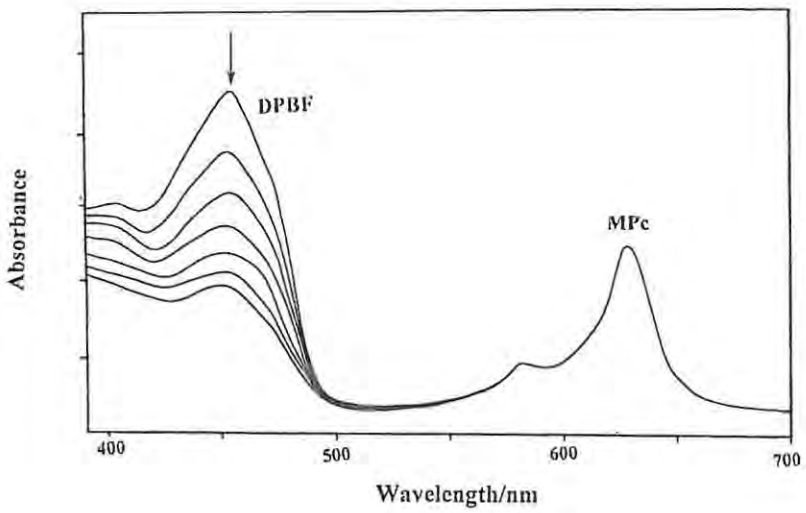

Figure 55 Spectral changes observed on photolysis of $[(CN)_2Ru(II)Pc]^{2-}$ in DMF in the presence of DPBF. (1.1×10^{-4} mol dm^{-3}).

Similar spectral changes were observed when $[(CN)_2Os(II)Pc]^{2-}$ instead of $[(CN)_2 RuPc]^{2-}$ was employed. There were no observable changes in the absorption spectra of the $[(CN)_2Ru(II)Pc]^{2-}$ or $[(CN)_2Os(II)Pc]^{2-}$ complexes during the photolysis indicating that the photosensitizer, $[(CN)_2Ru(II)Pc]^{2-}$ or $[(CN)_2Os(II)Pc]^{2-}$, were not consumed during the reaction. As **Figure 55** shows, there was a decrease in intensity in the absorption spectra of DPBF with photolysis time. This indicates that the concentration of DPBF was depleted as it reacted with singlet oxygen generated by the photoexcited $[(CN)_2Ru(II)Pc]^{2-}$ or

$[(CN)_2Os(II)Pc]^{2-}$ complexes. The fact that the absorption spectra of the $[(CN)_2$ Ru(II)Pc$]^{2-}$ or $[(CN)_2Os(II)Pc]^{2-}$ did not change in shape or decrease in intensity suggests that Type II mechanism was involved. We have mentioned in the introduction that Type II mechanism involves the energy transfer from the photosensitizer. Any changes in the absorption spectra of the photosensitiser would imply the involvement of Type I mechanism which involves an electron transfer and therefore would be accompanied by the oxidation of the $[(CN)_2Os(II)Pc]^{2-}$ or $[(CN)_2Ru(II)Pc]^{2-}$ and the formation of the π-cation radical species [19]. The absorption spectra of the $[(CN)_2Ru(II)Pc]^{2-}$ and $[(CN)_2Os(II)Pc]^{2-}$ would change drastically since oxidation in these complexes is known to occur at the phthalocyanine ring.

The absorbance of DPBF during photolysis was plotted against photolysis time. It was observed that the decrease in concentration of on the DPBF could be fitted to a straight line during the initial period in the quenching reaction, **Figure 56**.

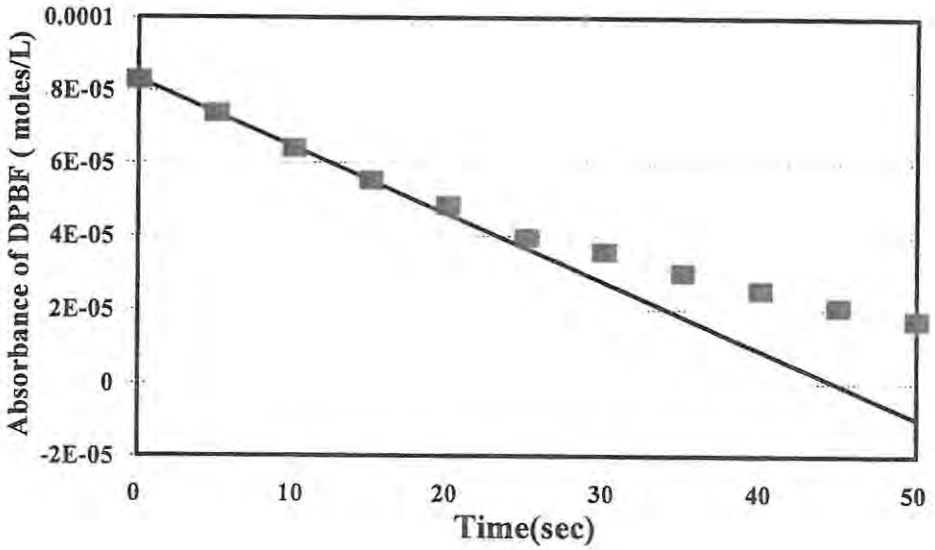

Figure 56 Plot of the absorbance of DPBF (1.1×10^{-4}) against photolysis time, for photolysis of $[(CN)_2RuPc]^{2-}$.

The quantum yield for singlet oxygen production by $[(CN)_2Ru(II)Pc]^{2-}$ and $[(CN)_2Os(II)Pc]^{2-}$, were calculated from **Equation 45** by plotting the inverse of the slopes of the plots in **Figure 56** versus the inverse of the concentration of DPBF, **Figure 57**.

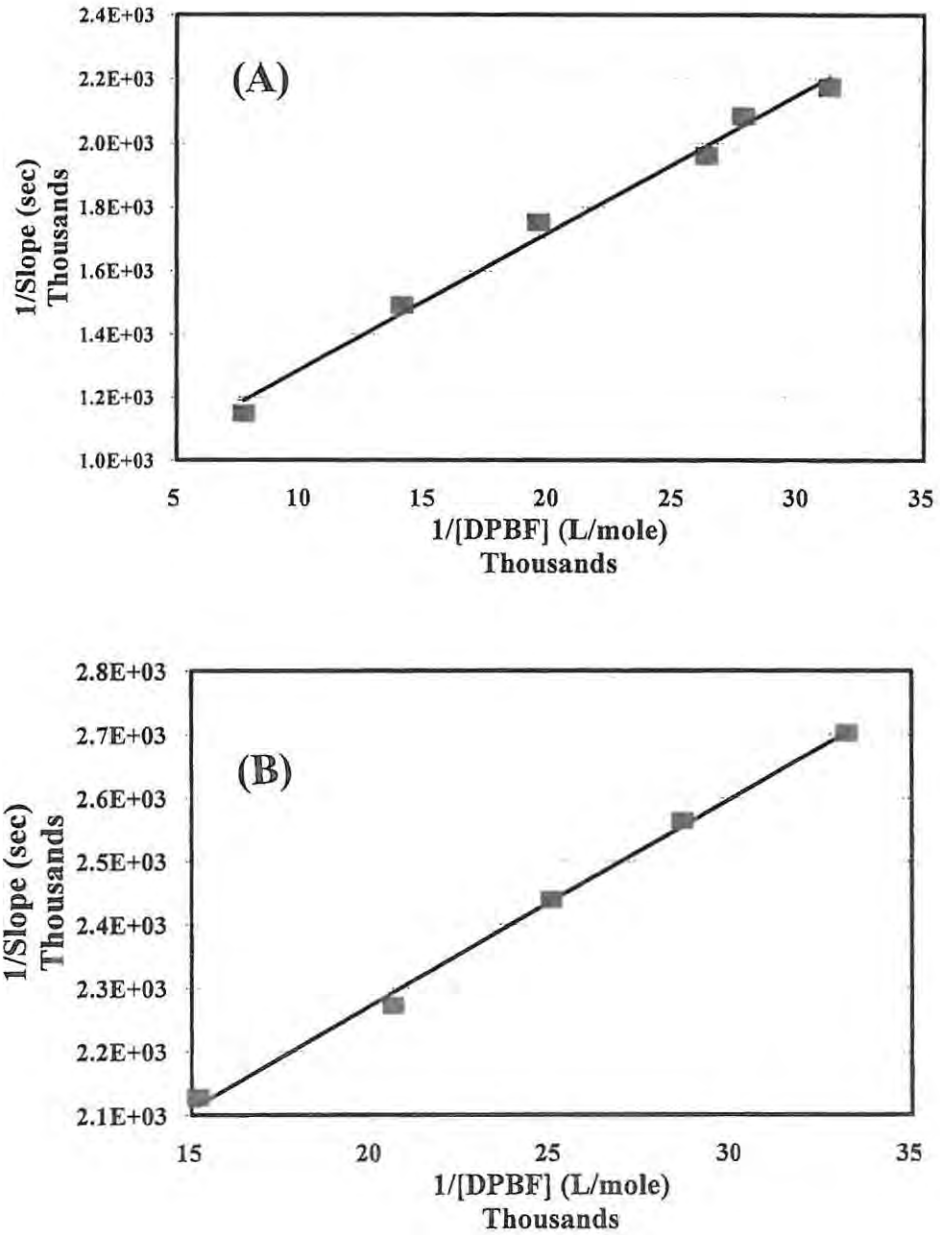

Figure 57 Plot of the inverse of slopes, obtained from Figure 56, versus the inverse of concentration of DPBF for photolysis of a) $[(CN)_2Ru(II)Pc]^{2-}$ and b) $[(CN)_2Os(II)Pc]^{2-}$.

From the intercept of the plots, shown above, and the intensity of radiation, I_o, calculated as outlined in section 2.7, the relative quantum yields for $[(CN)_2Ru(II)Pc]^{2-}$ and $[(CN)_2Os(II)Pc]^{2-}$ were calculated. The relative quantum yield values for singlet oxygen production by photosensitizers $[(CN)_2Os(II)Pc]^{2-}$ and $[(CN)_2Ru(II)Pc]^{2-}$ were 0.39 ± 0.05, and 0.76 ± 0.02 respectively.

It was found that $[(CN)_2Os(II)Pc]^{2-}$, as photosensitizer, has a lower quantum yield as compared to $[(CN)_2RuPc]^{2-}$. This differences in quantum yields values may be explained by considering the effects of the central metal on the triplet life times of the excited state of the photosensitizer. We have mentioned in the introduction that for the MPc complex to become a good photosensitizer, it should have a high triplet quantum yield and a long triplet life time[137,138]

The life time of the triplet excited states is largely determined by the nature of the central metal and the nature of the axial ligand. According to the literature [137,138], the increased $d\pi$-donor ability of the Os(II) ion is known to increase the electron density of the π-orbitals of the phthalocyanine ring in Os(II)Pc complexes as compared to the Ru(II)Pc complexes. This increases the mixing between the metal $d\pi$-orbitals and the ring $eg(\pi^*)$ lowest unoccupied molecular orbitals in Os(II)Pc complexes, thus increasing the spin orbit coupling. The increased spin orbit coupling tend to increase the intersystem crossing from the singlet excited state to the triplet excited state, and shortens the triplet lifetime. So, the lower quantum yields values for $[(CN)_2Os(II)Pc]^{2-}$ as compared to $[(CN)_2RuPc]^{2-}$ may be attributed to the more significant spin orbit coupling effects in $[(CN)_2Os(II)Pc]^{2-}$.

6.2 The effect of the axial ligand on the quantum yield for $O_2(^1\Delta_g)$ by Os(II) and Ru(II) phthalocyanine complexes

In order to investigate on the effect of the axial ligand on the quantum yield for singlet oxygen production by Os(II)Pc and Ru(II)Pc complexes, we also determined the quantum yields for the following MPc complexes: $Ru(II)Pc(py)_2$, $Os(II)Pc(py)_2$ and Ru(II)Pc(CO)(DMF). In order to make accurate the comparison of the quantum yields, the concentrations of the photosensitizers were kept constant (2.0×10^{-6} to 2.6×10^{-6} mol dm^{-3}), while the concentration of DBF was varied from 1.1×10^{-4} to 1.0×10^{-3} mol dm^{-3}. The amounts of oxygen bubbled in solution were kept the same and we maintained the same photolysis time for all the MPc complexes.

The spectral changes observed during photolysis of $Os(II)Pc(py)_2$, were very similar to that observed for the photolysis of cyano complexes of Ru(II)Pc and Os(II)Pc, in **Figure 57**, except that for the $RuPc(py)_2$, $OsPc(py)_2$ and RuPc(CO)(DMF) complexes the decrease in absorption spectra of DPBF were too fast to accurately determine the quantum yield. The fast decrease in DPBF spectra implies that larger concentrations of $O_2(^1\Delta_g)$ were generated for $RuPc(py)_2$, $OsPc(py)_2$ and RuPc(CO)(DMF) complexes. There were no changes in the absorption spectra of $Os(II)Pc(py)_2$ RuPc(CO)(DMF) and $(py)_2RuPc$ indicating that the photosensitizers were not involved in the chemical reaction.

The triplet life times of the excited states in MPc complexes is known to increase with increase in electron withdrawing character of the axial ligand. This increase in triplet life time is attributed to the changes in the energy gap between excited and ground states and the changes in vibrational frequencies that determine the rate of the radiationless relaxation processes. The slower reaction of the DPBF for the cyano complexes as compared to the bispyridine complexes may be explained in terms of the relative electron donor abilities of the cyanide and pyridine ligands. Cyanide as a ligand can either act as a sigma donor because of non-bonding pair on the

carbon atom, or it can act also act as a good π-acceptor because of the two vacant π* orbitals accompanying its triplet bond. When cyanide is coordinated to metal(II) phthalocyanine complexes, its sigma donor contribution dominates over the π-acceptor ability [19]. The sigma donor ligands are known to increase the mixing between the metal d-orbitals, thus increasing the spin orbit coupling in MPc complex, hence shortening the triplet life time of the excited states. The slower reaction of the DPBF for cyano complexes as compared to the bispyridine complexes suggest that the sigma donor effects of cyanide are stronger than the σ-donor effects of pyridine in Os(II)Pc and Ru(II)Pc complexes.

Reports by Ferraudi *et al* [86] have shown that RuPc(CO)(DMF) have the highest triplet life times and low quantum yield of the triplet state when compared with other axially coordinated Ru(II)Pc complexes. This may explain the fast decrease in intensity of the absorption spectra of DPBF on photolysis of Ru(II)Pc(CO)(DMF).

7. CONCLUSION

It has been shown in this thesis that GCE modified with the following MPc complexes: (DMSO)(Cl)Rh(III)Pc, $[(CN)_2Rh(III)Pc]^-$, $(DMSO)_2Ru(II)Pc$ or $(DMSO)_2Os(II)Pc$ show autocatalytic behaviour towards oxidation of cysteine, in that the peak current for the oxidation increase with repetitive scanning. When (py)ClRh(III)Pc, $(py)_2Ru(II)Pc$, and $(py)_2Os(II)Pc$ complexes (where the axial ligand was pyridine) were used to modify the electrode, the peak currents for oxidation of cysteine decreased rapidly after the first scan, showing that the electrode surface is poisoned by the oxidation products.

The autocatalytic behaviour exhibited by GCE modified with the above mentioned Rh(III), Ru(II) and Os(II) phthalocyanine complexes was observed at pHs >4 where cysteine oxidation currents have been reported to disappear very fast on cobalt phthalocyanine modified electrode [6]. The autocatalytic behaviour of Rh, Ru and Os phthalocyanine complexes has an advantage since it is achieved at pHs where proteins could be analyzed. This behaviour may be useful in analysis of the cysteine-containing proteins such as metallothionein. The detection limits for the determination of cysteine using Rh(III), Ru(II) and Os(II) phthalocyanine complexes are not as good as the limits reported for CoPc complex. This means that, even though Rh(III), Ru(II) and Os(II) phthalocyanine complexes improves the stability of the electrode surface when they are employed as chemical modifiers, they may not be used effectively for the analysis of biological systems where the concentration of cysteine is low. Further investigations may be required to find a catalyst that would improve both the stability of the electrode and the detection limits, and at the same time lower the potential at which oxidation of cysteine occurs.

Most of the applications of MPc complexes are limited by the insolubility of these complexes in aqueous solutions. The water soluble tetrasulphonated MPc complexes (MTSPcs) tend form dimers in aqueous solution and this is a serious drawback for the use of MPc complexes as photosensitizers, because dimers are photoinactive. The synthesis of water soluble MPc complexes which do not form aggregates in aqueous solutions is of great importance especially for the use of MPcs as photosensitizers in PDT. In this thesis, the MPc complex of and Os(II) containing cyanide on the axial positions, $[(CN)_2Os(II)Pc]^{2-}$, has been synthesized and this complex and the previously synthesized $[(CN)_2Ru(II)Pc]^{2-}$ show solubility in water without the formation of dimers. The tetramethyltetrapyridinoporphyrazine ($[MTmtppa]^{4+}$) complexes of Pd(II) and Pt(II) have also been synthesized. These complexes are highly soluble in water and they also do not form dimers.

The cyclic voltammetry studies of the Os(II) phthalocyanine complexes prepared in this thesis, $[(CN)_2Os(II)Pc]^{2-}$, $(py)_2Os(II)Pc$ and $(DMSO)_2Os(II)Pc$, show that the redox processes in these complexes occur on the phthalocyanine ring. The redox processes for these complexes are summarized in **Scheme 12.**

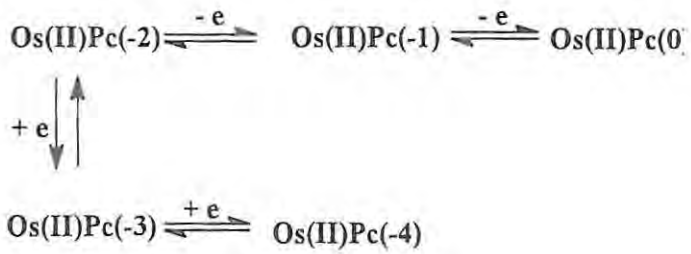

Scheme 12 Summary of the redox processes occurring in OsPc complexes.

The cyclic voltammetry studies of the Pd(II) and Pt(II) Tmtppa complexes exhibit two reduction processes. The first reduction is assigned to one-electron reduction of the ring in $[Pd(II)Tmtppa(-2)]^{4+}$ and $[Pt(II)Tmtppa(-2)]^{4+}$ with the formation of $[Pd(II)Tmtppa(-3)]^{3+}$ and $[Pt(II)Tmtppa(-3)]^{3+}$ species. The second reduction process is tentatively assigned to the electron transfer to the methylpyridinium substituents.

It has been shown that the $[Pd(II)Tmtppa(-2)]^{4+}$ and $[Pt(II)Tmtppa(-2)]^{4+}$ complexes are readily reduced in the presence of histidine and cysteine. The interaction of $[Co(II)TSPc]^{4-}$ with histidine facilitates the air oxidation of $[Co(II)TSPc]^{4-}$ to $[Co(III)TSPc]^{3-}$ species. On the other hand the interaction of $[Co(II)TSPc]^{4-}$ with cysteine results in the formation of $[Co(I)TSPc]^{5-}$ and cystine. The observed differences in the products obtained on interaction of histidine and cysteine may be explained by the fact that oxidation of cysteine is favoured relative to the oxidation of histidine due to the presence of sulfhydryl group in cysteine. Studies of the interaction of the MPc complexes with amino acids is an important step in understanding the mechanism involved in the interaction of MPc complexes with biological system since the MPc complexes are the porphyrin-type molecules which are important models of biological systems.

The fact that the MPc and the $[MTmtppa]^{4+}$ complexes mentioned above interact with amino acids, cysteine and histidine, suggests that these complexes may be of use in medicinal applications, where direct interaction of the MPc species with the biological substrate is required. However, there is a need for further investigation on the interaction of these complexes with a variety of amino acids and more importantly with variety of proteins. Attempts to interact the water soluble complexes, synthesized in this thesis, with proteins such as Bovine Serum Albumen (BSA) or metallothionein, were unsuccessful.

The relative quantum yield values for singlet oxygen production on photolysis of $[(CN)_2Os(II)Pc]^{2-}$ and $[(CN)_2Ru(II)Pc]^{2-}$ were 0.39 ± 0.05 and 0.76 ± 0.02 respectively. These values are slightly higher when compared with the reported quantum yields [106]. The quantum yields values may have been affected by the errors incurred in the determination of the intensity of radiation $\mathbf{I}_o$.
We have shown, however, that the relative quantum yields for singlet oxygen production is largely dependent on the nature of the central metal and also on the nature of the axial ligand. The lower quantum yield for the photosensitization of singlet oxygen production observed for $[(CN)_2Ru(II)Pc]^{2-}$ as compared to $[(CN)_2Os(II)Pc]^{2-}$ in an indication that π-donor ability of the central metal play an important role in photosensitization ability of the MPc complex.

The synthesis of water soluble MPc complexes with some other axial ligands other than cyanide would be a step further in realizing the use of MPc complexes in PDT. Even though Ru and Os phthalocyanine complexes with cyanide on the axial positions are soluble in water without the formation of dimers these complexes may not be suitable for medicinal applications since cyanide may be released in the body.

8. REFERENCES

1. R. L Migrom in *Colours of Life: An introduction to chemistry of porphyrins and related compounds*. Oxford University Press (1977).
2. D. Phillips, *Pure & Appl. Chem.*, 1995, **57(1)**, 126.
3. J. R Dawent, P. Douglas, A. Harriman, G. Porter and M-C Richoux, *Coord, Chem. Rev.*, 1982, **44**, 83.
4. N. Nensala, A. Nzimande and T. Nyokong, *J. Photochem. Photobiol. A: Chemistry* 98, 1996, 129.
5. N. Nensala and T. Nyokong, *Polyhedron*, 1997, **16(17)**, 2971.
6 T. Mafatle and T. Nyokong, *J. Electroanal. Chem.*, 1996, **408**, 213.
7. R. P Linstead, *J. Chem. Soc.*, 1934, 1016.
8. R. P Linstead and J.M Robertson, *J. Chem. Soc.*, 1936, 1195.
9. C. E Dent, R. P Linstead and A. R Lowe, *J. Chem. Soc.*, 1934, 1033.
10. J. H Webber and D. H Busch, *Inorg. Chem.*, 1965, **4(4)**, 469.
11. M. Hanack, P. Haisch, H. Lehman and Subramanian, *Synthesis*, 1993, 387.
12. J. M Robertson and I. J Woodward, *J. Chem. Soc.*, 1937, 219.
13. M. Gouterman, in D. Dolphin (ed) *The porphyrins: Physical chemistry*, Vol 3, part A, Academic Press New York, (1978), 1- 165.
14. M. J Stillman and T.Nyokong in C. C Leznoff and A. B. P Lever (ed) *Phthalocyanines: Properties and Applications*, VCH, vol. 1, chapt. 3, 1989.
15. A. B .P Lever, S. R Pickens, P. C Minor, S. Licoccia, B.S. Ramaswamy and K. Magnel, *J. Am. Chem. Soc.*, 1981,**103**, 6800.
16. W. A Nevin, M.R Hempstead, W. Liu, C. C Leznoff and A.B.P Lever, *Inorg. Chem.*, 1987 **26**, 570.

17. B. W Dale, *Trans. Faraday Soc.*, 1969, 65, 311.

18. M. J Stillman and T. Nyokong in C. C Leznoff and A. B. P Lever (ed) *Phthalocyanines: Properties and Application,* VCH, vol 1 chapt. 3, 1989.

19. T. Nyokong, *Polyhedron,* 1993, **12**, 375.

20. D. Dolphin, B. R James, A. J Murray and J. R Thornback, *Can. J. Chem.*, 1980, **321**, 309.

21. T. Nyokong, Z. Gasyna and M. J Stillman, *Inorg. Chem.*, 1987, **26**, 548.

22. T. Nyokong, Z. Gasyna and M. J. Stillman, *Inorg. Chim. Acta.*, 1986, **112**, 11.

23. P. C Minor, M. Gourterman and A.B.P Lever, *Inorg. Chem.*, 1985, **24**, 1894.

24. E. Ough, Z. Gasyna and M. Stillman, *Inorg. Chem.*, 1991, **30**, 2301.

25. D. W Clack and J. R. Yandle, *Inorg. Chem.*, 1972, **11**(8), 1738.

26. T. Nyokong, Z. Gasyna and M. J Stillman, *Am. Chem. Soc.*, 1986, 309.

27. A. J Bard and L. R Faulkner in *Electrochemical methods: Fundamentals and Applications,* John Wiley & Sons, New York (1980).

28. P. T Kissinger and W. R Heineman in *Laboratory Techniques in Electrochemistry,* Marcel Dekker (1996).

29. A. B. P Lever, Elena, R. Milaeva and G. Speier in C. C Leznoff and A. B. P Lever (ed) *Phthalocyanines: Properties and Applications,* VCH, vol.3, chapt 1, (1993). (same as 41)

30. A. B. P Lever and P. C Minor *Inorg. Chem.*, 1981, **20**, 4015.

31. R.O Loufty and C. Chang, *J. Chem. Phys.*, 1980, **73**, 2902.

32. A. Louati, M. El. Meray, J. J Andre, J. Smith, K. M. Kadish, M. Cross, and A. Giraudeau, *Inorg. Chem.*, 1985, **24**, 1175.

33. G. Fu, Y-S. Fu, K. Jayaraj and A. B. P Lever, *Inorg. Chem.*, 1990, **29**, 4090.

34. A. Giraudeau, A. Louati, M. Cross, J. J Andre, J. Simon, C. H Su and K. M Kadish, *J. Am. Chem. Soc.*, 1983, **105**, 2917.

35. A. B. P Lever and J. P Wilshire, *Can. J. Chem.*, 1976, **54**, 2514.

36. T. Nyokong, *Synth. Met.*, 1994, **66**, 107.

37. A. B. P Lever, S. Liccoccia, B. S Ramaswamy, S. A Kandil and D.V Stynes, *Inorg. Chim. Acta.*, 1981, **51**, 169.

38. A. Wolberg and J. Manasson, *J.Am. Chem.Soc.*, 1970, **92**, 2982.

39. H. Li and T.F Guarr, *J. Chem. Soc. Chem. Commun.*, 1989, 832.

40. C.C Leznoff, S. Creenberg, S. M Marcuccio, P. C Minor, P. Seymour and A. B. P Lever, *Inorg. Chim. Acta.*, 1984, **89**, L35.

41. A. B. P Lever, S. Licoccia, K. Magnell, P. C Minor and B. S Ramaswamy, *J. Am. Chem. Soc.*, 1982, 237.

42. L. D Rollman and R. T Iwamato, *J. Am. Chem. Soc.*, 1968, **90**, 1455.

43. R. H Campbell, G. A Heath, G. T Hefter and R. C. S McQeen, *J. Chem. Soc. Chem. Comm.*, 1983, 1128.

44. A. Giraudeau, F-R. F. Fau, and A. J. Bard, *J.Am.Chem.Soc.*, 1980, **102**, 5137.

45. A. B. P Lever, P. C Minor, and J. P Wilshire, *Inorg.Chem.*, 1981,**20**, 2550.

46. P. C Minor and A. B. P Lever, *Inorg.Chem.*, 1983, **22**, 826.

47. A. B. P Lever and P.C Minor, *Adv. Mol. Relax. Proc.*, 1980, **18**, 115.

48. A. Giraudeau, A. Louati, M.Cross, H. J Callot, L. K Hanson, R. Rhodes, and K. Kadish, *Inorg. Chem.*, 1982, **21**, 1581.

49. A. B. P Lever, *Adv.Inorg.Radiochem.*, 1965, 7, 27.

50. Y. Nishimura, Y. Kaneko, T. Arai, H. Sakuragi, K. Tokumaru, M. Kiteu, S. Yamamura and D. Matsunaga, *Chem. Lett*, 1990, 1935.

51. SAME AS 29

52. T. Nyokong, Z. Gasyna and M. J Stillman, *Am. Chem. Soc.*, 1986, 309.

53. T. Nyokong, *J. Chem. Soc. Dalton Trans*, 1994, 1359.

54. A. B. P Lever, Y. Tse, V. Manivannan, P. Seymour, V. V Strelets and L. S Persaud. *Inorg. Chem.*, 1996, **35**, 725.

55. H. Li and T. F Guarr, *J. Electroanal. Chem., Interfacial Electrochem.*, 1991, **297**, 169.

56. T. Nyokong, *SA Afr. J. Chem.*, 1995, **48(½)**, 23.

57. R. P Linstead, E. C Nobel and J. M Wright, *J. Chem. Soc.*, 1937, 911.

58. T. D Smith, J. Livorness, H. Taylor, J. R Pilbrow and G. R Sinclair, *J. Chem. Soc., Dalton Trans*, 1983, 1392.

59. D. Worhle and J. Getzel, *J. Chem. Soc., Perkin Trans (II)*, 1985, 1171.

60. P. Janda, J. Webber, L. Dunch and A. B. P Lever, *Anal. Chem.*, 1996, **68**, 960.

61. P. A Christensen and A. Hamnet in *Techniques and Mechanisms in Electrochemistry*, Chapman and Hall, New York, (1994).

62. J. Zhang, Y. H Tse, W.J. Pietro and A.B.P Lever, *J. Electroanal. Chem.*, 1996, **406**, 203.

63. G. Dougherty, *Inorg. Biochem.* 1988, **34**, 95.

64. K. Kasuga, M. Morisada and M. Handa, *Inorg. Chim Acta.* 1990, **174**, 161.

65. T. J. O'Shea, and S.M Lunte, *Anal. Chem.*, 1994, **66**, 307.

66. C. P Andreux and J. M Saveant, *J. Electroanal. Chem.*, 1978, **93**,163

67. M. .K. Halbert and R.P Baldwin, *Anal. Chem.*, 1985, **57**, 591.

68. Y-H. Tse, P. Janda and A.B.P Lever, *Anal. Chem.*, 1994, **66**, 384.

69. I. Juryan and D. Mandler, *Anal. Chem.*, 1994, **66**, 58.

70. J. Zagal and G. Fierro and R. Rozas, *J. Electroanal. Chem.*, 1981, **119**, 403.

71. J. H. Zagal, R.K. Sen and E. Yeager, *J. Electroanal. Chem.* 1977, **83**, 207.

72. J. Zagal an P. Herrea, *Electrochim. Acta*, 1985, **30**, 449.

73.. W. J. Pheth, in A J Bard (ed): *Encyclopedia of Electrochemistry of elements*, vol 8, Marcel

Derkker, Basel 1978.

74. F. A Cotton and G. Wilkinson, *Advanced Inorganinc Chemistry*, Weley Interscience, New York, 5th edn, 1988.

75. K. Tamura and K. Kahara, *J. Electrochem, Soc.*, 1976, **123**, 776.

76. J. H Zagal, *Coord. Chem. Revews*, 1992,119, 89.

77. P. Vasudevan, N. Phougat and A. K Shukla, *Appl. Organometallic Chem.*, 1996, **10**, 591.

78. J. D Cookson, T. D Smith, J.F Boas, P.R. Hicks and J. R Pilbrow, *J. Chem. Soc., Dalton Trans.*, 1977, 109.

79. K. M. K Korfhage, K. Ravichadran, R. P Baldwin, *Anal. Chem.*, 1984, **56**, 1577.

80. N. J Turro, in *Modern Molecular Photochemistry*, W. A Benjamin: New York, 1978.

81. D. R Arnold, N. C Bard, J.R Bolton, J.C.D Brand, P. W. M Jacobs, P. de Mayo, and W.R Ware, in *Photochemistry: An Introduction*, Academic Press: New York, (1974).

82. J. R Darwent, I. McCubbin and D. Phillips, *J. Chem. Soc. Faraday Trans* 2, 1982, **78**, 347.

83. A. Harriman, M-C. Richoux, G. Porter, *J. Chem . Soc., Faraday Trans* 2, 1981,**77**, 1175.

84. D. R Prasad and G. Ferraudi, *J. Phys. Chem.*, 1982, **86**, 4037.

85. D. R Prasad and G. Ferraudi, *Inorg. Chem.*, 1983, **22**, 1672.

86. G. Ferraudi and D.R Prasad, *J. Chem .Soc. Dalton. Trans.* 1984, 2137.

87. D. R Prasad and G. Ferraudi, *Inorg. Chem.*, 1982, **21**, 4241.

88. G. Ferraudi in C. C Leznoff and A. B. P Lever (ed) *Phthalocyanines: Properties and Applications*, VCH, vol. 1, chapt. 4, 1989.

89. G. Ferraudi and E.V Srisankar, *Inorg. Chem.*, 1978, **17**(11), 3164.

90. G. Ferraudi, *Inorg. Chem.*, 1979, **18**(4), 1005.

91. S. Muralidharan, G. Ferraudi and K. Schmatz, *Inorg. Chem.*, 1982, **21,** 2961.

92. I.. Rosenthal, C. Murali Krishna, P. Riesz an E. Ben-Hur, *Radiat. Res.*, 1986, **107**, 136.

93. J. R Darwent, P.Douglas, A. Harriman, G. Porter and M-C Richoux, *Coord. Chem. Rev.*, 1982, **44**, 83.

94. S. B Brown and T. G Truscott, *Chemistry in Britain*, Nov. 1993, 86.

95. N. Brasseur, H. Ali, J. Langlois and J.E van Lier, *Photochem. Photobiol.*, 1987, **46**(5), 739.

96. A. Harriman and M-C. Richoux, *J. Chem. Soc. Faraday Trans. 2.*, 1980, **76**,1618.

97. N. P Farell, A. J Murray, J. R Thornback, D. H Dolphin and B. R James, *Inorg. Chem.*, 1978, **28**, L144.

98. T. Nyokong, *Polyhedron* 1995, **14**, 643.

99. R. Behnisch and M. Hanack, *Synth. Met.* 1990, **36**, 387.

100. Y. Orihashi, H. Ohno, E. Tsuchida, H. Matsuda, H. Nakanishi and M. Kato, *Chem. Lett.*, 1987, 601.

101. J. Metz and M. Hanack, *J. Am. Chem. Soc.* 1983, **105**, 828.

102. D. Dolphin, B. R James, A. J Murray and J. R Thornback *Can. J. Chem.* 1980, **58**, 1125

103. M. Hanack and P. Vermelhren, *Inorg. Chem.* 1990, **29**, 134-136.

104. M. Hanack, A. Gul, L. R Subramarian, *Inorg. Chem.* 1992, **31**, 1542-1544.

105. W. Kobel and M. Hanack, *Inorg.* Chem. 1986, **25**, 103.

106. E. E Wegner and A. W Adamson, *J. Am. Chem. Soc.* 1996, **88:3** Feb 5.

107. J. G Calvert and J. N Pitts, Jr. in *Photochemistry*. John Wiley & Sons Inc. (1966)

108. P. Hambright, *Inorg. Chim. Acta.*, 1989, **157**, 95.

109. U. Zeiner, N. Fahny and M. Hanack., *Chem. Ber.*, 1983, **126**, 2559

110. T. Nyokong, *J. Chem. Soc., Dalton Trans.*, 1993, 3601.

111. K. Nakamoto in, *Infrared and Raman Spectra of Inorganic and coordination compounds*,

(3rd ed.) John Wiley & Sons, New York.

112. H. F shervil and L. Pinzuti, *Can. J. Chem.*, 1966, **44**, 125.

113. W. J Kroende and M. E Kenney, *Inorg. Chem.*, 1964, **3(5)**, 696.

114. J. Kobayashi, F. Kurokawa, N. Uyeda and E. Suito, *Spectrochim. Acta.*, 1970, **264**, 1305.

115. M. J Stillman, in C. C Leznoff and A. B. P Lever (eds), *phthalocyanines: properties and applications*, Vol 3, VCH, New York, (1993)

116. J. F Meyers, G. W Rayner-Canhan and A. B. P Lever, *Inorg. Chem.*, 1975, **14**, 461.

117. A. B. P Lever, *J. Chem. Soc.*, 1965, 1821.

118. W. P Griffith, in *Comprehensive Coordination Chemistry: The synthesis, reactions, preparations and applications of coordination compounds*, G. Wilknson and R. D Gullard and McCleverty (eds), Vol 4, Pergamon Press, Oxford, (1987).

119. J. E Scott, *Histochemie*, 1972, **30**, 215.

120. G. Araullo-McAdams and K. M Kadish, *Inorg. Chem.* 1990, **29**, 2749.

121. J. Limson and T. Nyokong, *Electroanalysis*, 1997, **9** 255.

122. S. Maroie, M. Savy and J. Verbist, *Inorg. Chem.*, 1979, **19**, 2560.

123. U. Zeiner, N. Fahny and M. Hanack, *Chem. Ber.* 1993, **126**, 2559.

124. A. Capobianchi, G. Pennisi, A. M Paolleti, G. Rossi, R. Caminiti, G. Sadun and E. Ercolani, *Inorog. Chem.*, 1996, **35**, 4643.

125. P. E Olsson, C. Haux, *Aquatic Toxilogy*, 1986, **9**, 4815.

126. R. W Olafson, *Int. Peptite Protein Res.*, 1984, **24**, 303.

127. L. C Gruen and R. J Blagrove *Aust. J. Chem.* 1973, **26**, 319.

128. A. B. P Lever, M. R Hempstead, C. C Leznoff, W. Leu, M. Melnik, W. A Nevin and P. Seymour, *Pure and Applied. Chem.*, 1986, **58**, 1467.

129. J. H Weber and D. H Busch, *Inorg. Chem.*, 1965, **4**, 472.

130. R. J. Sundberg and R. B Martin, *Chem. Rev.*, 1974, **74**, 496.

131. G. Pennesi, C. Ercolani, G. Rossi, P. Ascenzi, M Brunori and F. Monacell, *J. Chem. Soc., Dalton Trans,* 1985, 1113.

132. P. Asceni, M. Brunori, G. Pennesi, C. Ercolani and F. J. Monacelli, J. Chem. Soc., Dalton Trans., 1990, 105.

133. N. N Kundo and N. P Keir, Russ. *J. Phys. Chem.*, 1968, **42**, 707.

134. D. W Pang and Z. L Wang, *J. Electroanal. Chem.*, 1993, **358**, 235.

135. P. B Merkel and D. R Kearns., *J. Am. Chem. Soc.*, 1975, **97(2)**, 462.

136. M. G. Lagorio, L. E Decelio, E. A San Roman and S. E Bralavsky, *J. Photochem. Photobiol. B: Biol. 3.*, 1989, 615.

137. S. Gentemann, J. Albaneze, R. Garcia-Ferrer, S. Knapp, J. A Potenza, H. J Schuga and D. Holten, *J. Am. Chem. Soc.*, 1994, **116**, 281.

138. A. Antipas, J. W Buchler, M. Gouterman and P. D Smith, *J. Am. Chem. Soc.*, 1978, **100**, 3015.

139. R. T Morrison and R. N Boyd in *Organic Chemisty*, 5th edn., Allyn & Bacon (London) 1987.

APPENDIX 1

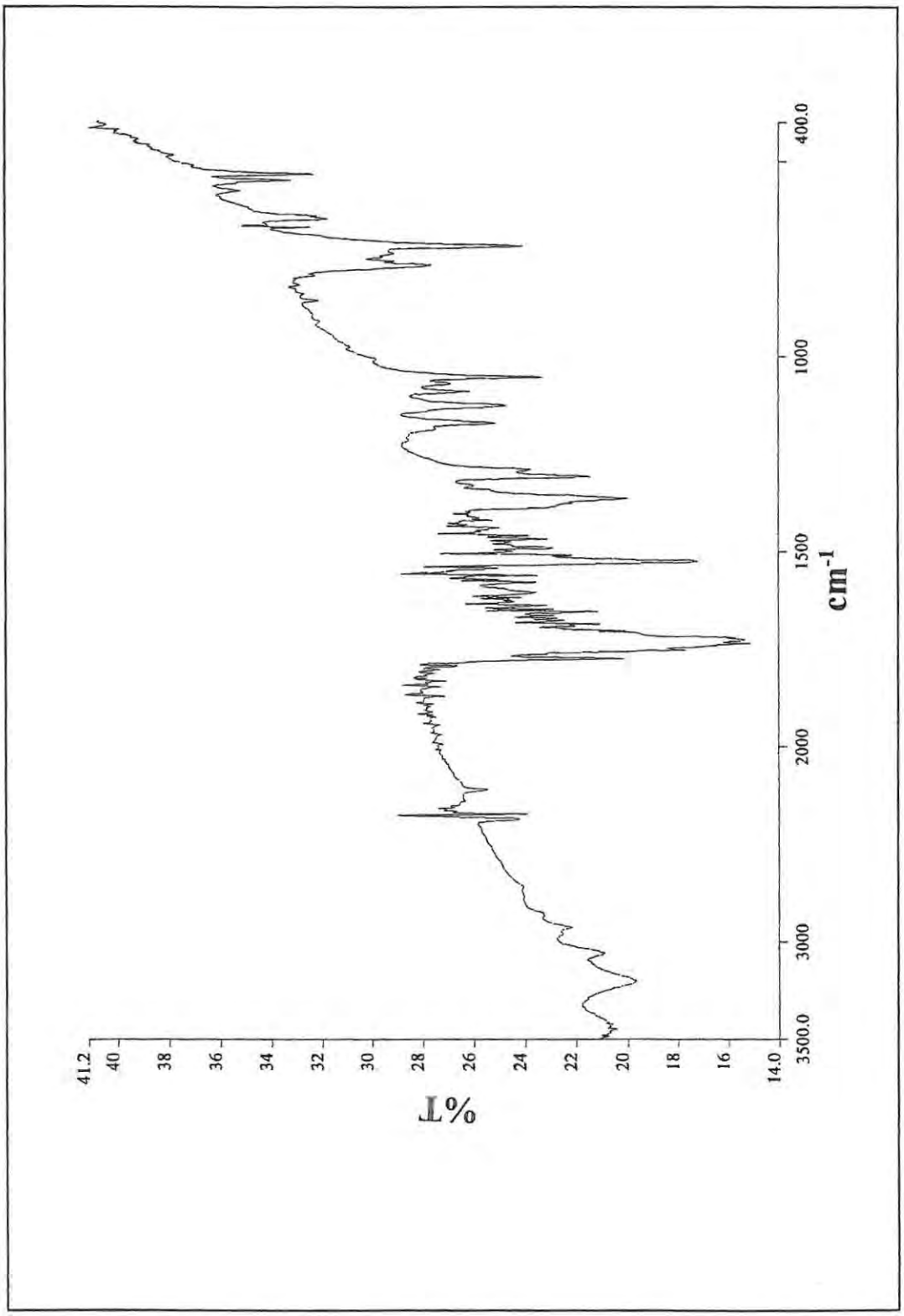

IR spectra of $(py)_2Os(II)Pc$

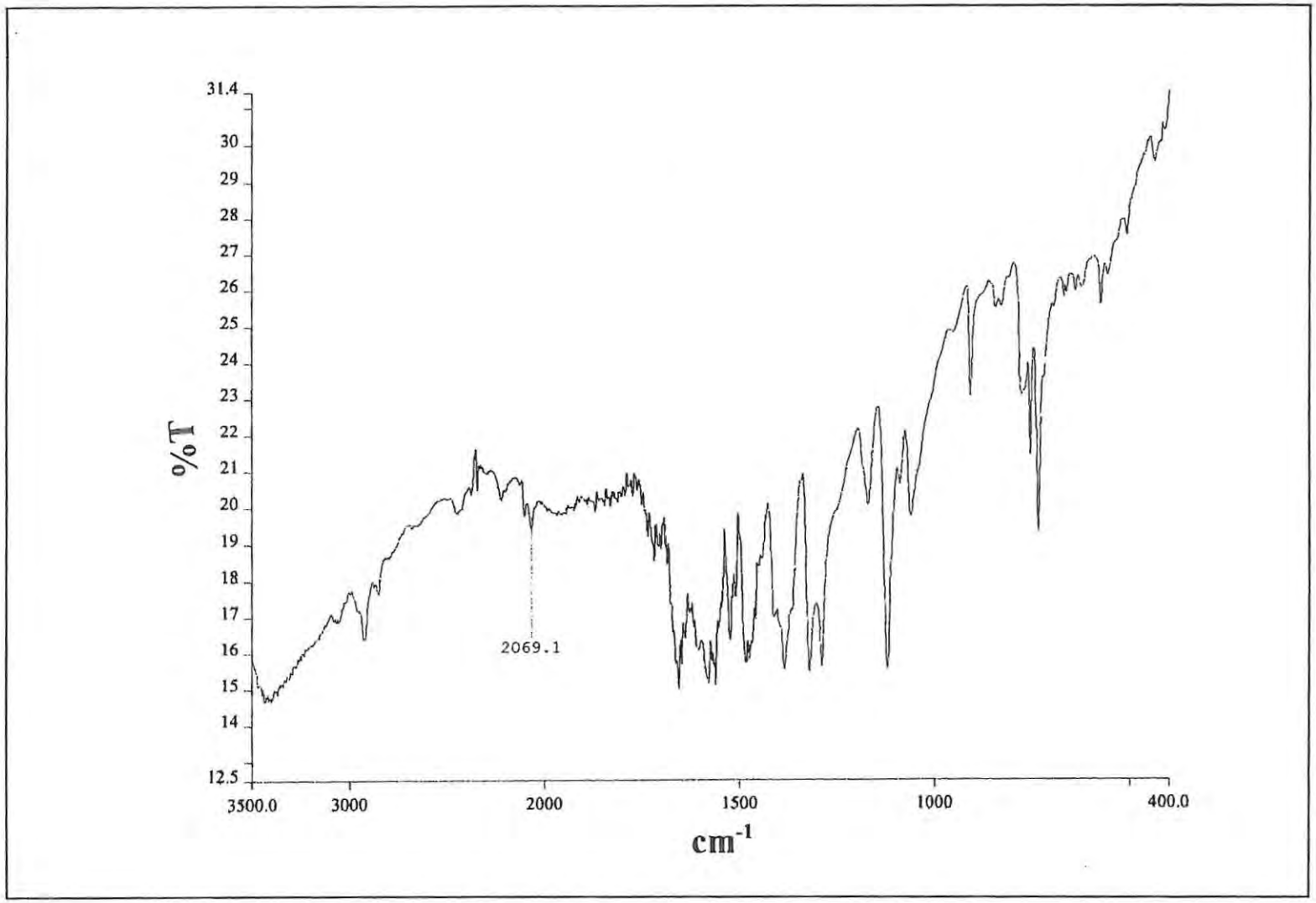

IR spectra of $K_2[(CN)_2Os(II)Pc]$

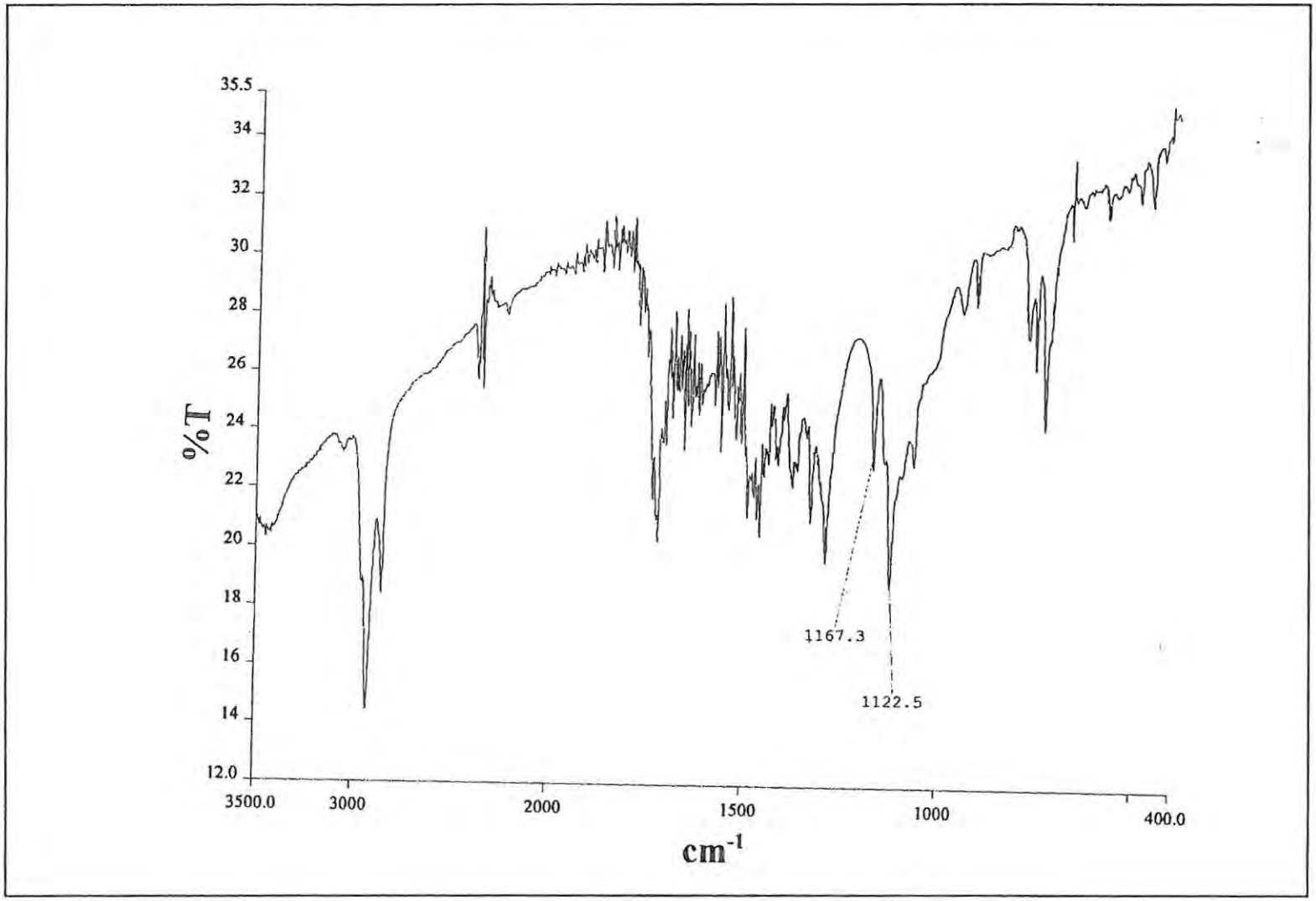

IR spectra of $(DMSO)_2Os(II)Pc$

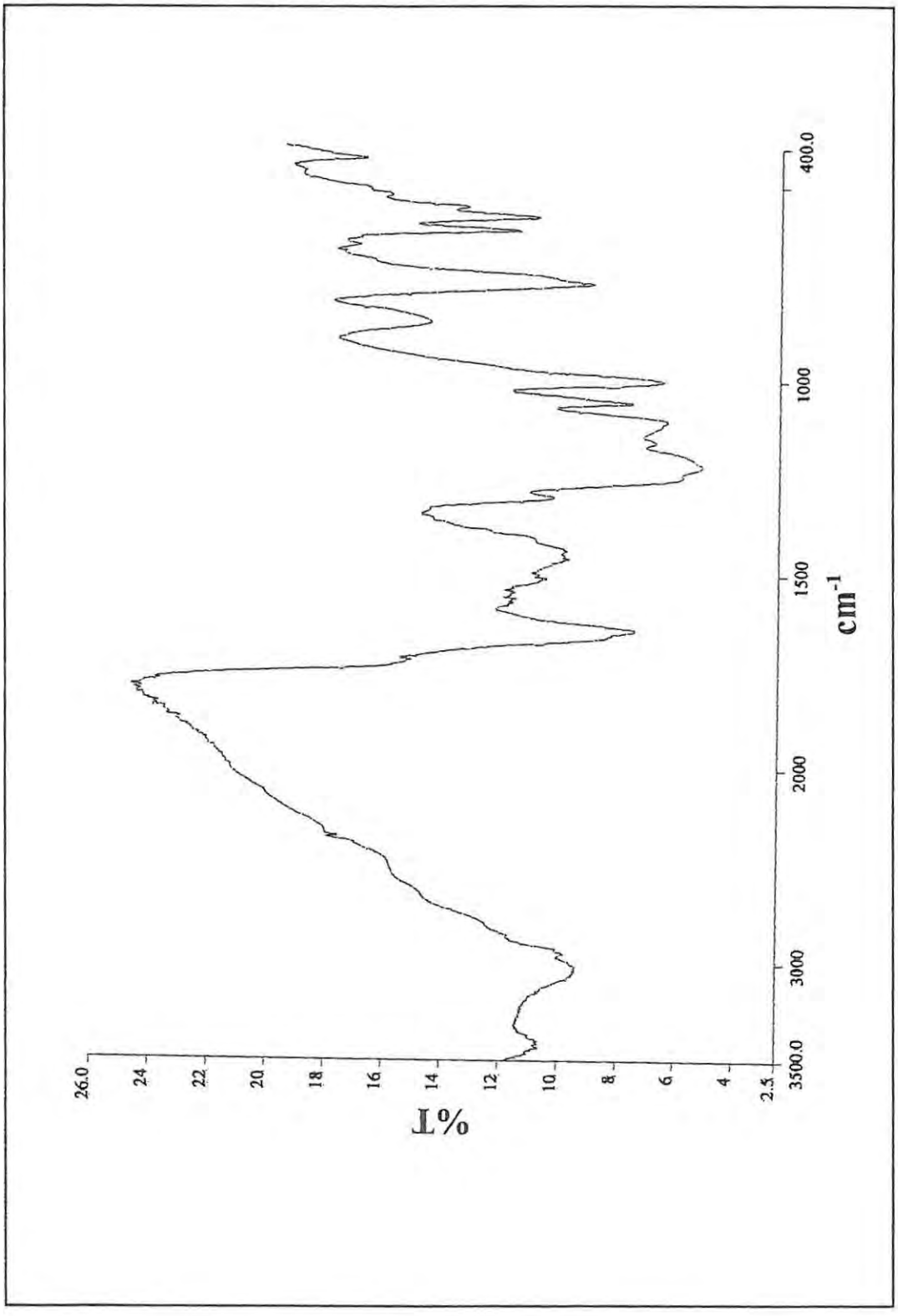

IR spectra of [Pd(II)3,4Tmtppa(-2)]$^{4+}$

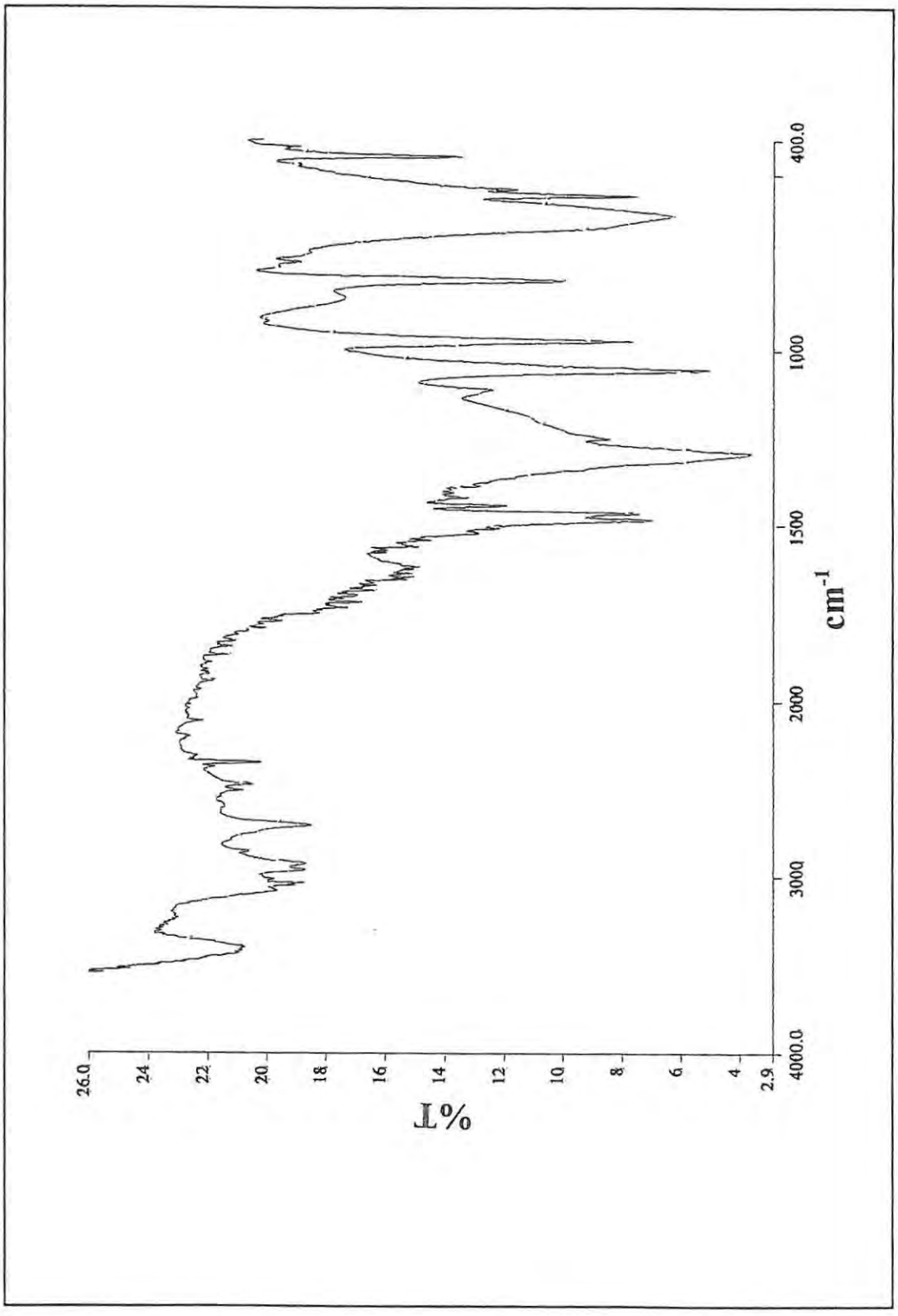

IR spectra of $[Pd(II)2,3Tmtppa(-2)]^{4+}$

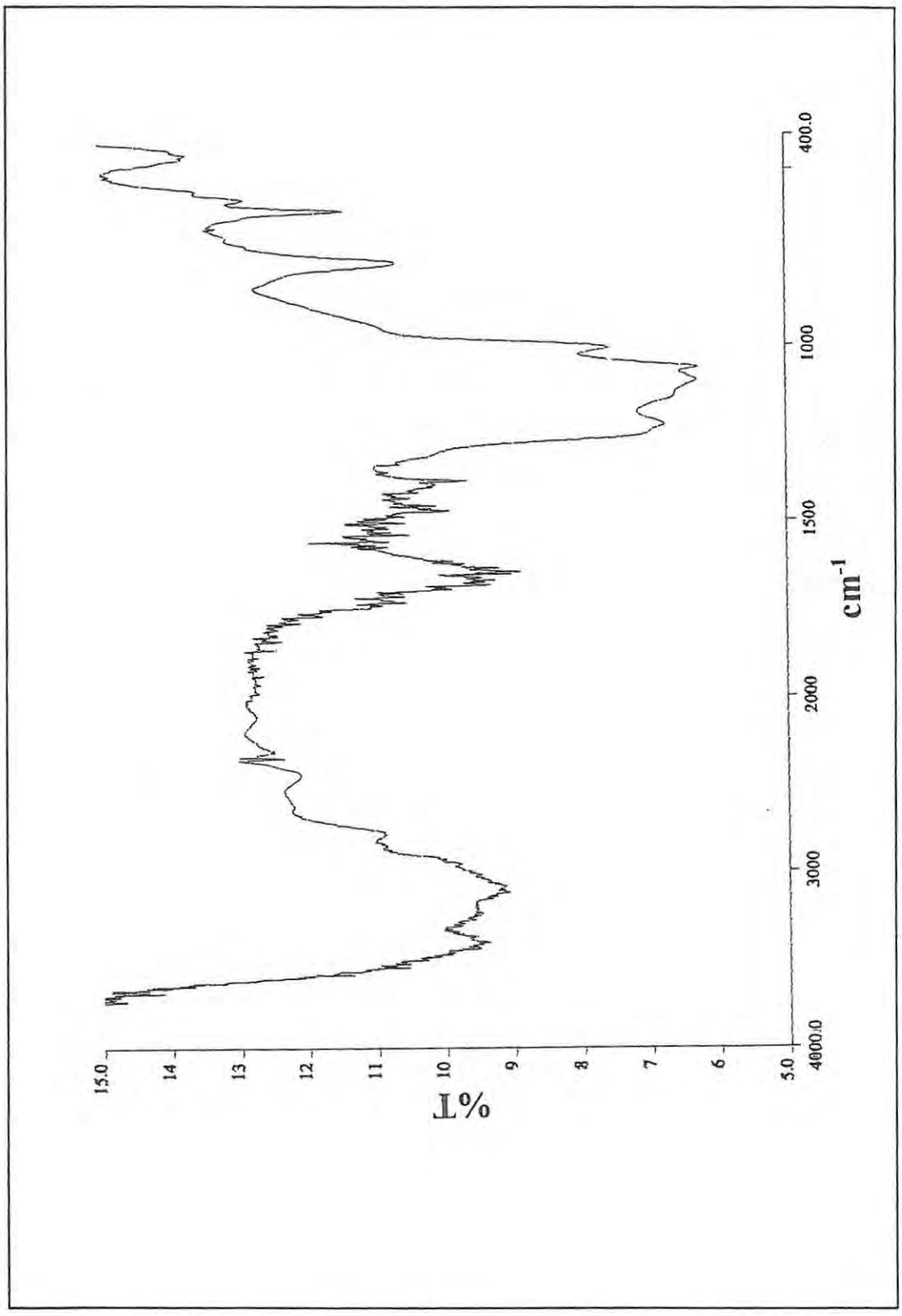

IR spectra of $[Pt(II)3,4Tmtppa(-2)]^{4+}$

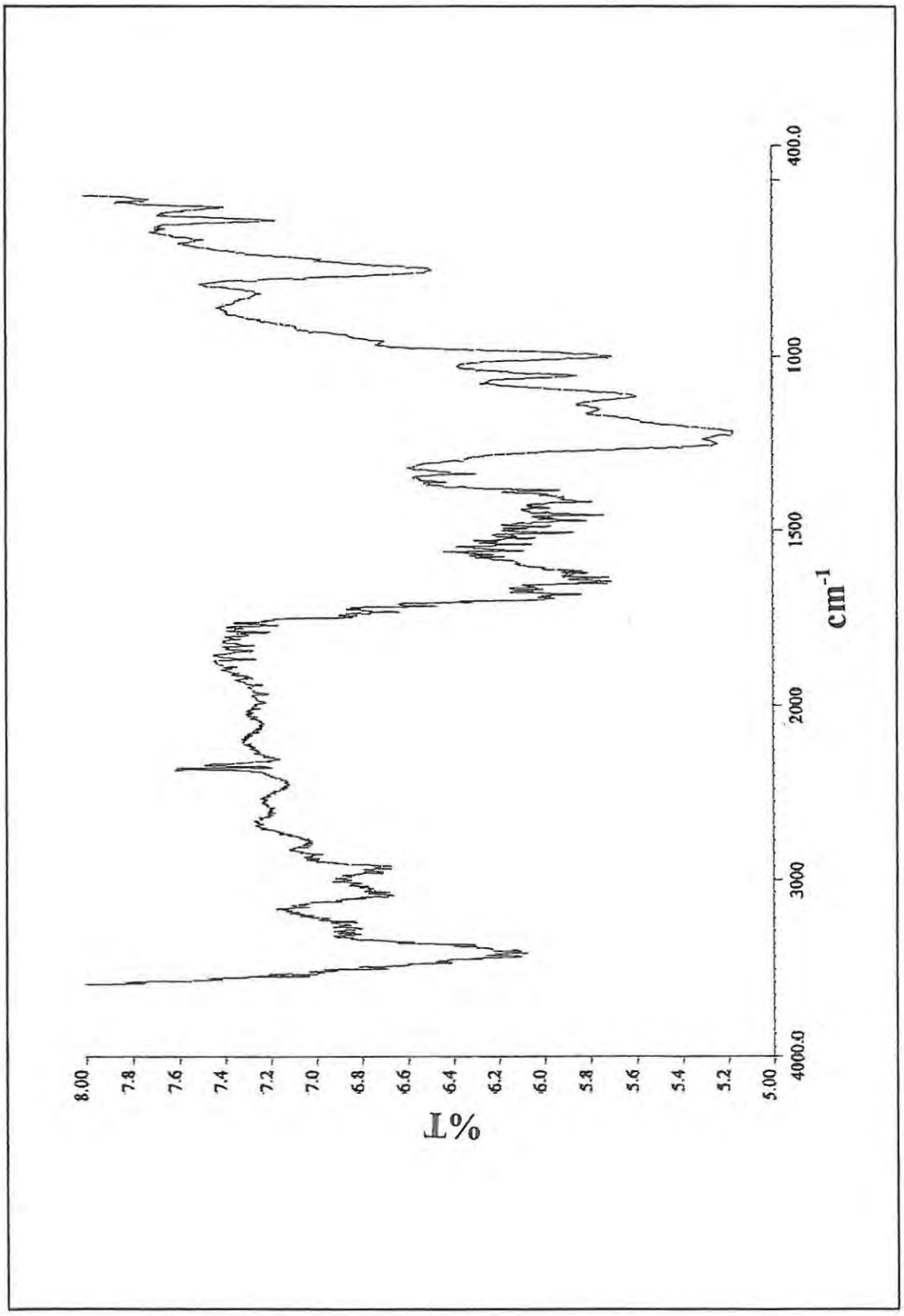

IR spectra of $[Pt(II)2,3Tmtppa(-2)]^{4+}$

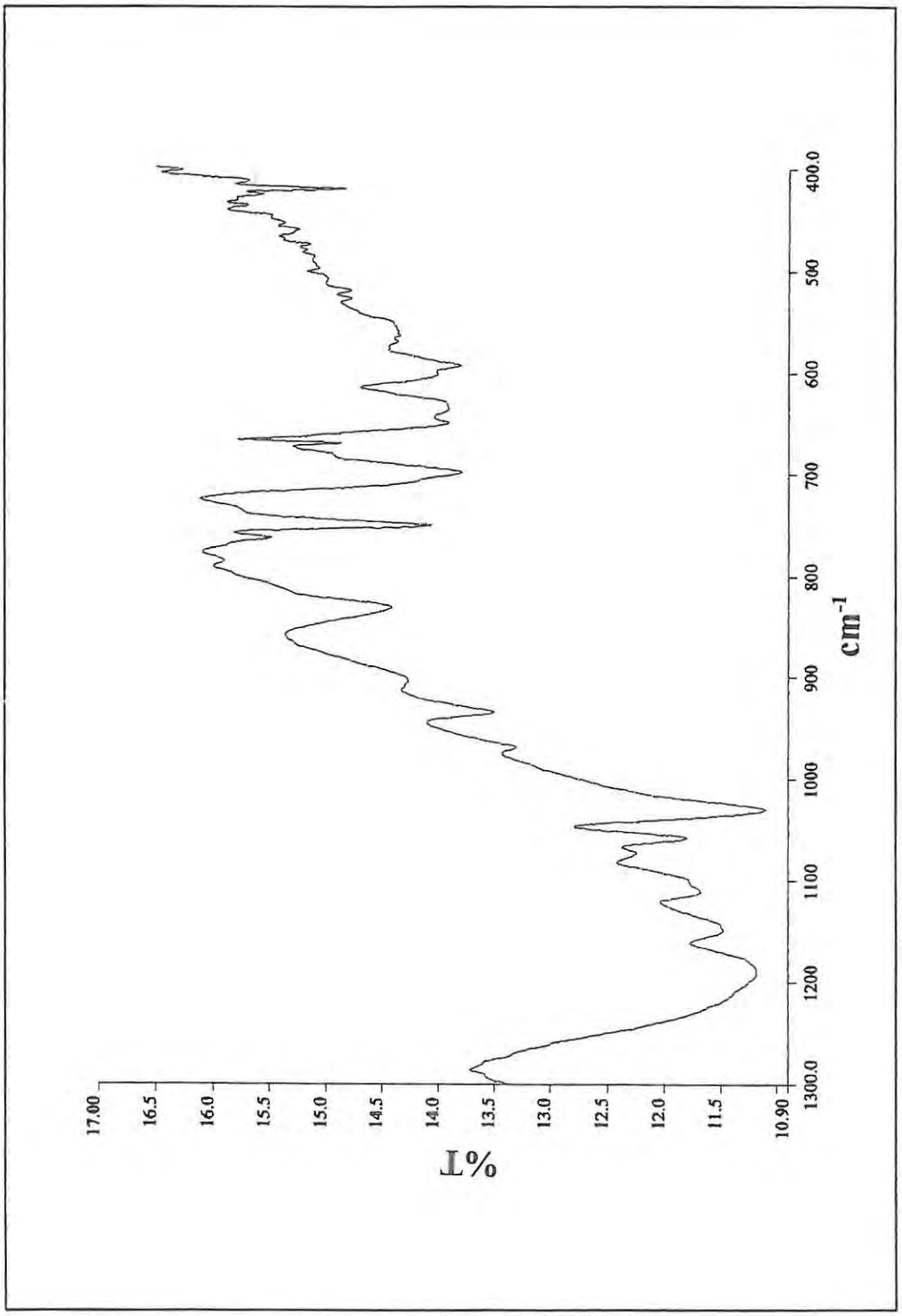

IR spectra of $[Co(II)TSPc]^{4-}$

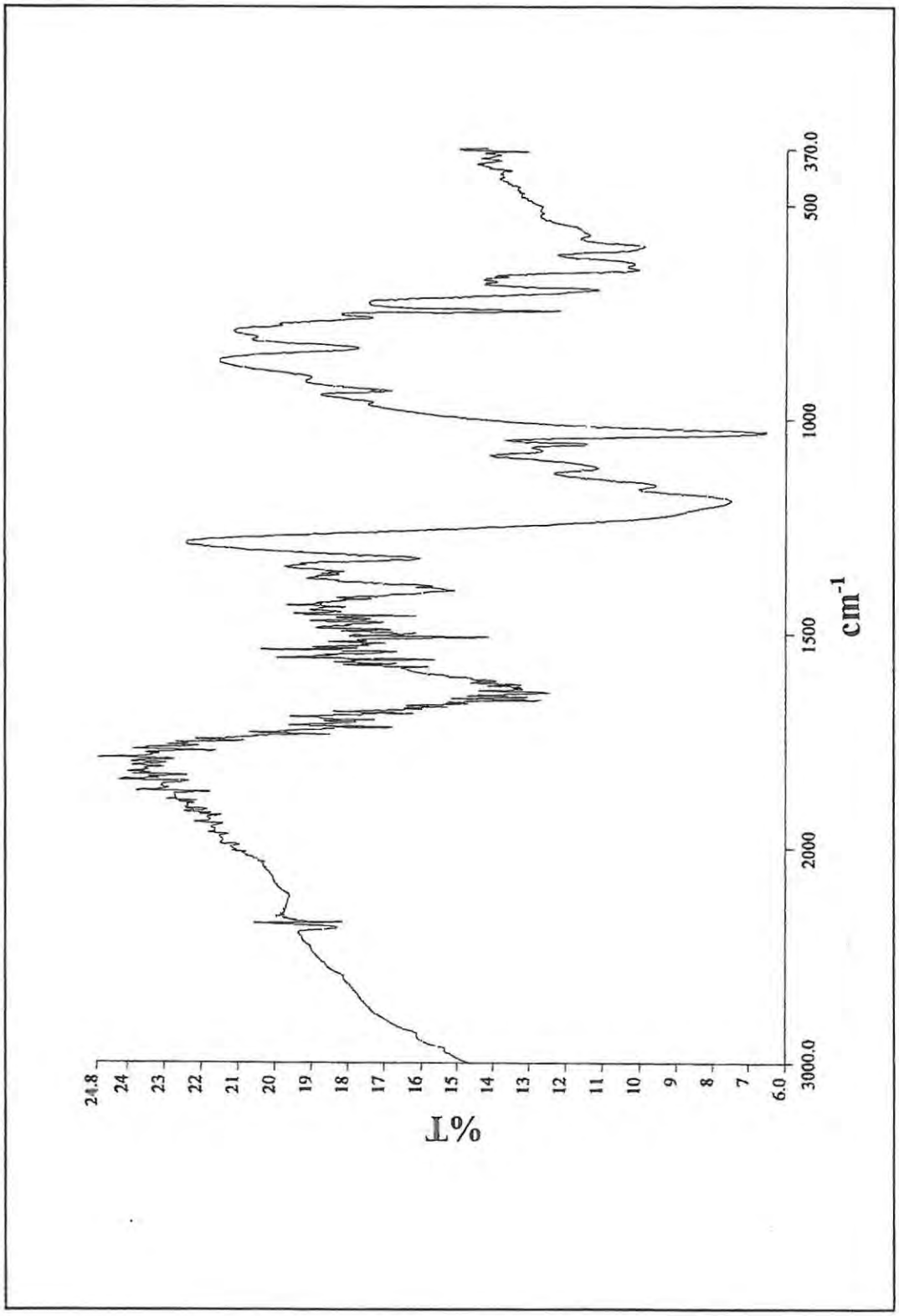

IR spectra of $[Pd(II)TSPc]^{4-}$

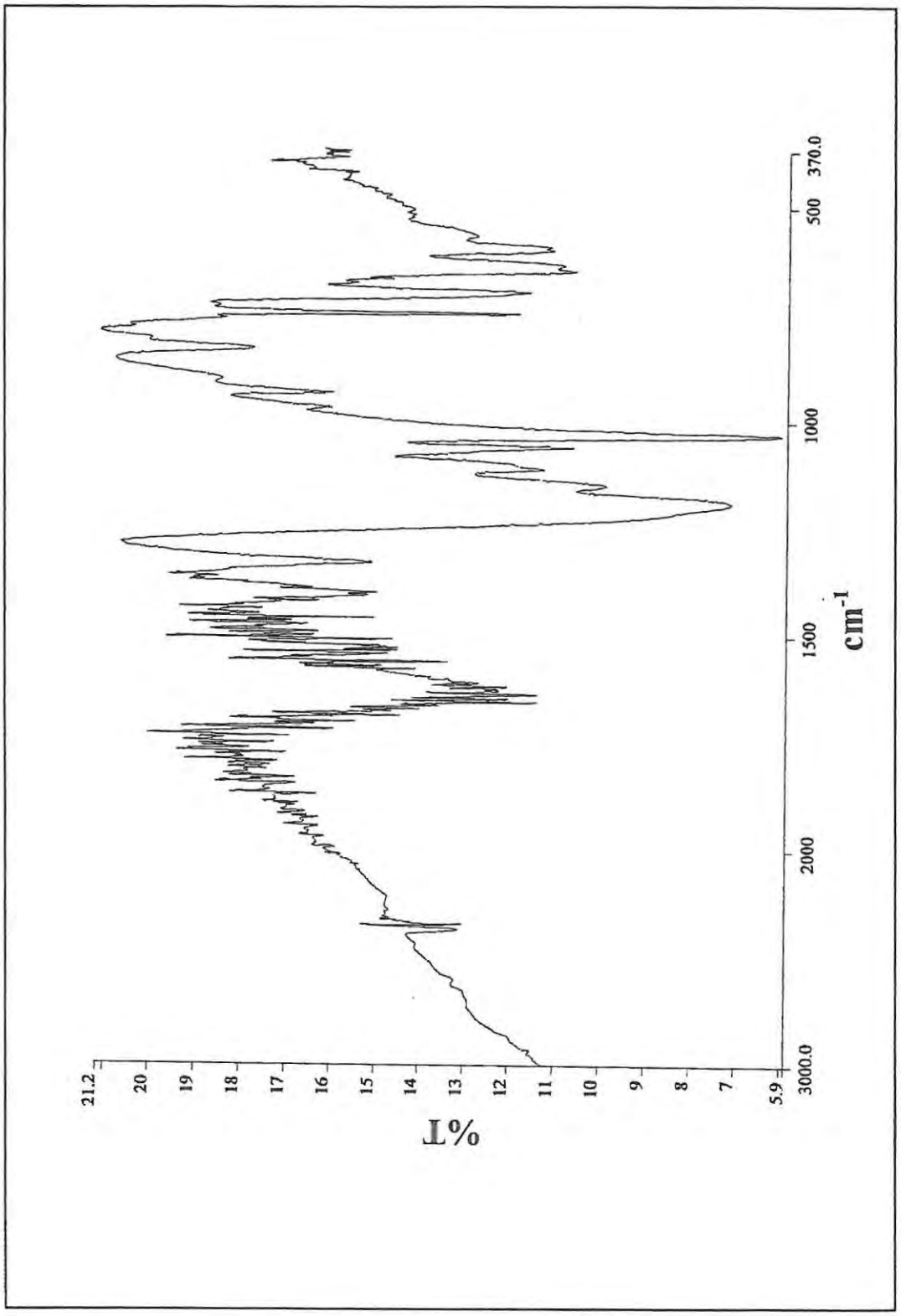

IR spectra of $[Ni(II)TSPc]^{4-}$